

AD-A034 946

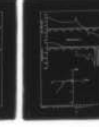
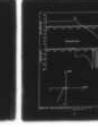
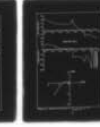
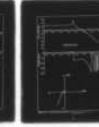
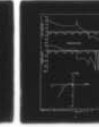
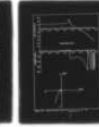
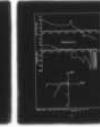
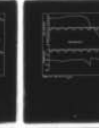
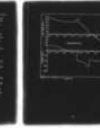
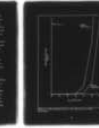
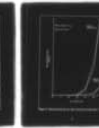
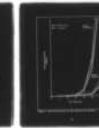
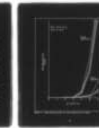
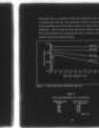
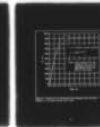
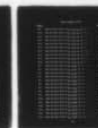
AIR FORCE INST OF TECH WRIGHT-PATTERSON AFB OHIO SCH--ETC F/G 1/2  
A CONTROL THEORETIC STUDY OF THE NUCLEAR VULNERABILITY OF THE A--ETC(U)  
DEC 76 J T MERRIFIELD

UNCLASSIFIED

GA/MC/76D-10

NL

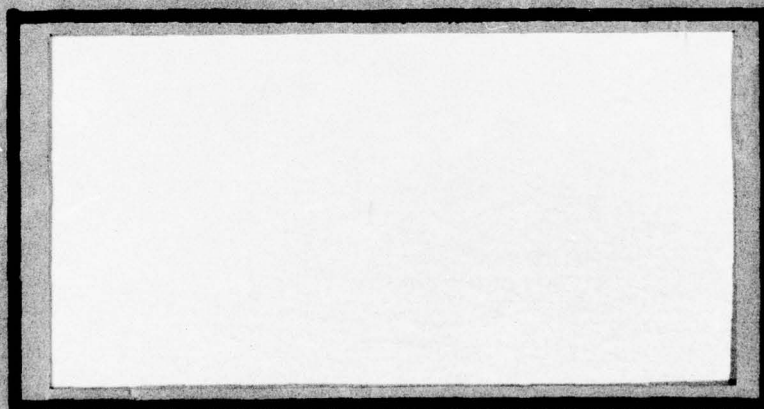
1 OF 2  
ADA034946



ADA034946



71



DDC  
JAN 28 1977  
RECEIVED

UNITED STATES AIR FORCE  
AIR UNIVERSITY  
AIR FORCE INSTITUTE OF TECHNOLOGY  
Wright-Patterson Air Force Base, Ohio

DISTRIBUTION STATEMENT A  
Approved for public release;  
Distribution Unlimited



1

A CONTROL THEORETIC STUDY OF  
THE NUCLEAR VULNERABILITY OF  
THE AIR REFUELING TASK

THESIS

GA/MC/76D-10

John T. Merrifield  
Capt USAF

D D C  
RECEIVED  
JAN 28 1977  
ALBUQUERQUE

ACCESSION for	
NTIS	White Section <input checked="" type="checkbox"/>
D.C.	Buff Section <input type="checkbox"/>
UNANNOUNCED	<input type="checkbox"/>
JUSTIFICATION.....	
BY.....	
DISTRIBUTION/AVAILABILITY CODES	
Dist.	AVAIL. 223/27 SPURIAL
A	

14 GA/MC/76D-10

6  
A CONTROL THEORETIC STUDY OF  
THE NUCLEAR VULNERABILITY OF  
THE AIR REFUELING TASK

THESIS 9 Master's thesis

Presented to the Faculty of the School of Engineering  
of the Air Force Institute of Technology  
Air University  
in Partial Fulfillment of the  
Requirements for the Degree of  
Master of Science

16 7930  
17 09

12 148p.

10 by  
John T. Merrifield B.S.  
Capt USAF

Graduate Astronautical Engineering

11 December 1976

Approved for public release; distribution unlimited.

1473  
012225  
LB

## Preface

This thesis presents my attempts to model the complex air refueling task in a relatively simplistic manner in order to obtain some "first cut" predictions as to its vulnerability to the adverse effects of air turbulence and pilot irradiation. The study was done at the United States Air Force School of Aerospace Medicine, at Brooks Air Force Base, Texas, where a large data base had already been established for the work. Several very broad assumptions and simplifications were made to reduce this problem to manageable proportions considering the time and equipment constraints under which I worked. As a result, I believe that the trends exhibited by the data and its sensitivity to changes in the simulation variables are more significant than the specific times computed for the refueling task.

I have tried to simulate the refueling task as realistically as time and equipment permitted. To this end I observed the "flying abilities" of the pilot models to assure that they were not controlling in a superhuman fashion. There is considerable doubt in some areas as to the limitations of the human pilot. For example, it seems uncertain as to how rapidly and over how large a range the pilot can be reasonably expected to move the throttles to maintain position in the refueling task. I tried also to keep the execution of the refueling task itself within established limits. A good example of this action is the setting of realistic limits on the closure rate during hookup.

I wish to thank the staff of the Aerodynamics Branch of Boeing/Wichita for the hours of telephone time as well as the copies of technical reports I needed for this work; the personnel of the Biometrics



Section of the USAF School of Aerospace Medicine for their always eager support and assistance; Dr. Charles P. Hatsell for his help in enabling me to gain a background in the theory behind this work, and for his very flexible consultation hours during the period spent in doing this study; and my partner in marriage, Sandra, and our two children, Patrick and Kris, who did all they could to help me through this difficult time of our lives.

John T. Merrifield

## Contents

	<u>Page</u>
Preface . . . . .	11
List of Figures . . . . .	vi
List of Tables . . . . .	ix
List of Symbols . . . . .	x
Abstract . . . . .	xvi
 I. Introduction . . . . .	 1
II. Definition of the Problem . . . . .	3
The Coordinate Systems . . . . .	3
The Air Refueling Task . . . . .	6
Assumptions, Approximations and Simplifications . .	9
III. Analytical Development . . . . .	12
The Pilot-Aircraft Control System . . . . .	12
Engine Dynamics . . . . .	12
The Downwash Model . . . . .	17
B-52H Equations of Motion . . . . .	18
Derivation of the Controlled Elements . . . . .	21
The Gust Model . . . . .	24
The Pilot Model . . . . .	24
Analysis of the Pilot-Aircraft System . . . . .	26
Effects of Irradiation on the Human Pilot . . . . .	31
IV. Analog Simulation . . . . .	33
Apparatus . . . . .	33
General . . . . .	33
Observation of Hookup Procedure . . . . .	34
The Simulation Variables . . . . .	35
Monte Carlo Simulation of the Air Refueling Task .	41
V. Results and Discussion . . . . .	44
Overview . . . . .	44
Variation of Mean Refueling Time with Gust	
Intensity . . . . .	44
Variation of Mean Refueling Time with Thrust	
Authority . . . . .	48
Variation of Mean Refueling Time with $T_L$ . . . . .	48
Variation of Mean Refueling Time with Radiation	
Dose . . . . .	48
Results of No-Downwash Simulations . . . . .	49
VI. Conclusions and Recommendations . . . . .	52

## Contents (contd)

Bibliography . . . . .	54
Appendix A: Linearization of Induced Effects Data by the Method of Least Squares . . . . .	56
Appendix B: Calculation of Steady State Angle of Attack in Downwash . . . . .	58
Appendix C: Details of the Derivation of the Controlled Elements . . . . .	60
Appendix D: Gust Model . . . . .	66
Appendix E: Bode and Polar Plots of the Open-Loop Pilot- Aircraft Transfer Functions Without Downwash. .	71
Appendix F: Bode and Polar Plots of the Open-Loop Pilot- Aircraft Transfer Functions With Downwash . . .	90
Appendix G: Analog Patching Diagram . . . . .	109
Appendix H: Plots of Components of Mean Refueling Time . .	112
Vita . . . . .	128



# List of Figures

<u>Figure</u>		<u>Page</u>
1	Coordinate Systems . . . . .	4
2	Block Diagram of Pilot-Aircraft Control System . . .	13
3	Reduced Block Diagram of Pilot-Aircraft Control System . . . . .	14
4	Comparison of B-52H Thrust Time Response and the Time Response of the Approximation . . . . .	16
5	Pilot Gain Factor versus Time . . . . .	32
6	No-Gust Hookup Flight Paths . . . . .	36
7	Mean Refueling Time vs Gust Intensity for 0 Rads . .	45
8	Mean Refueling Time vs Gust Intensity for 500 Rads .	46
9	Mean Refueling Time vs Gust Intensity for 1000 Rads.	47
10	Mean Refueling Time vs Gust Intensity for 0 Rads, No Downwash . . . . .	50
C-1	Bode Plot of $Y_{c_E}$ ) No DW . . . . .	62
C-2	Bode Plot of $Y_{c_T}$ ) No DW . . . . .	63
C-3	Bode Plot of $Y_{c_E}$ ) DW . . . . .	64
C-4	Bode Plot of $Y_{c_T}$ ) DW . . . . .	65
D-1	Bode Plot of Gust Model . . . . .	70
E-1	Bode and Polar Plots of $Y_{p_E}$ $Y_{c_E}$ ) No DW, $T_L = 8$ . . .	72
E-2	Bode and Polar Plots of $Y_{p_T}$ $Y_{c_T}$ ) No DW, $T_L = 8$ . . .	73
E-3	Bode and Polar Plots of $Y_{p_E}$ $Y_{c_E}$ ) No DW, $T_L = 7$ . . .	74
E-4	Bode and Polar Plots of $Y_{p_T}$ $Y_{c_T}$ ) No DW, $T_L = 7$ . . .	75
E-5	Bode and Polar Plots of $Y_{p_E}$ $Y_{c_E}$ ) No DW, $T_L = 6$ . . .	76
E-6	Bode and Polar Plots of $Y_{p_T}$ $Y_{c_T}$ ) No DW, $T_L = 6$ . . .	77
E-7	Bode and Polar Plots of $Y_{p_E}$ $Y_{c_E}$ ) No DW, $T_L = 5$ . . .	78
E-8	Bode and Polar Plots of $Y_{p_T}$ $Y_{c_T}$ ) No DW, $T_L = 5$ . . .	79

# List of Figures (Contd)

<u>Figure</u>		<u>Page</u>
E-9	Bode and Polar Plots of $Y_{PE} Y_{CE}$ ) No DW, $T_L = 4$ . . . .	80
E-10	Bode and Polar Plots of $Y_{PT} Y_{CT}$ ) No DW, $T_L = 4$ . . . .	81
E-11	Bode and Polar Plots of $Y_{PE} Y_{CE}$ ) No DW, $T_L = 3$ . . . .	82
E-12	Bode and Polar Plots of $Y_{PT} Y_{CT}$ ) No DW, $T_L = 3$ . . . .	83
E-13	Bode and Polar Plots of $Y_{PE} Y_{CE}$ ) No DW, $T_L = 2$ . . . .	84
E-14	Bode and Polar Plots of $Y_{PT} Y_{CT}$ ) No DW, $T_L = 2$ . . . .	85
E-15	Bode and Polar Plots of $Y_{PE} Y_{CE}$ ) No DW, $T_L = 1.5$ . . . .	86
E-16	Bode and Polar Plots of $Y_{PT} Y_{CT}$ ) No DW, $T_L = 1.5$ . . . .	87
E-17	Bode and Polar Plots of $Y_{PE} Y_{CE}$ ) No DW, $T_L = 1$ . . . .	88
E-18	Bode and Polar Plots of $Y_{PT} Y_{CT}$ ) No DW, $T_L = 1$ . . . .	89
F-1	Bode and Polar Plots of $Y_{PE} Y_{CE}$ ) DW, $T_L = 8$ . . . . .	91
F-2	Bode and Polar Plots of $Y_{PT} Y_{CT}$ ) DW, $T_L = 8$ . . . . .	92
F-3	Bode and Polar Plots of $Y_{PE} Y_{CE}$ ) DW, $T_L = 7$ . . . . .	93
F-4	Bode and Polar Plots of $Y_{PT} Y_{CT}$ ) DW, $T_L = 7$ . . . . .	94
F-5	Bode and Polar Plots of $Y_{PE} Y_{CE}$ ) DW, $T_L = 6$ . . . . .	95
F-6	Bode and Polar Plots of $Y_{PT} Y_{CT}$ ) DW, $T_L = 6$ . . . . .	96
F-7	Bode and Polar Plots of $Y_{PE} Y_{CE}$ ) DW, $T_L = 5$ . . . . .	97
F-8	Bode and Polar Plots of $Y_{PT} Y_{CT}$ ) DW, $T_L = 5$ . . . . .	98
F-9	Bode and Polar Plots of $Y_{PE} Y_{CE}$ ) DW, $T_L = 4$ . . . . .	99
F-10	Bode and Polar Plots of $Y_{PT} Y_{CT}$ ) DW, $T_L = 4$ . . . . .	100
F-11	Bode and Polar Plots of $Y_{PE} Y_{CE}$ ) DW, $T_L = 3$ . . . . .	101
F-12	Bode and Polar Plots of $Y_{PT} Y_{CT}$ ) DW, $T_L = 3$ . . . . .	102
F-13	Bode and Polar Plots of $Y_{PE} Y_{CE}$ ) DW, $T_L = 2$ . . . . .	103
F-14	Bode and Polar Plots of $Y_{PT} Y_{CT}$ ) DW, $T_L = 2$ . . . . .	104
F-15	Bode and Polar Plots of $Y_{PE} Y_{CE}$ ) DW, $T_L = 1.5$ . . . . .	105

# List of Figures (contd)

<u>Figure</u>		<u>Page</u>
F-16	Bode and Polar Plots of $Y_{PT} Y_{CT})_{DW}$ , $T_L = 1.5$ . . . . .	106
F-17	Bode and Polar Plots of $Y_{PE} Y_{CE})_{DW}$ , $T_L = 1$ . . . . .	107
F-18	Bode and Polar Plots of $Y_{PT} Y_{CT})_{DW}$ , $T_L = 1$ . . . . .	108
G-1	Analog Patching Diagram . . . . .	110
H-1	Mean Hookup Time vs Gust Intensity for 0 Rads, Thrust Authority A . . . . .	113
H-2	Mean Hookup Time vs Gust Intensity for 0 Rads, Thrust Authority B . . . . .	114
H-3	Mean Time-on-Boom vs Gust Intensity for 0 Rads . . . . .	115
H-4	Mean Inadvertant Disconnect Time vs Gust Intensity for 0 Rads . . . . .	116
H-5	Mean Hookup Time vs Gust Intensity for 500 Rads, Thrust Authority A . . . . .	117
H-6	Mean Hookup Time vs Gust Intensity for 500 Rads, Thrust Authority B . . . . .	118
H-7	Mean Time-on-Boom vs Gust Intensity for 500 Rads . . . . .	119
H-8	Mean Inadvertant Disconnect Time vs Gust Intensity for 500 Rads . . . . .	120
H-9	Mean Hookup Time vs Gust Intensity for 1000 Rads, Thrust Authority A . . . . .	121
H-10	Mean Hookup Time vs Gust Intensity for 1000 Rads, Thrust Authority B . . . . .	122
H-11	Mean Time-on-Boom vs Gust Intensity for 1000 Rads. . . . .	123
H-12	Mean Inadvertant Disconnect Time vs Gust Intensity for 1000 Rads . . . . .	124
H-13	Mean Hookup Time vs Gust Intensity for 0 Rads, No Downwash . . . . .	125
H-14	Mean Time-on-Boom vs Gust Intensity for 0 Rads, No Downwash . . . . .	126
H-15	Mean Inadvertant Disconnect Time vs Gust Intensity for 0 Rads, No Downwash . . . . .	127



List of Tables

<u>Table</u>		<u>Page</u>
I	Position Coordinates . . . . .	6
II	B-52H Longitudinal Aerodynamic Characteristics for the Refueling Task . . . . .	7
III	Eigenanalysis of B-52H Characteristic Equation . . .	22
IV	Transfer Functions of the Controlled Elements . . .	23
V	Summary of Pilot-Aircraft System Analysis . . . .	28
VI	Pilot Gain Decrements Due to Irradiation . . . . .	32
VII	Summary of Results of No-Gust Hookup Runs . . . . .	37
VIII	Simulation Variables and Their Values . . . . .	38
IX	Induced Effects Data . . . . .	56
X	Analog Potentiometer Settings . . . . .	111

# List of Symbols

<u>Symbol</u>	<u>Definition</u>	<u>Usual Dimension</u>
$\bar{c}$	Mean aerodynamic (geometric) chord	ft
CAS	Calibrated Air Speed	knots
$C_{D1}$	Aircraft drag coefficient at equilibrium	
$C_{D\alpha}$	Variation of drag coefficient with angle of attack	rad <sup>-1</sup>
$C_{Du}$	Variation of drag coefficient with speed	
$C_{L0}$	Lift coefficient for zero angle of attack, zero elevator angle and zero stabilizer angle	
$C_{L1}$	Aircraft lift coefficient at equilibrium	
$C_{L\alpha}$	Aircraft lift curve slope	rad <sup>-1</sup>
$C_{L\dot{\alpha}}$	Variation of lift coefficient with rate of change of angle of attack	sec-rad <sup>-1</sup>
$C_{L\delta_E}$	Variation of lift coefficient with elevator angle	rad <sup>-1</sup>
$C_{Lq}$	Variation of lift coefficient with pitch rate	sec-rad <sup>-1</sup>
$C_{Lu}$	Variation of lift coefficient with speed	sec-ft <sup>-1</sup>
$C_{m0}$	Pitching moment coefficient for zero angle of attack, zero elevator angle and zero stabilizer angle	
$C_{m1}$	Aircraft pitching moment coefficient at equilibrium	
$C_{m\alpha}$	Variation of pitching moment coefficient with angle of attack	rad <sup>-1</sup>
$C_{m\dot{\alpha}}$	Variation of pitching moment coefficient with rate of change of angle of attack	sec-rad <sup>-1</sup>

# List of Symbols (Contd)

$C_{m\delta E}$	Variation of pitching moment coefficient with elevator angle	rad <sup>-1</sup>
$C_{mq}$	Variation of pitching moment coefficient with pitch rate	sec-rad <sup>-1</sup>
$C_{mu}$	Variation of pitching moment coefficient with speed	sec-ft <sup>-1</sup>
$\Delta C_{L1}$	Induced change in aircraft lift coefficient due to downwash	
$\Delta C_{m1}$	Induced change in aircraft pitching moment coefficient due to downwash	
$dT$	Moment arm of thrustline	ft
$g$	Acceleration of gravity	ft/sec <sup>2</sup>
$I_{yy}$	Moment of inertia about Y axis	slug-ft <sup>2</sup>
$K_F$	Gain needed to compensate for gust filter loss	
$K_{PE}$	Pilot model gain for the elevator loop	
$K_{PT}$	Pilot model gain for the throttle loop	
$L_w$	Scale of turbulence for the Z gust	ft
$m$	Mass of aircraft	slugs
$M$	Mach number	
$MRT$	Military Rated Thrust	lbs
$M_u$	Dimensional variation of pitching moment with speed	ft <sup>-1</sup> sec <sup>-1</sup>
$M_w$	Dimensional variation of pitching moment with perturbed velocity along Z axis	rad/ft-sec
$M_{\dot{w}}$	Dimensional variation of pitching moment with perturbed acceleration along Z axis	rad/ft
$M_q$	Dimensional variation of pitching moment with pitch rate	sec <sup>-1</sup>



# List of Symbols (Contd)

$M_{\delta E}$	Dimensional variation of pitching moment with elevator angle	sec <sup>-2</sup>
$M_{\delta T}$	Dimensional variation of pitching moment with thrust	rad/lb-sec <sup>2</sup>
$q$	Perturbed pitch rate	rad/sec
$\bar{q}_1$	Dynamic pressure	lb/ft <sup>2</sup>
$R$	Radial distance from tanker boom pod	ft
RMS	Root-mean-square	
$S$	Wing surface area	ft <sup>2</sup>
SAS	Stability augmentation system	
TAS	True Air Speed	knots
$T_L$	Pilot rate to displacement weighting (pilot lead)	sec
$u$	Perturbed velocity along X-stability axis	ft/sec
$U_1$	Equilibrium velocity along X-stability axis	ft/sec
$w$	Perturbed velocity along Z-stability axis	ft/sec
$w_g$	Gust velocity along Z-stability axis	ft/sec
$x$	Horizontal displacement of B-52 center of mass from tanker boom pod	ft
$x'$	Horizontal displacement of B-52 boom receptacle from tanker boom pod	ft
$\hat{x}$	Horizontal displacement of B-52 center of mass from center of refueling envelope	ft
$\hat{x}'$	Horizontal displacement of B-52 boom receptacle from center of refueling envelope	ft
$X_{CG}$	Distance of the center of gravity from the wing leading edge	ft

### List of Symbols (Contd)

$X_u$	Dimensional variation of X-force with speed	$\text{sec}^{-1}$
$X_w$	Dimensional variation of X-force with perturbed velocity along Z axis	$\text{sec}^{-1}$
$X_{\delta E}$	Dimensional variation of X-force with elevator angle	$\text{ft}/\text{sec}^2$
$X_{\delta T}$	Dimensional variation of X-force with thrust	$\text{ft}/\text{lb-sec}^2$
$Y_{CE}$	Aircraft transfer function (controlled element) for the elevator control	$\text{ft}/\text{inch}$
$Y_{PE}$	Pilot model transfer function for the elevator control	$\text{inch}/\text{ft}$
$Y_{CT}$	Aircraft transfer function (controlled element) for the throttle control	$\text{ft}/\text{lb}$
$Y_{PT}$	Pilot model transfer function for the throttle control	$\text{lb}/\text{ft}$
$z$	Vertical displacement of B-52 center of mass from tanker boom pod	$\text{ft}$
$z'$	Vertical displacement of B-52 boom receptacle from tanker boom pod	$\text{ft}$
$\hat{z}$	Vertical displacement B-52 center of mass from center of refueling envelope	$\text{ft}$
$\dot{\hat{z}}$	Vertical velocity of B-52 center of mass relative to center of refueling envelope	$\text{ft}/\text{sec}$
$\hat{z}'$	Vertical displacement of B-52 boom receptacle from center of refueling envelope	$\text{ft}$
$\dot{\hat{z}'}$	Vertical velocity of B-52 boom receptacle relative to center of refueling envelope	$\text{ft}/\text{sec}$
$\ddot{\hat{z}'}$	Vertical (normal) acceleration of B-52 boom receptacle relative to center of refueling envelope	$\text{ft}/\text{sec}^2$
$Z_u$	Dimensional variation of Z-force with speed	$\text{sec}^{-1}$

# List of Symbols (Contd)

$Z_{\dot{w}}$	Dimensional variation of Z-force with perturbed velocity along Z-axis	sec <sup>-1</sup>
$Z_{\ddot{w}}$	Dimensional variation of Z-force with perturbed acceleration along Z axis	
$Z_q$	Dimensional variation of Z-force with pitch rate	ft/sec
$Z_{\delta_E}$	Dimensional variation of Z-force with elevator angle	ft/sec <sup>2</sup>
$\rho$	Air density	slug/ft <sup>3</sup>
$\theta_1$	Equilibrium pitch attitude angle	rad
$\theta$	Perturbed pitch attitude angle	rad
$\alpha_1$	Equilibrium angle of attack	rad
$\alpha$	Perturbed angle of attack	rad
$\eta$	Angle of the refueling boom with the local horizontal	deg
$\delta_E$	Perturbed elevator angle	rad
$\delta_{PE}$	Output of pilot model transfer function for the elevator loop	inch
$\delta_{stab}$	Horizontal stabilizer angle	rad
$\delta_T$	Perturbed thrust	lbs
$\delta_{PT}$	Output of pilot model transfer function for the throttle loop	lbs
$\omega$	Frequency	rad/sec
$\omega_c$	Crossover frequency	rad/sec
$\omega_n$	Undamped natural frequency	rad/sec
$\omega_{ns.p.}$	Short period undamped natural frequency	rad/sec
$\omega_{np}$	Phugoid undamped natural frequency	rad/sec
$\zeta$	Damping ratio	
$\zeta_{s.p.}$	Short period damping ratio	



List of Symbols (Contd)

$\zeta_p$	Phugoid damping ratio	
$\tau_e$	Pilot's effective time delay	sec
$\sigma_w$	Root-mean-square intensity of vertical gust velocity	ft/sec
$\phi_m$	Phase margin	deg
$\xi$	RMS value of Gaussian random noise	volts

## ABSTRACT

A hypothetical air refueling operation involving a B-52H bomber and a KC-135 tanker is modeled on an analog computer for the purpose of determining its vulnerability to air turbulence and pilot gain decrement due to irradiation. The model includes the following elements: (1) the longitudinal small perturbation equations of motion for the B-52H in the downwash flow field of the KC-135; (2) pilot models to operate the elevator and throttle of the B-52H; and (3) a stochastic gust model which provides vertical gust disturbances to the equations of motion.

The controlled elements with and without downwash are derived for the refueling task. Comparison of these transfer functions shows that the downwash causes instability. Stability analyses are conducted on the pilot-aircraft open-loop transfer functions over a range of pilot rate to displacement weighting,  $T_L$ , and pilot gains are found which will stabilize the system for each value of  $T_L$ .

By means of no-gust hookup simulations the range of  $T_L$  is narrowed by eliminating those values of  $T_L$  which yield unrealistically long hookup times or poor aircraft control during hookup.

Monte Carlo simulations of the refueling task are run at varying combinations of  $T_L$ , rms gust intensity, pilot thrust authority, and pilot gain decrement due to irradiation. Trends of mean refueling time are predicted. Using mean refueling time as a basis for comparison, optimum values of  $T_L$  are found for the irradiated and the non-irradiated pilot.

Results also are presented on a small group of Monte Carlo simulations conducted with the downwash effects removed from the equations of motion.

A CONTROL THEORETIC STUDY OF THE NUCLEAR  
VULNERABILITY OF THE AIR REFUELING TASK

I. Introduction

There is much current interest in determining the ability of the pilot of a B-52 aircraft performing a strategic bombing mission to suffer the radiation effects of a nuclear encounter and still continue on to mission completion. A typical mission consists of a takeoff, climbout, cruise, air refueling, low level phase, and a penetration to the target. The air refueling portion of the mission is one of the most vulnerable to the effects of pilot irradiation because it requires flying in close formation with a tanker aircraft in order to receive enough fuel to complete the mission. This study treats the air refueling portion of the B-52 mission.

The longitudinal small perturbation equations of motion of the B-52H aircraft were programmed on an analog computer and a two-dimensional simulation of the air refueling was made. These linearized equations included the force and moment induced on the B-52 by the KC-135 tanker downwash flow field. The pitch stability augmentation system (SAS) and the engine dynamics also were modeled on the analog computer.

Pilot models were developed which enabled a closed-loop analysis of the elevator and throttle control loops of the simulated B-52. The parameters of these pilot models were chosen on the basis of human operator theory and stability considerations. To this end it was necessary to perform frequency domain analyses on the transfer functions of the controlled elements and the pilot-aircraft open-loop



transfer functions. Although the analog simulation was concerned primarily with the pilot-aircraft systems having downwash effects included, the frequency domain analyses were performed with equal emphasis on the systems with and without downwash.

The variables considered in this study are listed below:

1. Pilot lead time,  $T_L$
2. RMS vertical gust intensity,  $\sigma_w$
3. Thrust (throttle) authority limits
4. Radiation dose level

The pilot lead was the only variable in the theoretical analyses, whereas all four variables were considered in the analog simulation.

The primary objective of this study was to predict the length of time required to accomplish an air refueling under the adverse conditions of air turbulence gusts and pilot performance degradation due to irradiation. Determination of the values of  $T_L$  which produced the lowest values of predicted refueling time was a secondary objective.

## II. Definition of the Problem

### The Coordinate Systems

Three coordinate systems were used in this study. These are depicted in Figure 1. The X,Z system has its origin at the boom pod of the tanker aircraft. These axes are aligned with the local horizontal and vertical. The perturbed displacements of the B-52 center of mass along these axes are  $x$  and  $z$ , respectively. Since the displacements of the B-52 boom receptacle are of primary interest to this problem, these displacements,  $x'$  and  $z'$ , are defined as

$$x' = x + 54 \cos\theta \quad (1)$$

$$z' = z - 54 \sin\theta \quad (2)$$

where 54 is the distance in feet from the B-52 center of mass to the refueling boom receptacle and  $\theta$  is the perturbed pitch attitude. The B-52 fuselage is assumed here to have zero vertical dimension. If it is further assumed that all perturbations in  $\theta$  are small, the above relationships reduce to

$$x' = x + 54 \quad (3)$$

$$z' = z - 54\theta \quad (4)$$

Since only perturbed quantities are of interest to this study, the constant 54 ft can be eliminated from the first of these equations. This simplification yields

$$x' = x \quad (5)$$

$$z' = z - 54\theta \quad (6)$$

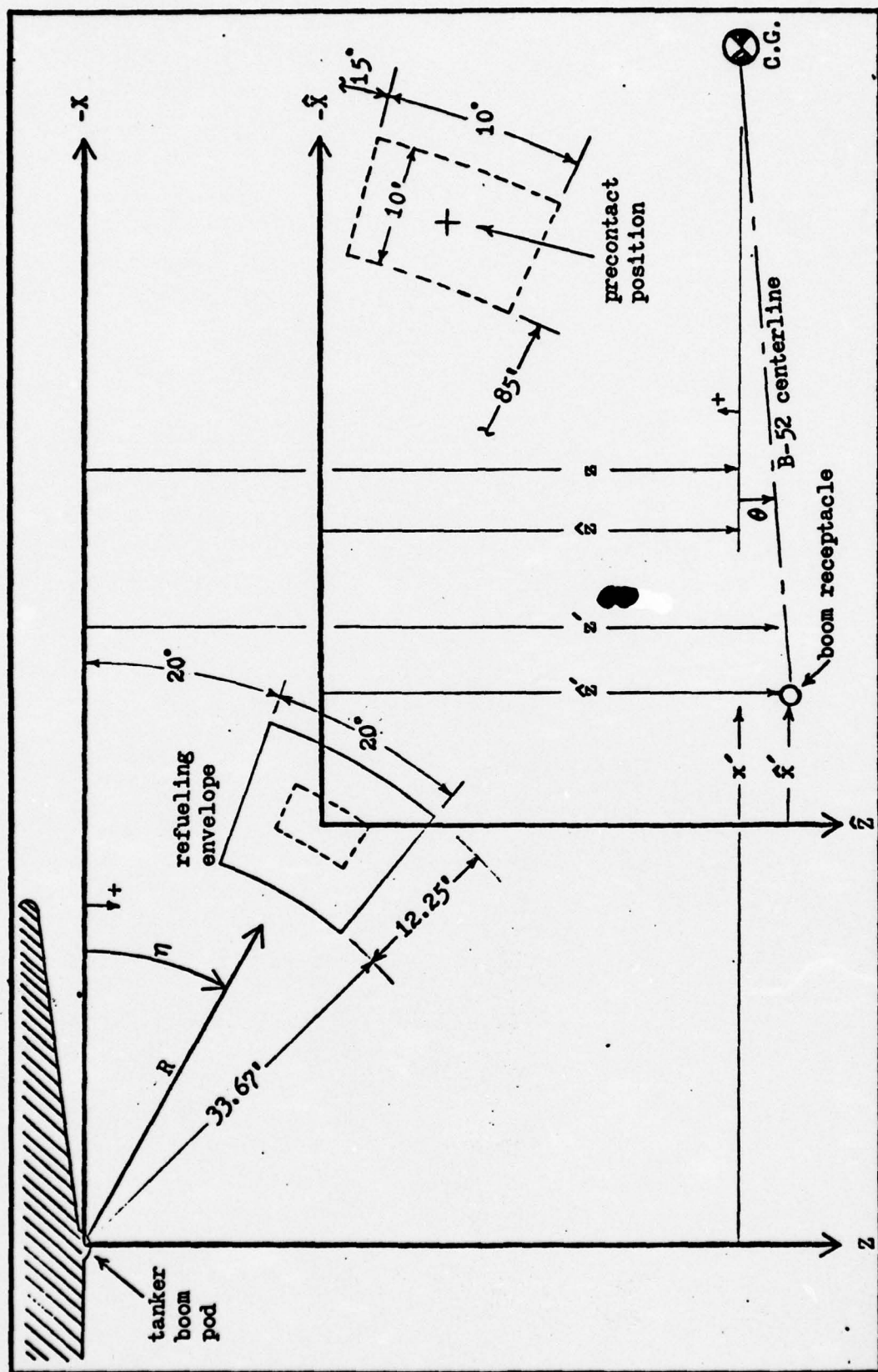


Figure 1. Coordinate Systems.



The  $R, \eta$  coordinate system is derived from the  $X, Z$  system by the following relationships:

$$R = \sqrt{x'^2 + z'^2} \quad (7)$$

$$\eta = \tan^{-1} \frac{z'}{-x'} \quad (8)$$

where  $R$  is the magnitude of the radius vector from the tanker boom pod to the B-52 boom receptacle and  $\eta$  is the angle of the radius vector from the local horizontal. When the refueling boom is connected to the B-52,  $R$  and  $\eta$  represent the boom length and boom angle, respectively.

The refueling envelope is the region in space defined by

$$33.67' \leq R \leq 45.92' \quad (9)$$

$$20^\circ \leq \eta \leq 40^\circ \quad (10)$$

(Ref 1:1-6)

The  $\hat{X}, \hat{Z}$  system of coordinates has its origin at the center of the refueling envelope. These axes also are aligned with the local horizontal and vertical. Since small perturbations in  $\theta$  are assumed, the B-52 stability axes always remain approximately aligned with the  $\hat{X}, \hat{Z}$  axes.  $\hat{x}$  and  $\hat{z}$  are the perturbed displacements of the B-52 center of mass from the center of the refueling envelope.  $\hat{x}'$  and  $\hat{z}'$  are the perturbed displacements of the boom receptacle from the center of the envelope, where

$$\hat{x}' = \hat{x} \quad (11)$$

$$\hat{z}' = \hat{z} - 54\theta \quad (12)$$

which are derived in a manner identical to the derivation of Eqs (5) and (6).

The  $\hat{X}, \hat{Z}$  system is related to the  $X, Z$  system by the relationships listed below.

$$\hat{x} = x + 34.47 \text{ ft} \quad (13)$$

$$\hat{z} = z - 19.90 \text{ ft} \quad (14)$$

The precontact position, where the B-52 is stabilized before attempting hookup, is depicted on Figure 1 as

$$\hat{x} = -50 \text{ ft} \quad (15)$$

$$\hat{z} = +10 \text{ ft} \quad (16)$$

(Ref 1:4-2)

Table I, below, presents the coordinates of the refueling envelope center and the precontact position in all three coordinate systems.

TABLE I

Position	Position Coordinates		
	Coordinate Systems		
	$\frac{X, Z}{\text{ft, ft}}$	$\frac{R, \eta}{\text{ft, deg}}$	$\frac{\hat{X}, \hat{Z}}{\text{ft, ft}}$
Center of Refueling Envelope	-34.47, 19.90	39.79, 30	0, 0
Precontact	-84.47, 29.90	89.61, 19.5	-50, 10

#### The Air Refueling Task

The air refueling phase of the hypothetical strategic bombing mission was assumed to take place approximately five and one half hours after takeoff. The B-52 takes on 120,000 lbs of fuel during an "on-boom" time of twenty minutes. The aircraft parameters and flight conditions assumed for that point in the mission are given in Table II.

Table II  
B-52H Longitudinal Aerodynamic Characteristics for the Refueling Task  
(Stability Axis System)

W = 450,000 lbs (max. gross weight)		M = .72	$\bar{c} = 22.96 \text{ ft}$
Mass = 13,970 slugs		$\rho = .0007945 \text{ slug/ft}^3$	$x_{CG} = 25 \text{ ft}$
Altitude = 32,700 ft		$\bar{q}_1 = 198 \text{ lb/ft}^2$	$d_T = 2.78 \text{ ft}$
CAS = 255 kts		$I_{yy} = 8.15 \times 10^6 \text{ slug-ft}^2$	$\alpha_1 = .03 \text{ deg (no downwash)}$
TAS = 706 kts		$S = 4000 \text{ ft}^2$	$\theta_1 = 0$

Dimensionless Derivatives	Dimensional Derivatives	Dimensionless Derivatives	Dimensional Derivatives
$C_{D_u} = 0$	$X_u = -.000465 \text{ sec}^{-1}$	$C_{L_{\delta_E}} = .00251 \text{ deg}^{-1}$	$Z_{\delta_E} = -8.153 \text{ ft/sec}^2\text{-rad}$
$C_{D_1} = .0278$	$X_{\delta_T} = .0000715 \text{ slug}^{-1}$	$C_{m_\alpha} = -.0151 \text{ deg}^{-1}$	$M_w = -.002734 \text{ rad/ft-sec}$
$C_{D_\alpha} = .00441 \text{ deg}^{-1}$	$X_w = .02548 \text{ sec}^{-1}$	$C_{m_\alpha} = -.0479 \text{ deg}^{-1}$	$M_w = -.0001408 \text{ rad/ft}$
$C_{L_1} = .57$	$Z_{\delta_T} = 0$	$C_{m_q} = -.4360 \text{ deg}^{-1}$	$M_q = -.9063 \text{ sec}^{-1}$
$C_{L_u} = 0$	$Z_u = -.09154 \text{ sec}^{-1}$	$C_{m_{\delta_E}} = -.00491 \text{ deg}^{-1}$	$M_{\delta_E} = -.6277 \text{ sec}^{-2}$
$C_{L_\alpha} = .0891 \text{ deg}^{-1}$	$Z_w = -.4122 \text{ sec}^{-1}$	$C_{L_{\delta_{stab}}} = .01079 \text{ deg}^{-1}$	$M_{\delta_T} = 3.411 \times 10^{-7} \text{ lb}^{-1}\text{sec}^{-2}$
$C_{L_\alpha} = .0158 \text{ deg}^{-1}$	$Z_w = -.001182$	$C_{m_{\delta_{stab}}} = -.0327 \text{ deg}^{-1}$	
$C_{L_q} = .0719 \text{ deg}^{-1}$	$Z_q = -3.798 \text{ ft/sec}$		

(Ref 2:10.13 - 10.15)



Also listed in that table are the B-52 stability derivatives which will be used in the equations of motion in later sections.

The air refueling maneuver requires the pilot to perform three types of procedures. They are:

1. hookup
2. boom tracking
3. inadvertant disconnect, if required

The air refueling task begins with the B-52 stabilized in the pre-contact position, depicted in Figure 1. The initial hookup procedure is begun when the pilot advances the throttles enough to establish a slow closure rate with respect to the tanker. The pilot climbs until the B-52 boom receptacle is slightly below the refueling boom, which has been extended into the refueling envelope. As the B-52 boom receptacle approaches the center of the refueling envelope the pilot reduces power in order to arrive at the center of the envelope with zero closure rate. The boom operator aboard the tanker then inserts the boom nozzle into the B-52 boom receptacle (Ref 1:4.2).

The boom tracking procedure requires the B-52 pilot to keep his aircraft within the limits of the refueling envelope until the refueling is completed or until the occurrence of an inadvertant disconnect.

An inadvertant disconnect occurs when the boom receptacle moves outside the limits of boom travel as defined by the refueling envelope. If refueling is not completed the B-52 pilot returns his aircraft to the precontact position and stabilizes before attempting another hookup.

### Assumptions, Approximations, and Simplifications

The complexity of the air refueling problem required that the task be reduced to a simpler form for this study. The statements listed below define the manner in which this was done.

1. The B-52 was treated as a rigid body.
2. The weight of the B-52 remained constant at 450,000 lbs during refueling. It was assumed that maximum gross weight represented the worst case from the standpoint of pilot control.
3. The KC-135 tanker was treated as a stable platform, unaffected by the vertical air turbulence gusts.
4. The B-52 was assumed to have accomplished a successful hookup when it had remained for fifteen seconds within an envelope defined by

$$37.79' \leq R \leq 41.79' \quad (17)$$

$$25^\circ \leq \eta \leq 35^\circ \quad (18)$$

This envelope is shown by dashed lines within the larger refueling envelope in Figure 1.

5. In the inadvertant disconnect procedure, the B-52 was assumed to have stabilized in the precontact position when it had remained for fifteen seconds within an envelope defined by

$$85' \leq R \leq 95' \quad (19)$$

$$15^\circ \leq \eta \leq 25^\circ \quad (20)$$

This envelope also is defined by dashed lines in Figure 1.

6. During the hookup procedure the B-52 closure rate was required to remain between one and two feet per second relative to the tanker.

7. The B-52 was assumed to be affected only by vertical air turbulence gusts. Head-on and side gusts were not considered.

8. The derivative of the vertical gust velocity,  $\dot{w}_g$ , was neglected.

9. Small perturbations in  $u, w, q$ , and  $\theta$  were assumed.

10. The B-52 stability axes were assumed to be always approximately aligned with the local horizontal and vertical.

11. The engine dynamics were approximated by a first order lag transfer function.

12. The B-52 pitch SAS was simplified to that shown in Figure 2 by neglecting several high frequency terms in the transfer functions of its components (Ref 3:17).

13. A linear form of pilot model,  $Y_p = K_p(T_L j\omega + 1)e^{-j\omega\tau_e}$ , was assumed both for the elevator and the throttle control. This model will be the subject of discussion in later sections.

14. The  $e^{-j\omega\tau_e}$  terms in the pilot models were represented in the analog simulations by second order Pade' approximations.

15. The pilot models applied control inputs directly into the pitch SAS and the engine throttles. Connecting linkages and gear reductions normally present between the cockpit and these control units were disregarded. The gains of the pilot models were calculated on the basis of these approximations.

16. The B-52 was assumed to be trimmed at all times for flight at the center of the refueling envelope. As shown later this



assumption simplified the downwash equations.

17. The B-52 was assumed to be aligned at all times on the centerline of the KC-135 tanker with all lateral variables equal to zero.

18. The hypothetical nuclear encounter was assumed to occur at the time of takeoff.

### III. Analytical Development

#### The Pilot-Aircraft Control System

A block diagram of the pilot-aircraft control system is shown in Figure 2.  $Y_{p_E}$  is the transfer function of the pilot model for elevator control and  $Y_{p_T}$  is the pilot model for throttle control.

The stability characteristics of the closed-loop control system can be analyzed if  $Y_{p_E}$ ,  $Y_{c_E}$  and  $Y_{p_T}$ ,  $Y_{c_T}$ , the open-loop pilot-aircraft transfer functions, are derived.  $Y_{c_E}$  and  $Y_{c_T}$ , the transfer functions of the elevator and throttle controlled elements, take the following forms for the air refueling task:

$$Y_{c_E} = \frac{\hat{z}}{\delta_{p_E}} \quad (21)$$

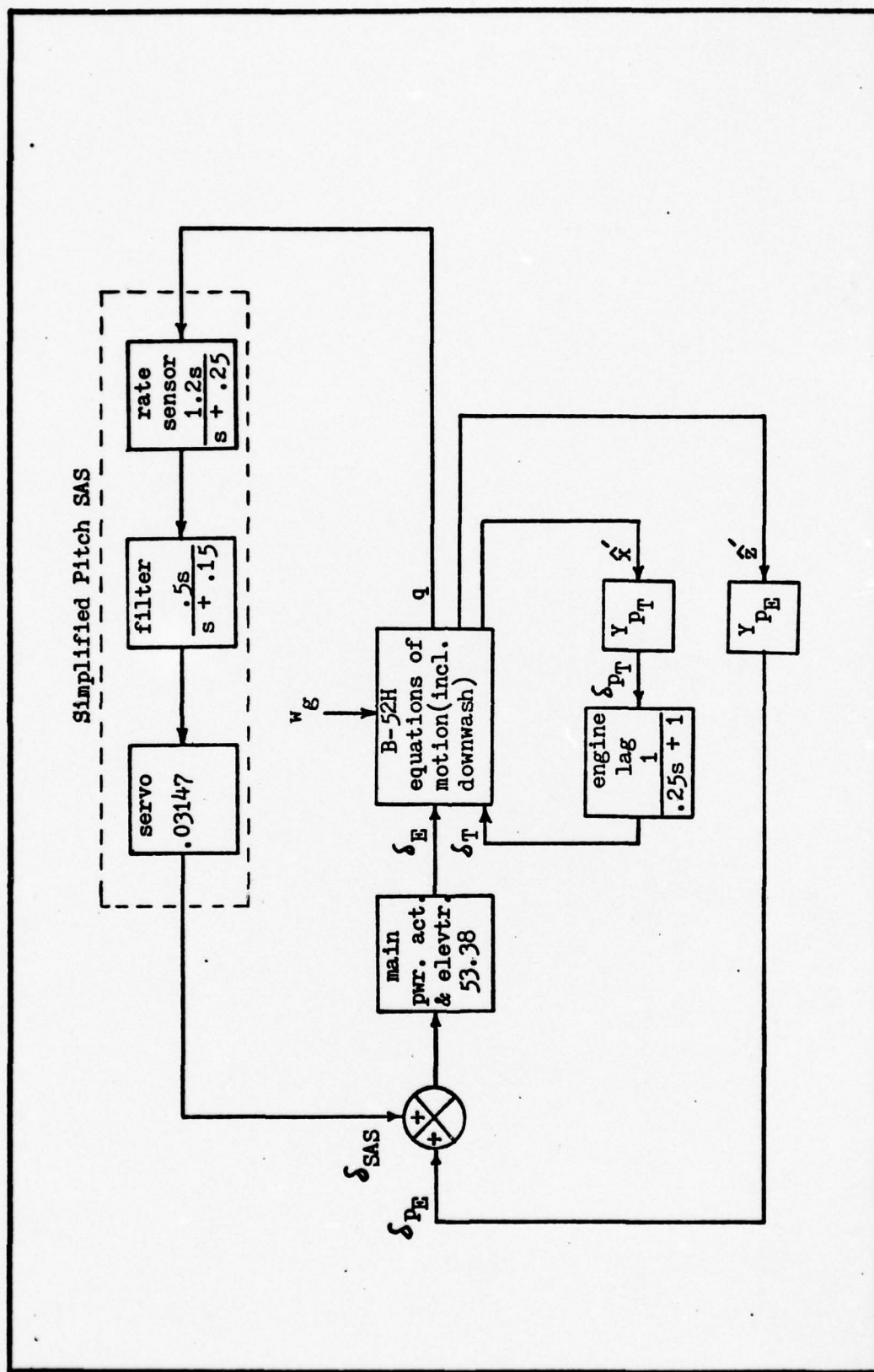
$$Y_{c_T} = \frac{\hat{x}}{\delta_{p_T}} \quad (22)$$

where  $\delta_{p_E}$  represents the pilot's input to the pitch SAS and  $\delta_{p_T}$  is the pilot's input to the engine throttle.

The system shown in Figure 2 can be modeled in terms of pilot models operating on controlled elements as shown by Figure 3. The succeeding sections will lead up to the derivation of the terms of the two controlled elements.

#### Engine Dynamics

At the refueling altitude of 32,700 ft the thrust required to maintain equilibrium flight is calculated from the equilibrium drag coefficient,  $C_{D_1}$ , as shown below.





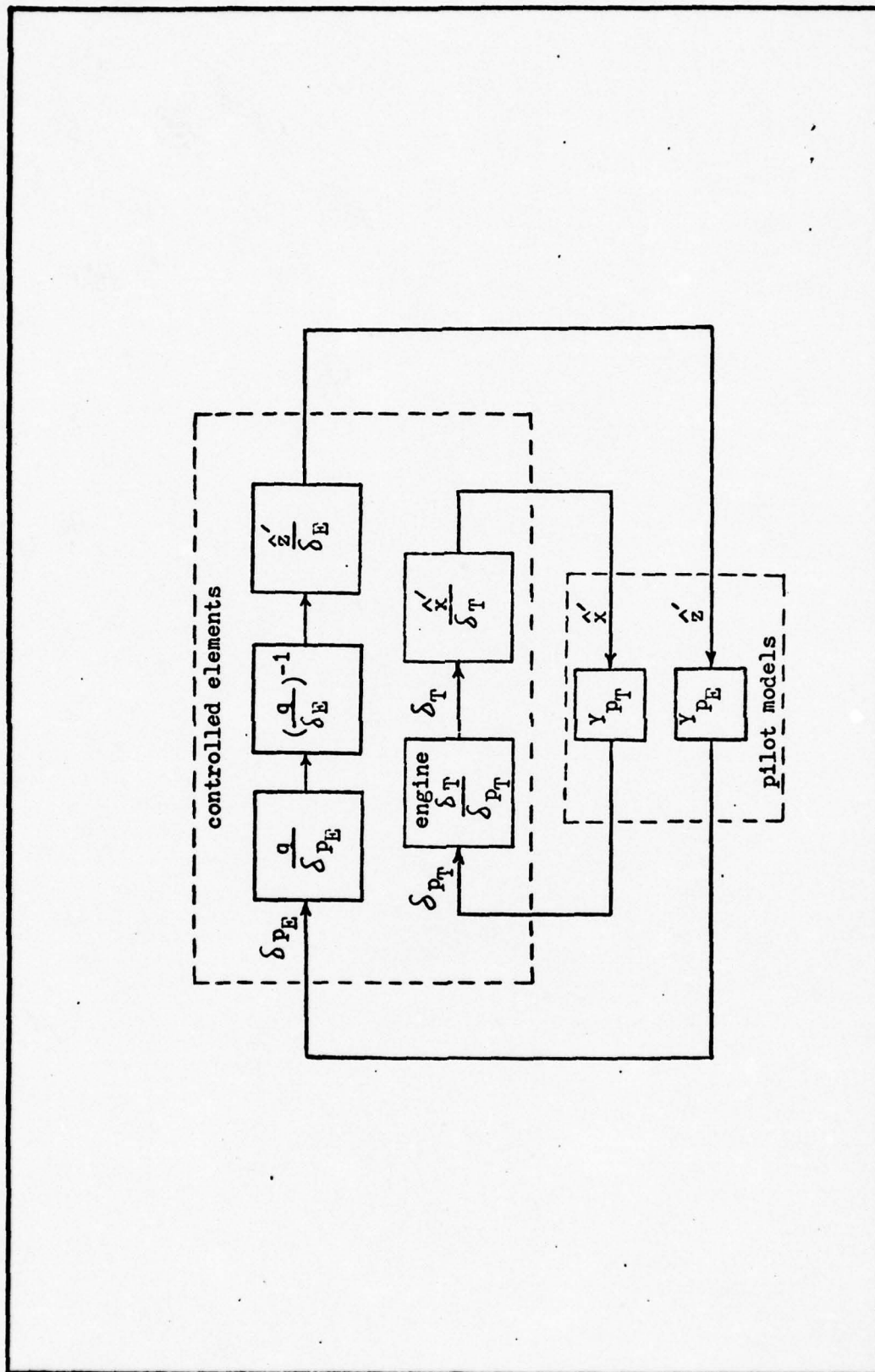


Figure 3. Reduced Block Diagram of Pilot-Aircraft Control System.

$$\begin{aligned} T_{eq} = \text{Drag} &= C_{D1} \bar{q}_1 S = (.0278)(198)(4000) \\ &= \underline{22017.6 \text{ lbs}} \end{aligned} \quad (23)$$

$$\text{Equilibrium thrust per engine} = 22017.6/8 = \underline{2752.2 \text{ lbs}}$$

The above value of equilibrium thrust defines an operating point about which positive or negative changes,  $\delta_T$ , are commanded by the pilot.

The thrust time response of the TF33-P-3 engine of the B-52H for a step throttle movement from idle to military rated thrust (MRT) is plotted in Reference 4. That portion of the curve representing the time response of  $\delta_T$  to a step throttle movement,  $\delta_{p_T}$ , from the equilibrium thrust setting to MRT is reproduced in Figure 4. By trial and error it was determined that the time response for this particular case can be approximated by

$$\delta_T(t) = \delta_{p_T} (1 - e^{-4t}) = 926(1 - e^{-4t}) \quad (24)$$

which is also plotted on Figure 4 for comparison. Taking Laplace transforms of both sides of the above expression yields the transfer function

$$\frac{\delta_T}{\delta_{p_T}} = \frac{1}{.25 s + 1} \quad (25)$$

This transfer function is used in the analog simulations to represent the engine dynamics. It is by no means meant to provide a close approximation to the engine response in the general case. On the contrary, the approximation was based on the response to only one of the many possible throttle inputs--that of a step input from equilibrium to MRT thrust. A step throttle input from idle thrust to the equilibrium thrust setting, for example, will result in a much slower engine

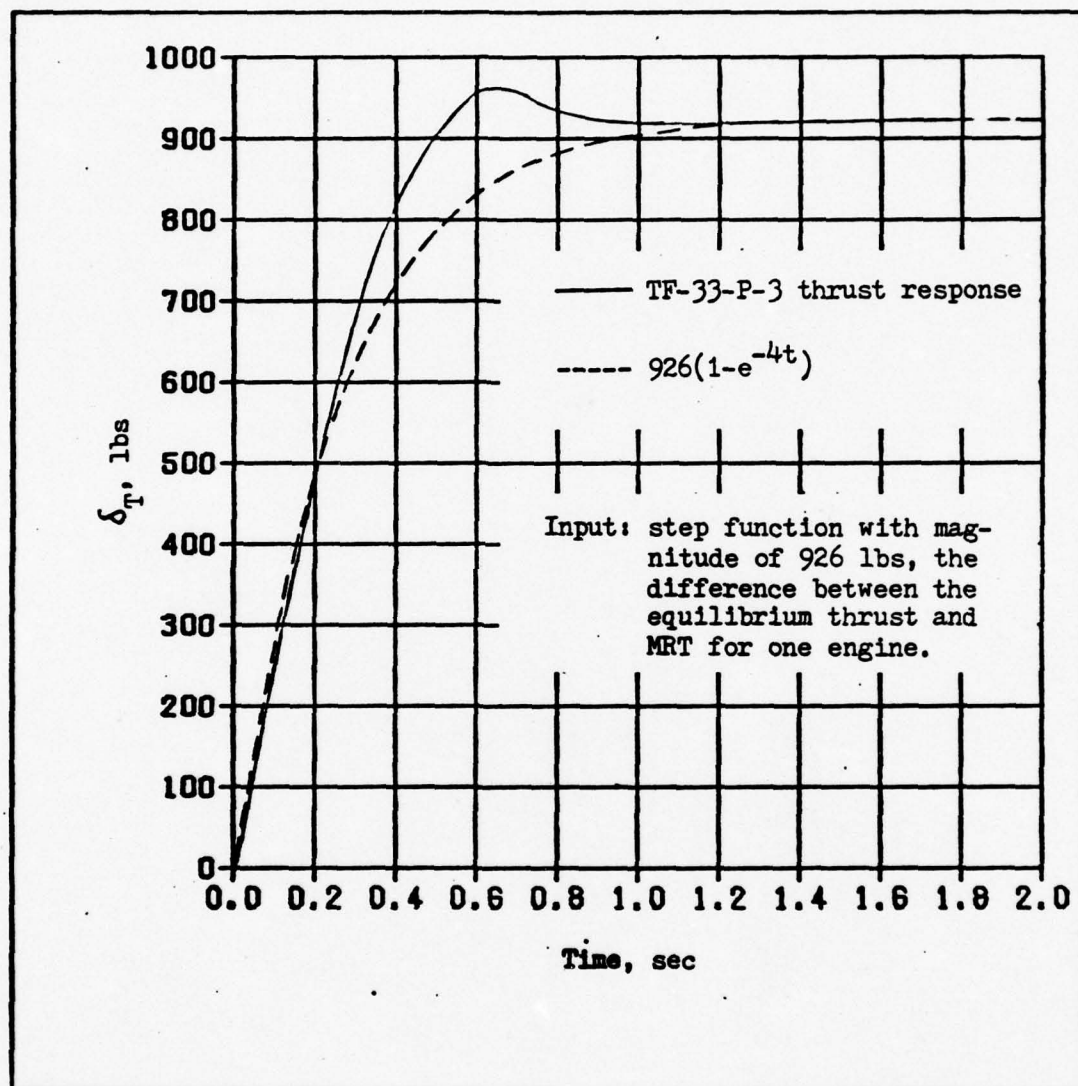


Figure 4: Comparison of B-52H Thrust Time Response with the Time Response of the Approximation (Ref 4:142).



response than given by the approximation. However, it is assumed that the approximation of the engine response in the neighborhood of the equilibrium thrust setting will also be a valid approximation to the engine response in a statistical sense; i.e., the average response experienced over many simulations of the air refueling.

#### The Downwash Model

The effects of the KC-135 flow field on the B-52 were derived from graphical data in the form of induced changes in the B-52 equilibrium lift and moment coefficients,  $C_{L1}$  and  $C_{m1}$  (Ref 5:2-79,4-95). This data is given as a function of the variable  $z$ . A linear fit is made to this data as shown in Appendix A. The resultant equations for the induced changes, converted to the variable  $\hat{z}$ , are

$$\Delta C_{L1} = -.077 + .00114\hat{z} \quad (26)$$

$$\Delta C_{m1} = .068 - .00102\hat{z} \quad (27)$$

This study assumed that the effects of tanker downwash are trimmed out when the B-52 is flying at the center of the refueling envelope. In that case the conditions

$$\Delta C_{L1} \Big|_{\hat{z}=0} = 0 \quad (28)$$

$$\Delta C_{m1} \Big|_{\hat{z}=0} = 0 \quad (29)$$

must hold since the aircraft must have the same total lift (= weight) and moment (= 0) as in the case with no downwash. Therefore, when the aircraft is trimmed for flight at the center of the refueling envelope the constant terms drop out of the downwash equations, reducing them to simple linear terms in  $\hat{z}$ :

$$\Delta C_{L1} = .00114\hat{z} \quad (30)$$

$$\Delta C_{m1} = -.00102\hat{z} \quad (31)$$

The changes in lift and moment caused by the tanker downwash are

$$\Delta L = \Delta C_{L1} \bar{q}_1 S \quad (32)$$

$$\Delta M = \Delta C_{m1} \bar{q}_1 S \bar{c} \quad (33)$$

where  $\bar{q}_1$  is the dynamic pressure,  $S$  is the wing area, and  $\bar{c}$  is the mean geometric chord of the wing.

In order to trim out the induced effects of the tanker flow field, the B-52 pilot must change the steady state angle of attack  $\alpha_1$ , by changing the horizontal stabilizer angle by an increment  $\delta_{stab}$ . A new stability axis system is thus defined. The steady state angle of attack which is required for flight at the center of the refueling envelope is .68 deg, as shown by the calculations in Appendix B. This value of  $\alpha_1$  was assumed to be small enough to be treated as equal to zero in the ensuing derivation of the B-52H equations of motion.

#### B-52H Equations of Motion

The B-52H equations of motion, using the dimensional form of the stability derivatives, are presented below. These equations include the vertical gust disturbance,  $w_g$ , and the lift and moment terms induced by the KC-135 downwash.

$$\dot{u} = X_u u + X_w (w - w_g) - g\theta + X_{\delta_T} \delta_T \quad (34)$$

$$\dot{w} - U_1 q = Z_u u + Z_w (w - w_g) + Z_q q + \frac{Z_{\dot{q}}}{U_1} \dot{w}_g + Z_{\dot{w}} (\dot{w} - \dot{w}_g) + Z_{\delta_E} \delta_E - \frac{\bar{q}_1 S}{m} \Delta C_{L1} \quad (35)$$

$$\dot{q} = M_u u + M_w (w - w_g) + M_q q + \frac{M_{\dot{q}}}{U_1} \dot{w}_g + M_{\dot{w}} (\dot{w} - \dot{w}_g) + M_{\delta_E} \delta_E + M_{\delta_T} \delta_T + \frac{\bar{q}_1 S c}{I_{yy}} \Delta C_{m1} \quad (36)$$

(Ref 6:9.83)

Neglecting the  $\dot{w}_g$  terms, rearranging the equations, and substituting in values for the coefficients as listed in Table II, yields

$$\dot{u} = -.004465u + .02548w - 32.2\theta - .02548w_g + .0000715\delta_T \quad (37)$$

$$\dot{w} = -.09143u - .4117w + 701.37q + .4117w_g - 8.143\delta_E + \hat{A}z \quad (38)$$

$$\begin{aligned} \dot{q} = .000013u - .002676w - 1.00505q + .002676w_g - .62655\delta_E \\ + 3.411 \times 10^{-7} \delta_T + B\hat{z} \end{aligned} \quad (39)$$

$$\dot{\theta} = q \quad (40)$$

where the coefficients of the downwash variable,  $\hat{z}$ , are:

$$A = \frac{-\bar{q}_1 S}{m} (.00114) = -.06471 \quad (41)$$

$$B = \frac{\bar{q}_1 S c}{I_{yy}} (-.00102) = -.002269 \quad (42)$$

which are derived from Table II and Eqs (30) and (31).

By introducing the equation,

$$\dot{\hat{z}} = w - U_1 \theta \quad (43)$$

and by letting  $u, w, q, \theta, \hat{z}$  be the state variables and  $\delta_E, \delta_T$  be the control variables of the system, the equations of motion can be put into matrix format as shown below.



$$\begin{Bmatrix} \dot{u} \\ \dot{w} \\ \dot{q} \\ \dot{\theta} \\ \dot{z} \end{Bmatrix} = \begin{bmatrix} -.004465 & .02548 & 0 & -32.2 & 0 \\ -.09143 & -.4117 & 701.37 & 0 & A \\ .000013 & -.002676 & -1.00505 & 0 & B \\ 0 & 0 & 1 & 0 & 0 \\ 0 & 1 & 0 & -706 & 0 \end{bmatrix} \begin{Bmatrix} u \\ w \\ q \\ \theta \\ z \end{Bmatrix}$$

$$+ \begin{bmatrix} -.02548 \\ .4117 \\ .002676 \\ 0 \\ 0 \end{bmatrix} w_g + \begin{bmatrix} 0 & .0000715 \\ -8.143 & 0 \\ -.62655 & 3.411 \times 10^{-7} \\ 0 & 0 \\ 0 & 0 \end{bmatrix} \begin{Bmatrix} \delta_E \\ \delta_T \end{Bmatrix} \quad (44)$$

The characteristic equation of this system is

$$\begin{aligned}
\text{C.E.} = & s^5 + 1.4212s^4 + (2.2994-A)s^3 + (.012756-1.00953A+4.6B)s^2 \\
& + (.0080505-1.89374A+290.6807B)s + (-.00862A-.001525B) \quad (45)
\end{aligned}$$

The eigenvalues and eigenvectors of the system without the downwash effects were calculated by letting A and B go zero, reducing the system to fourth order. The resultant characteristic equation is

$$\text{C.E.}_{\text{NoDW}} = s^4 + 1.4212s^3 + 2.2994s^2 + .012756s + .0080505 \quad (46)$$

Substituting the numerical values for A and B into Eq (45) yields the characteristic equation

$$\text{C.E.}_{\text{DW}} = s^5 + 1.4212s^4 + 2.3641s^3 + .067645s^2 - .52896s + .0005612 \quad (47)$$

which represents the system with downwash. The eigenvalues and eigenvectors for this system also were calculated. A comparison of the eigenanalysis for the B-52 with and without downwash is presented in

Table III. The downwash terms introduce two poles in the right half s-plane, thus causing the aircraft to be unstable. Additionally, the phugoid oscillatory roots are eliminated.

#### Derivation of the Controlled Elements

The controlled elements  $Y_{cE}$  and  $Y_{cT}$  have been defined as

$$Y_{cE} = \frac{\hat{z}'}{\delta_{pE}} = \frac{\hat{z}'}{\delta_E} \left( \frac{q}{\delta_E} \right)^{-1} \frac{q}{\delta_{pE}} = \left( \frac{\hat{z}}{\delta_E} - 54 \frac{\theta}{\delta_E} \right) \left( \frac{q}{\delta_E} \right)^{-1} \frac{q}{\delta_{pE}} \quad (48)$$

and

$$Y_{cT} = \frac{\hat{x}'}{\delta_{pT}} = \frac{\hat{x}'}{\delta_T} \frac{\delta_T}{\delta_{pT}} = \frac{1}{s} \frac{u}{\delta_T} \frac{\delta_T}{\delta_{pT}} \quad (49)$$

where  $\frac{\delta_T}{\delta_{pT}}$  is the transfer function of the engine dynamics.  $Y_{cE}$  and  $Y_{cT}$  represent the vertical and horizontal displacements of the B-52 boom receptacle due to the respective pilot inputs  $\delta_{pE}$  and  $\delta_{pT}$ . The throttle controlled element can be derived in a straightforward manner from the equations of motion, but the derivation of the elevator controlled element requires a complicated block diagram reduction of the pitch SAS feedback control loop. Details of the derivation of the controlled elements are shown in Appendix C.

Table IV presents a summary of the controlled elements in factored frequency domain form. Inspection of these controlled elements reveals that the downwash terms have caused them to become unstable by introducing two positive real poles. In addition to eliminating the phugoid oscillation, the tanker downwash changes the short-period response of the elevator controlled element by decreasing its damping while increasing its damped frequency.

Table III  
Eigenanalysis of B-52H Characteristic Equation

Without Downwash		With Downwash	
EIGVAL (1)		EIGVAL (1)	
-.7089110	1.337319	-.6379154	1.411451
EIGVEC (1)		EIGVEC (1)	
.1097337D-01	.5121876D-02	.1062842D-01	.5919335D-02
1.000000	.0	1.000000	.0
-.4223274D-03	.1907391D-02	-.3104689D-03	.2001139D-02
.1244091D-02	-.3436895D-03	.1259858D-02	-.3494375D-03
		.1157477	-.1306298
EIGVAL (2)		EIGVAL (2)	
-.7089110	-1.337319	-.6379154	-1.411451
EIGVEC (2)		EIGVEC (2)	
.1097337D-01	-.5121876D-02	.1062842D-01	-.5919335D-02
1.000000	.0	1.000000	.0
-.4223274D-03	-.1907391D-02	-.3104689D-03	-.2001139D-02
.1244091D-02	.3436895D-03	.1259858D-02	.3494375D-03
		.1157477	.1306298
EIGVAL (3)		EIGVAL (3)	
-.1696463D-02	.5925515D-01	.1061246D-02	.0
EIGVEC (3)		EIGVEC (3)	
1.000000	.0	.9193964	.0
-.3619953D-01	-.1044339D-02	-.2516848	.0
.1092860D-03	-.3668806D-05	-.3788101D-06	.0
-.1146243D-03	-.1841048D-02	-.3569485D-03	.0
		.3022661	.0
EIGVAL (4)		EIGVAL (4)	
-.1696463D-02	-.5925515D-01	-.5484181	.0
EIGVEC (4)		EIGVEC (4)	
1.000000	.0	.9630291D-02	.0
-.3619953D-01	.1044339D-02	-.6662926	.0
.1092860D-03	.3668806D-05	.1999292D-03	.0
-.1146243D-03	.1841048D-02	-.3645562D-03	.0
		.7456281	.0
EIGVAL (5)		EIGVAL (5)	
		.4019726	.0
EIGVEC (5)		EIGVEC (5)	
		.6342205D-01	.0
		-.4873993	.0
		-.4768249D-03	.0
		-.1186212D-02	.0
		.8708719	.0

Note: Elements of eigenvectors correspond to elements of state vector of Eq (44).



Table IV  
Transfer Functions of the Controlled Elements

	$\frac{Y_{cE}}{N_{oDW}}$	$\frac{Y_{cT}}{N_{oDW}}$	$\frac{Y_{cE}}{DW}$	$\frac{Y_{cT}}{DW}$
<b>Numerator</b>				
K	-7.766	.02034	-112.237	-.06857
T <sub>1</sub>	6.667	-	-2500	1.82
T <sub>2</sub>	4.0	-	-	-2.453
T <sub>3</sub>	-2500	-	-	-
$\omega_{n1}$	2.544	-	2.557	-
$\zeta_1$	.058	-	.058	-
<b>Denominator</b>				
T <sub>s</sub>	1	-	-	1
T <sub>1</sub>	4.5	.25	1.585	.25
T <sub>2</sub>	6.0	-	-2.57	1.824
T <sub>3</sub>	-	-	-952.38	-2.488
T <sub>4</sub>	-	-	-	-943.4
$\omega_{n1}$	1.514	.0593	1.471	-
$\zeta_1$	.68	.028	.62	-
$\omega_{n2}$	.0593	-	-	-
$\zeta_2$	.028	-	-	-

General form of numerator or denominator:

$$G = K(T_s j\omega) \prod_{i=1}^n (T_i j\omega + 1) \prod_{k=1}^m \left( \frac{-\omega^2}{\omega_{nk}^2} + \frac{2\zeta_k}{\omega_{nk}} j\omega + 1 \right)$$

### The Gust Model

As previously stated, the B-52 is assumed to be affected only by vertical gusts. The random vertical gust model used in this study is defined by the following transfer function, which is based on the Dryden scales for clear air turbulence.

$$\frac{w_g}{\xi} = \sigma_w \left[ \frac{2.85 (4.29j\omega+1)}{(2.48j\omega+1)^2} \right] \quad (50)$$

where

$w_g$  = random vertical gust velocity

$\sigma_w$  = rms value of random vertical gust velocity

$\xi$  = rms value of Gaussian random noise input  
(Ref 7:459)

The bandwidth of the random noise,  $\xi$ , was 1.5 Hz. Calculation of the terms in this gust model is shown in Appendix D.

Bode magnitude and phase angle plots of the gust transfer function are shown in Figure D-1. It is seen that the log magnitude of the transfer function is at its half-power point, or 3 db down, at a frequency of approximately .82 rad/sec. This frequency was considered to be the highest frequency at which effective gusts could be generated by the model.

### The Pilot Model

The form of the pilot model which was chosen for this air refueling simulation is the linear describing function

$$Y_p = K_p (T_L j\omega + 1) e^{-j\omega\tau_e} \quad (51)$$

where  $K_p$  = pilot gain

$T_L$  = lead time constant, sec

$\tau_e$  = effective time delay, sec

This model has been used with success in previous work with compensatory control systems (Ref 8:4). The parameters  $K_p$ ,  $T_L$  and  $\tau_e$  must be chosen as those which best fit each particular control problem under consideration whether it be the air refueling with downwash or without downwash.

The pilot's time delay,  $\tau_e$ , was chosen as 0.3 seconds for all cases. This value of time delay has been used in many other pilot modeling applications and has been verified in many human operator tracking experiments. It may be possible that for the air refueling task the human pilot could work at a lower value of time delay, but there is currently no data in existence to support that theory.

Since the controlled elements under consideration here are unstable (with downwash) and are more complicated than those investigated in many of the previous human operator tracking experiments, their forms did not suggest appropriate values for  $T_L$ . It has been shown that in an actual flight environment a pilot may generate a value of  $T_L$  as high as eight seconds (Ref 8:4). For this reason, the value of  $T_L$  was varied over a range of from one to eight seconds to determine which values provided the best performance in the air refueling task. There are indications from previous work in the literature that a highly trained pilot would be operating with the optimum  $T_L$ , if one exists.



The pilot gains,  $K_p$ , were calculated individually for each value of  $T_L$ . Stability considerations were the primary bases for determining values of  $K_p$ , as shown in the following section.

It has been found that the human pilot adapts the form of his equalizing characteristics to achieve stable control, good low frequency closed loop system response to the forcing function, and maintenance of high frequency system stability (Ref 9:18-19). These considerations were important in choosing the parameters of the pilot models used in this study.

#### Analysis of the Pilot-Aircraft System

In this section the open-loop transfer functions  $Y_p Y_c$  are analyzed in the frequency domain in order to determine the stability characteristics of the corresponding closed-loop systems. The objective of this analysis is to find values of pilot gain,  $K_p$ , which are most suitable with respect to stability and system following characteristics as  $T_L$  is varied. The Nyquist stability criterion is the basis for these stability analyses (Ref 10:272-287).

The pilot-aircraft open-loop transfer functions for the case without downwash are analyzed first. These transfer functions are shown below for the elevator and the throttle control loops.

$$Y_{P_E} Y_{C_E})_{No\ DW} = K_{P_E} (T_L j\omega + 1) e^{-j\omega \cdot 3} \left[ Y_{C_E} \right)_{No\ DW} \right] \quad (52)$$

$$Y_{P_T} Y_{C_T})_{No\ DW} = K_{P_T} (T_L j\omega + 1) e^{-j\omega \cdot 3} \left[ Y_{C_T} \right)_{No\ DW} \right] \quad (53)$$

$Y_{C_E})_{No\ DW}$  and  $Y_{C_T})_{No\ DW}$  are given by Table IV. Bode plots and polar plots of these open-loop transfer functions are provided in Appendix E

for values of  $T_L$  from 1 to 8. Applying the Nyquist criterion to the polar plots showed that the corresponding closed-loop pilot-aircraft systems are stable for values of pilot gain between zero and certain maximum limits, above which the systems are unstable. These maximum limits are given in Table V.

Values of  $K_{p_E}$  and  $K_{p_T}$  were calculated by applying the "Primary Rule of Thumb" of frequency response synthesis, stated below:

"Find or create a fair stretch of -20db/decade slope for the amplitude ratio, and then make it the crossover region by putting the 0 db line through it" (Ref 9:27).

Additional considerations when using this method, in order of decreasing importance, are

1. The system must have a positive phase margin.
2. For a "good" feedback control system the pilot's describing function,  $Y_p$ , must be adjusted so that the crossover frequency,  $\omega_c$ , exceeds the highest important frequency of the forcing function (Ref 9:27). The forcing function in this problem is the vertical gust,  $w_g$ . It has already been shown that the -3 db frequency of the gust model is .82 rad/sec. If this frequency is taken to be the highest important frequency of the input then the crossover frequencies of the open-loop transfer functions should always exceed .82 rad/sec.

After using the Primary Rule of Thumb to define the crossover region, the values of  $K_{p_E}$  were calculated for a crossover frequency of .82 rad/sec. These are given in Table V. The systems are shown to be unstable for  $T_L$ 's of 1.5 and 1 sec. Those two cases would require

Table V

## Summary of Pilot-Aircraft System Analysis

$T_L$	$Y_{PE}$	$Y_{CE}$	No DW	$Y_{PT}$	$Y_{CT}$	No DW
	$K_{PE}$	$\omega_c$	$\phi_m$	$K_{PT}$	$\omega_c$	$\phi_m$
8	.001698 (0-.002927)	.82 r/s	23 deg	753 (0-6469)	.45 r/s	61 deg
7	.001905 (0-.003302)	.82	22	933 (0-7338)	.49	59
6	.002238 (0-.003706)	.82	20	1124 (0-8477)	.51	56
5	.002660 (0-.004222)	.82	18	1520 (0-10034)	.58	53
4	.003283 (0-.004953)	.82	15	2031 (0-12291)	.62	49
3	.004240 (0-.005723)	.82	9	2991 (0-15859)	.70	43
2	.005752 (0-.005934)	.82	1	5029 (0-22347)	.83	33
1.5	.007076 (0-.004250)	.82	-7	6848 (0-26720)	.90	26
1	.008756 (0-.000303)	.82	-20	9111 (0-30921)	.93	14

Note: Values in parentheses are the minimum and maximum values of stable  $K_p$ .

(Table V continued on next page)



Table V  
(contd)

$T_L$	$Y_{PE} \quad Y_{CE} \quad )_{DW}$			$Y_{PT} \quad Y_{CT} \quad )_{DW}$		
	$K_{PE}$	$\omega_c$	$\phi_m$	$K_{PT}$	$\omega_c$	$\phi_m$
8	.003531 (.003406-.003667)	1.24 r/s	2 deg	794 (1.9 - $\infty$ )	.47 r/s	61 deg
7	.003731 (.003406-.004125)	1.19	6	939 (2.2 - $\infty$ )	.49	59
6	.003953 (.003404-.004714)	1.12	10	1183 (2.7 - $\infty$ )	.53	56
5	.004195 (.003403-.005466)	1.03	16	1526 (3.4 - $\infty$ )	.58	53
4	.004467 (.003402-.006503)	.90	23	2037 (4.4 - $\infty$ )	.62	49
3	.004695 (.003402-.007816)	.70	30	2996 (5.9 - $\infty$ )	.70	43
2	.004924 (.003402-.008910)	.47	26	5033 (9.8 - $\infty$ )	.83	33
1.5	.004925 (.003403-.008910)	.39	18	6848 (14.9 - $\infty$ )	.90	26
1	.004929 (.003407-.008910)	.34	10	9115 (30.4 - $\infty$ )	.93	14

Note: Values in parentheses are the minimum and maximum values of stable  $K_p$ .

$\omega_c$  to be decreased to a value less than .82 rad/sec in order to achieve stability. The values of  $K_{pT}$  were calculated at the  $\omega_c$ 's which provided the greatest phase margins in the crossover regions. These values also are presented in Table V.

The pilot-aircraft open-loop transfer functions including the tanker downwash are

$$Y_{pE} Y_{cE})_{DW} = K_{pE}(T_L j\omega + 1)e^{-j\omega \cdot 3} \begin{bmatrix} Y_{cE} \\ )_{DW} \end{bmatrix} \quad (54)$$

$$Y_{pT} Y_{cT})_{DW} = K_{pT}(T_L j\omega + 1)e^{-j\omega \cdot 3} \begin{bmatrix} Y_{cT} \\ )_{DW} \end{bmatrix} \quad (55)$$

where  $Y_{cE})_{DW}$  and  $Y_{cT})_{DW}$  can be derived from Table IV. Bode and polar plots of these transfer functions are presented in Figures F-1 through F-18.

Nyquist analysis of the polar plots of  $Y_{pE} Y_{cE})_{DW}$  showed that the systems with downwash are conditionally stable. There exists a region of stability within each polar plot corresponding to a particular range of  $K_{pE}$ . Values of  $K_{pE}$  for which the  $-1+j0$  point lies outside this specific region cause the pilot-aircraft system to be unstable. These regions of stability are marked with cross-hatching on the polar plots. It can be seen that the stable region is quite small for  $T_L = 8$  and increases in size as the value of  $T_L$  decreases. The values of  $K_{pE}$  which placed the  $-1+j0$  points at the graphical centers of the stable regions were calculated. These values, given in Table V, were used in the analog simulations. Table V also lists the range of stable  $K_{pE}$  for each value of  $T_L$ .

Applying the Nyquist stability criterion to the polar plots of  $Y_{pT} Y_{cT})_{DW}$  in Appendix F showed that these transfer functions do not exhibit the conditionally stable characteristic. They are unstable

only if the pilot gain falls below some minimum value. Lacking stability considerations other than to keep  $K_{pT}$  above this minimum value, the Primary Rule of Thumb was employed to calculate the values of  $K_{pT}$ . As in the case of  $Y_{pT} Y_{cT}$  ) No DW, the values chosen for  $K_{pT}$  were those which gave the maximum phase margins in the crossover regions. Table V presents these gains in addition to the minimum values of  $K_{pT}$  which are stable.

The pilot gains calculated in this section apply only to the model of the non-irradiated pilot. The following section introduces factors which can be applied to these gains to simulate performance decrements due to irradiation.

#### Effects of Irradiation on the Human Pilot

It has been shown that a pilot who has suffered a lethal dose of radiation is likely to suffer a decrement in performance which varies as a function of time after the dose is received. Data which support this conclusion were obtained in laboratory experiments with trained monkeys performing flight-simulating tasks. The clinical response to radiation exhibited by monkeys is essentially the same as that of humans.

Generally the data showed that the monkeys suffered substantial degradations in performance shortly after irradiation, followed by periods of partial recovery lasting for several hours (Ref 11:946).

It is assumed here that a decrement in pilot performance due to a nuclear encounter can be simulated by reductions in the gains  $K_{pE}$  and  $K_{pT}$ . It is further assumed that such a nuclear encounter occurs at the time of takeoff. Figure 5 illustrates the variation of



pilot gain factor as a function of time after exposure for four levels of radiation dose (Ref 12). The pilot gains of Table V are multiplied by the appropriate gain factor from this figure to simulate pilot irradiation. Table VI lists the pilot gain factors which are applicable to the beginning of the refueling simulation occurring at five and one-half hours after radiation exposure.

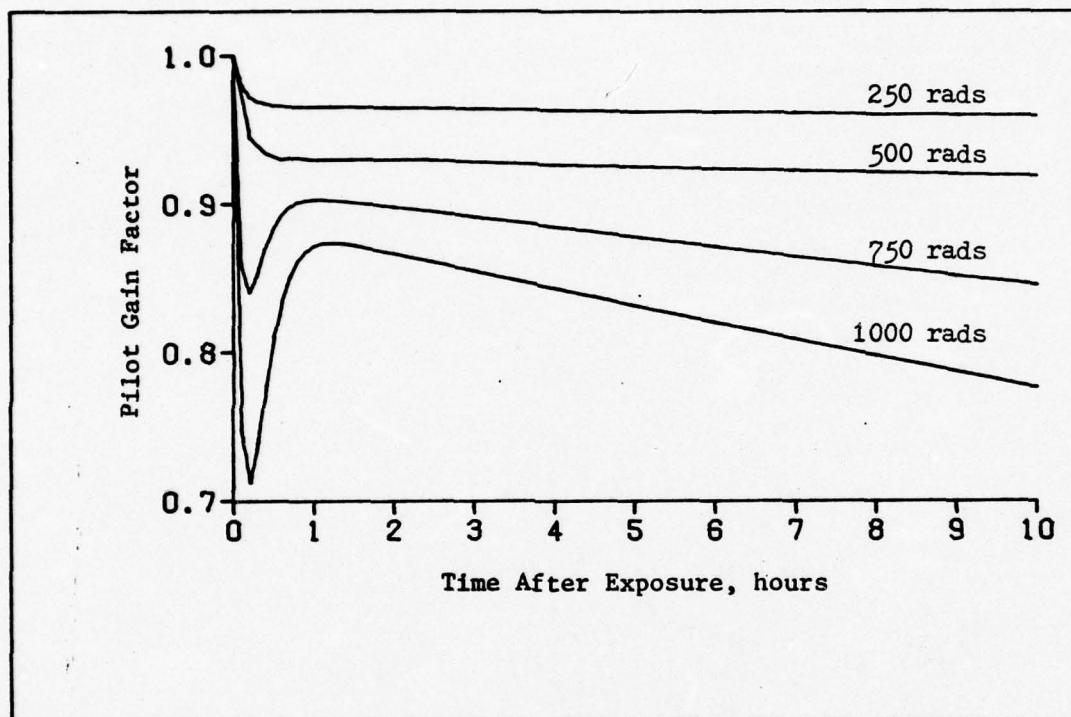


Figure 5. Pilot Gain Factor versus Time (Ref 12).

Table VI

Pilot Gain Decrements Due to Irradiation

Radiation Dose (rads)	Pilot Gain Factor ( $t = 5\frac{1}{2}$ hours)
250	0.96
500	0.93
750	0.87
1000	0.83

(Ref 12)

#### IV. Analog Simulation

##### Apparatus

The analog simulation was patched on an Electronics Associates, Inc. (EAI) Model 680 analog computer. This computer was interfaced with a Digital Equipment Corporation (DEC) PDP-12 digital computer by means of an analog-to-digital converter. The PDP-12 was equipped with an RK05 disk drive and an LP08 high speed line printer. Strip chart data was collected by means of an EAI 8875 recorder.

A Hewlett-Packard HOI-3722A Noise Generator supplied the random Gaussian noise to the gust filter.

##### General

Except where otherwise noted all experimental work presented in this chapter involved the simulated B-52 as affected by the downwash field of the KC-135 tanker.

The pilot-aircraft control system was patched on the EAI 680 analog computer according to the diagram shown in Figure G-1. Also shown on this patching diagram is the error detection and logic circuitry. Potentiometer settings are listed in Table X. The pure time delay term in the pilot model was represented by the second order Pade' approximation,

$$e^{-Ts} = \frac{1 - .5Ts + .083T^2s^2}{1 + .5Ts + .083T^2s^2} \quad (56)$$

As shown earlier in this report the frequency domain analyses were performed on the pilot-aircraft open-loop transfer functions over a range of  $T_L$ 's from 1 to 8. For the analog simulation a narrowing of this range by elimination of undesirable  $T_L$ 's seemed feasible.

The critical and demanding task of accomplishing a hookup procedure was chosen as the basis on which to evaluate the performance of the pilot model at the various values of  $T_L$ .

#### Observation of Hookup Procedure

The characteristics of the pilot-aircraft system accomplishing a hookup procedure in smooth air ( $w_g = 0$ ) were evaluated by considering the following factors:

1. Maximum closure rate experienced during hookup
2. Hookup flight path
3. Amount of negative thrust required to drive the closure rate to zero at the center of the refueling envelope
4. Time required to accomplish the hookup

To preclude the danger of overrunning the tanker during an attempted hookup maneuver, the B-52 must be limited to a very slow closure rate. This restriction was accounted for in the analog simulation by limiting the forward (positive) thrust authority of the pilot model to 500 lbs. With this limit imposed on the system the no-gust closure rates always remained less than 2 ft/sec for all values of  $T_L$ .

A "good" hookup flight path was defined as one in which the B-52 gained most of its required altitude, with minimum overshoot, before entering the refueling envelope. It was assumed that such an approach would offer the B-52 pilot better visual references on the tanker than would be possible in a "low" approach.

Negative thrust authority was limited to 10,000 lbs during the hookup runs. In other words, the pilot model was able to reduce



thrust as much as 10,000 lbs below the equilibrium thrust setting in order to stop the closure rate. As would be expected, as  $T_L$  decreased the model required increased amounts of negative thrust to stop the closure rate due to its lesser ability to "anticipate" arrival at the contact position. Negative thrust requirements more than 5000 lb were considered excessive.

The time required for hookup was that time required to enter and remain for 15 seconds within the small hookup envelope depicted by dashed lines in Figure 1.

Figure 6 presents the hookup flight path for each  $T_L$ . These are the trajectories of the B-52 boom receptacle as plotted from the analog computer. Table VII gives a comparison of the maximum closure rates, negative thrust requirements, and time to hookup. Based on the above stated criteria,  $T_L$ 's equal to 3, 4, 5, and 6 seemed to offer the best compromises between the factors. These four values of  $T_L$  were selected for further experimentation.

#### The Simulation Variables

Table VIII lists the four variables and the ranges over which they were varied in the simulations.

The rms gust intensity,  $\sigma_w$ , was varied from 0 to 6 ft/sec as shown. The actual random gust velocities,  $w_g$ , produced by the gust filter achieved peaks of roughly three times the rms values. Thus, for  $\sigma_w = 6$  ft/sec, the actual gusts affecting the B-52 included peak velocities in the neighborhood of 18 ft/sec.

It became evident in the initial analog runs that the time required to accomplish the simulated air refueling was strongly

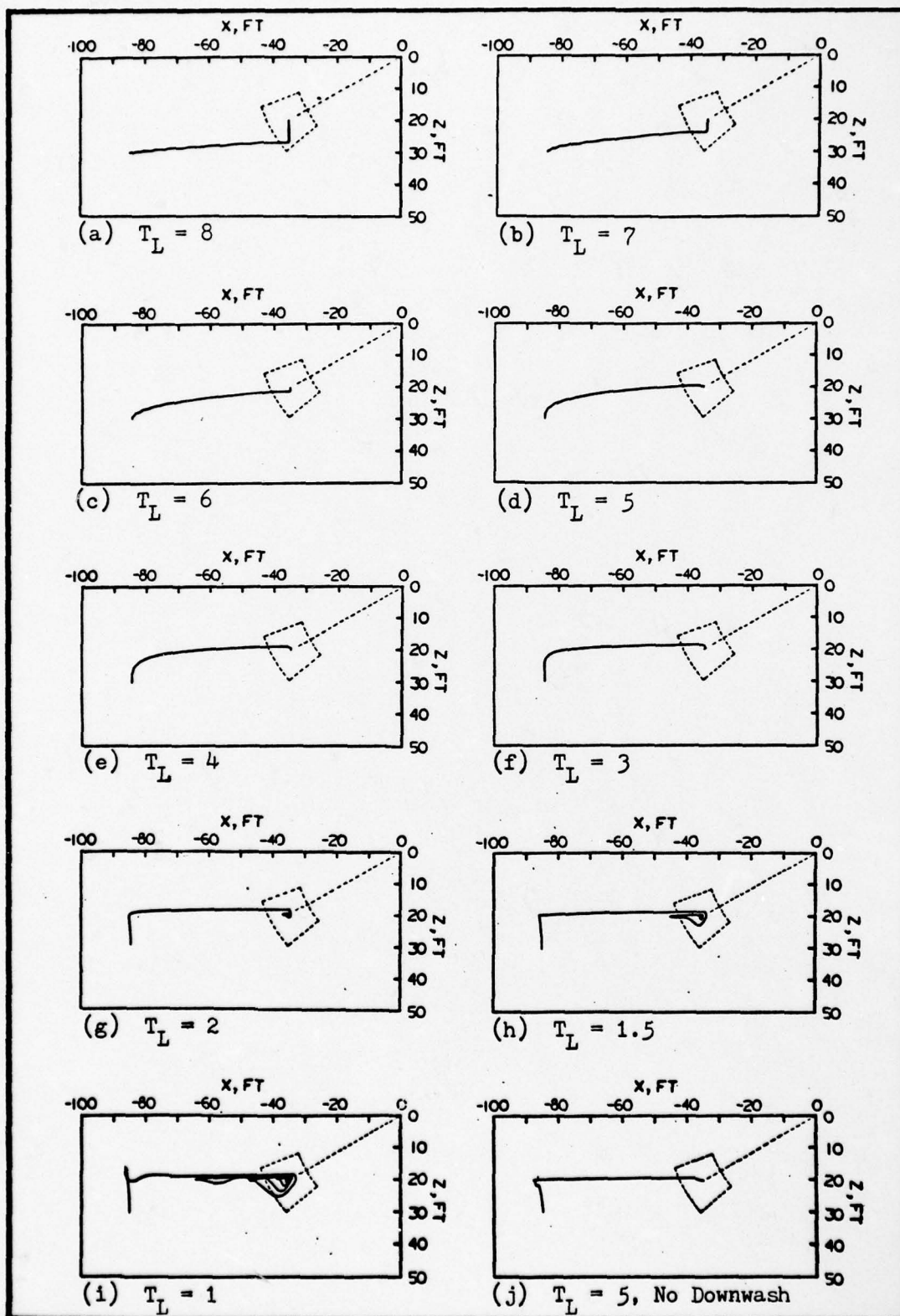


Figure 6. No-Gust Hookup Flight Paths.

Table VII

## Summary of Results of No-Gust Hookup Runs

<u>T<sub>L</sub></u>	<u>K<sub>P</sub>E</u>	<u>K<sub>P</sub>T</u>	<u>Time Required to Hookup(sec)</u>	<u>Negative Thrust Used (lbs)</u>	<u>Maximum Forward Closure Rate (ft/sec) before Negative Thrust Applied</u>
8	.003531	794	385	2700	1.8
7	.003731	939	72	2800	1.7
6	.003953	1183	63	3000	1.6
5	.004195	1526	63	3600	1.5
4	.004467	2037	66	4500	1.6
3	.004695	2996	70	6100	1.6
2	.004924	5033	74	9200	1.6
1.5	.004925	6848	125	>10000	1.7
1	.004929	9115	257	>10000	1.8



Table VIII

Simulation Variables and Their Values

<u>Variable</u>	<u>Units</u>	<u>Values Used in Analog Simulations</u>
$T_L$	sec	3, 4, 5, 6
$\sigma_w$	ft/sec (rms)	0, 1, 2, 3, 4, 5, 6
Radiation Dose	rads	0, 500, 1000 (simulated via pilot gain decrements)
Thrust	lbs	Thrust Authority A*, Thrust Authority B**

- \*Thrust Authority A:
1. Hookup: -5000 to 500 (2500)
  2. Boom Track: -5000 to 2500
  3. Inadvertant Disconnect: -5000 to 2500

- \*\*Thrust Authority B:
1. Hookup: -10000 to 500 (5000)
  2. Boom Track: -10000 to 5000
  3. Inadvertant Disconnect: -10000 to 5000

Values in parentheses are the limits of the graduated forward thrust for hookup as explained in the text.

influenced by the amount of throttle authority allowed the pilot model. The thrust is, of course, limited by the capabilities of the engines to a range of approximately -20000 lbs to +13000 lbs. The negative limit is based on the fact that not all of the 22000 lbs of equilibrium thrust can be eliminated by pulling back on the throttles; a small amount (approximately 2000 lbs) remains after all eight throttles are pulled back to the idle position. The positive limit reflects the additional thrust which is available as all eight engine throttles are advanced from the equilibrium setting (1.48 EPR) to MRT (2.0 EPR) (Ref 4:104, 116).

The decision was made to use more restrictive thrust limits in the analog simulations. This decision was based on the following thoughts:

1. The B-52 may be flying the mission with one or more engines inoperative.
2. The pilot may not be working all eight throttles during the refueling operation.
3. Adverse engine behavior such as compressor stalling often results from varying the engine throttles rapidly over their full ranges.

Two different ranges of thrust authority were treated in the analog simulations. The boom track and inadvertant disconnect procedures were simulated using thrust ranges of -5000 to 2500 lbs (Thrust Authority A) and -10000 to 5000 lbs (Thrust Authority B). It will be noted that the negative thrust limits were two times as large as the positive limits. Aside from the fact that there simply is more

thrust available on the negative side of equilibrium than on the positive side, these limits were established mainly to fulfill the desire to make the simulation more realistic by imposing a passive type of safety factor. Since forward movement of the B-52 is the more dangerous, due to the collision hazard, it was assumed that the pilot would need more thrust authority in the negative direction in order to more quickly stop forward closure rates.

While the thrust limitations were easily applied to the boom track and inadvertant disconnect procedures, the simulation of the hookup procedure presented some unique problems. As stated earlier, the forward (positive) thrust for hookup was limited to 500 lbs in order to keep the no-gust closure rate at a value less than 2 ft/sec. At the same time, the negative thrust limits imposed on the hookup simulations were much greater— -5000 or -10000 lbs, depending on the thrust range under investigation. This large imbalance of available forces caused no problems as long as the hookup simulations were run under no-gust conditions. As a matter of fact, the hookup simulations seemed quite realistic--the pilot model put in the full 500 lbs of forward thrust at the precontact position; the B-52 accelerated slowly, attaining a forward velocity in the neighborhood of 1.5 to 1.8 ft/sec as it neared the refueling envelope, at which time the pilot model put in a large amount of negative thrust to drive the closure rate to zero as the aircraft arrived at the contact position.

When wind gusts were introduced into the B-52 equations of motion the small forward thrust limit of 500 lbs was insufficient to allow the pilot model to adequately correct for backward movements caused by the gust-induced perturbations. As a result, the simulated B-52 often



was caused to move backwards to the limits of the analog scaling of the  $\hat{x}$ -axis, which was 200 ft. The time required to effect a hookup in these instances was usually quite long. The assumption was made that the pilot would not maintain the low positive thrust setting (500 lbs) while his aircraft drifted backwards. In an attempt to make the hookup simulation more realistic in the wind gust environment, a type of graduated forward throttle was developed.

By means of analog patching, the forward throttle limit was allowed to increase above 500 lbs if a negative velocity along the  $\hat{x}$ -axis was experienced. The limit increased in proportion to negative  $u$  up to the maximums allowed for the boom track and inadvertant disconnect procedures (i.e., 2500 or 5000 lbs). The thrust limit imposed by this graduated throttle is given by the schedule

$$\begin{aligned} \text{Forward thrust (lbs)} &= 500 & u \geq 0 \\ &= 500(1-u) & u < 0 \end{aligned} \quad (57)$$

#### Monte Carlo Simulation of the Air Refueling Task

Each part of the refueling mission--hookup, boom track, and inadvertant disconnect--was simulated using the ranges of variables given in Table VIII. Because the B-52 equations of motion were subjected to gust disturbances of a random nature, a series of 500 refuelings were simulated for each combination of variables, and statistics were compiled on the duration of each of the three components of the air refueling. Each of these simulations was timed for 2000 seconds unless sooner terminated by the error detection and logic circuitry on the analog computer.

For the boom track procedure this early termination occurred at the time of first boom disconnect (i.e., when the B-52 boom receptacle first went outside the limits of the refueling envelope).

For the hookup and inadvertant disconnect procedures the runs were terminated in less than 2000 seconds only when the B-52 boom receptacle had remained for fifteen seconds within the hookup and pre-contact envelope, respectively.

All of the simulations were run on the analog computer at a rate of 1000 times real time. Thus only 2 seconds of real time were required to simulate 2000 seconds of flight. For this purpose the frequency bandwidth of the random noise input to the gust filter also was increased by a factor of 1000, to 1.5 KHz.

At the termination of each run the duration in seconds for that run was collected and stored by the PDP-12 digital computer. After the time statistics were collected for each series of 500 runs, the mean time for that series was calculated.

Using the mean times for hookup, boom track, and inadvertant disconnect the mean total refueling time was calculated as shown below.

$$RT = \text{Integer} \left( \frac{1200}{BT} \right) \times (HU + ID) + HU + 1200 \quad (58)$$

where RT = mean refueling time

BT = mean time-on-boom (boom track time)

HU = mean hookup time

ID = mean inadvertant disconnect time

1200 = total time-on-boom required to accomplish the refueling

$\text{Integer} \left( \frac{1200}{BT} \right)$  = integer value of  $\frac{1200}{BT}$ , which represents the number of inadvertant disconnects which occur during the refueling.

The initial hookup time is accounted for in the total time, but the final disconnect is not included because the B-52 need not return to the pre-contact position and stabilize after the refueling is completed.

To offer a comparison of the results of these simulations with the results had the downwash from the KC-135 been neglected, a group of runs at  $T_L = 5$  were made with the downwash effects excluded.



## V. Results and Discussion

### Overview

The data collected in the Monte Carlo simulations of the air refueling task are presented in this chapter. The data are in the form of plots of the trends of mean refueling time as functions of rms gust intensity,  $\sigma_w$ . The other three simulation variables--thrust authority,  $T_L$ , and radiation dose--are presented as parameters on these plots. The following four sections will discuss the variation of mean refueling time with each of the simulation variables. Finally, a brief discussion will be presented on the results of the simulation runs with no tanker downwash. Appendix H includes supplementary plots of the components of mean refueling time--hookup time, time-on-boom, and inadvertant disconnect time--as functions of gust intensity.

### Variation of Mean Refueling Time with Gust Intensity

Figure 7 shows a plot of the trend of mean refueling time versus gust intensity for the non-irradiated pilot. Inspection of the curves for Thrust Authority A (narrow range of thrust authority) reveals that the mean refueling time increases slowly for gusts of 3 ft/sec rms or less. Above 3 ft/sec rms the refueling time increases sharply, much like an exponential function of gust intensity. Similar variations are exhibited by the plots for 500 and 1000 rads, Figures 8 and 9, respectively. The mean refueling times at Thrust Authority B (wide range of thrust authority) indicate a sharp rise only when  $\sigma_w$  exceeds 5 ft/sec rms.

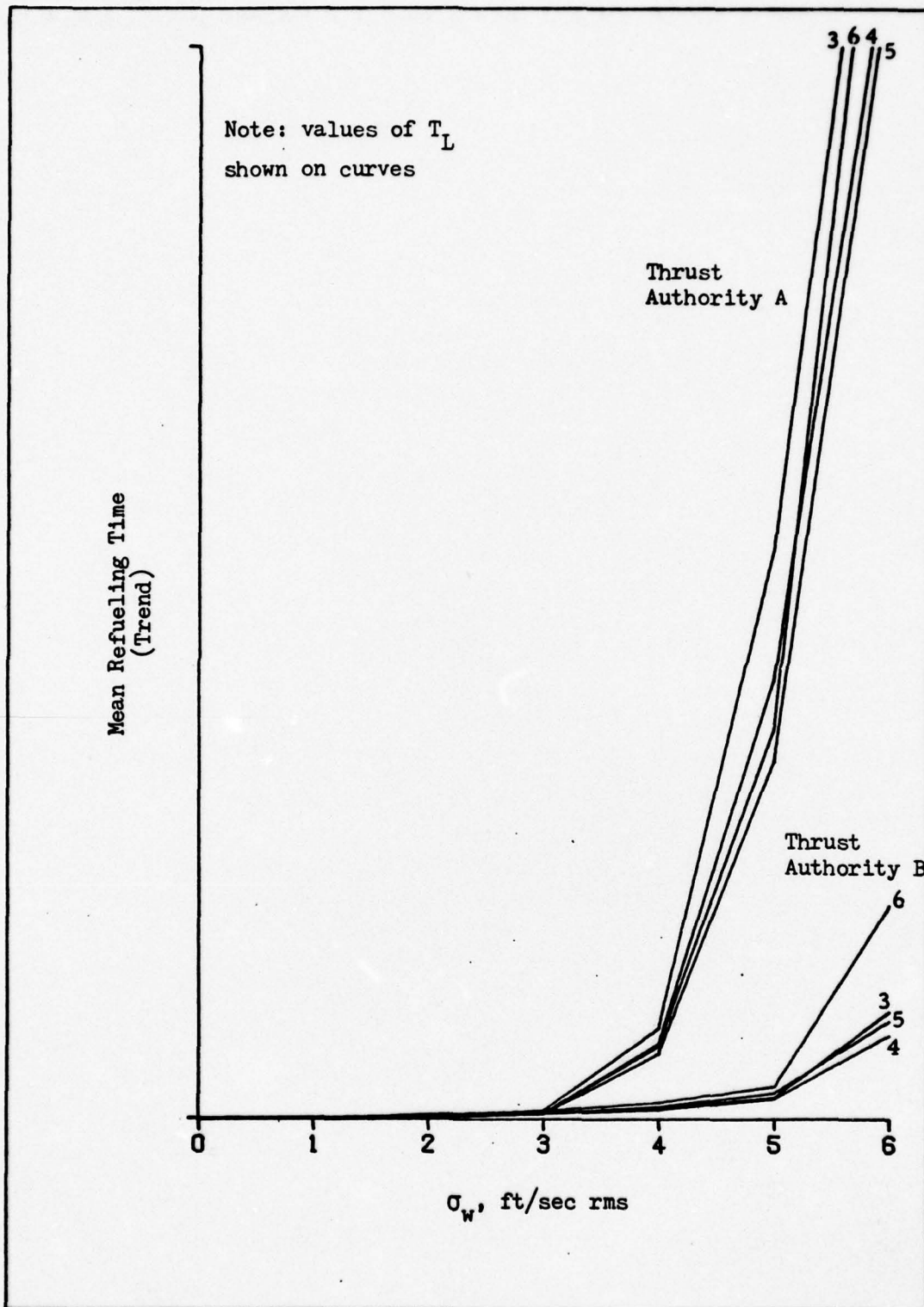


Figure 7. Mean Refueling Time vs. Gust Intensity for 0 Rads.

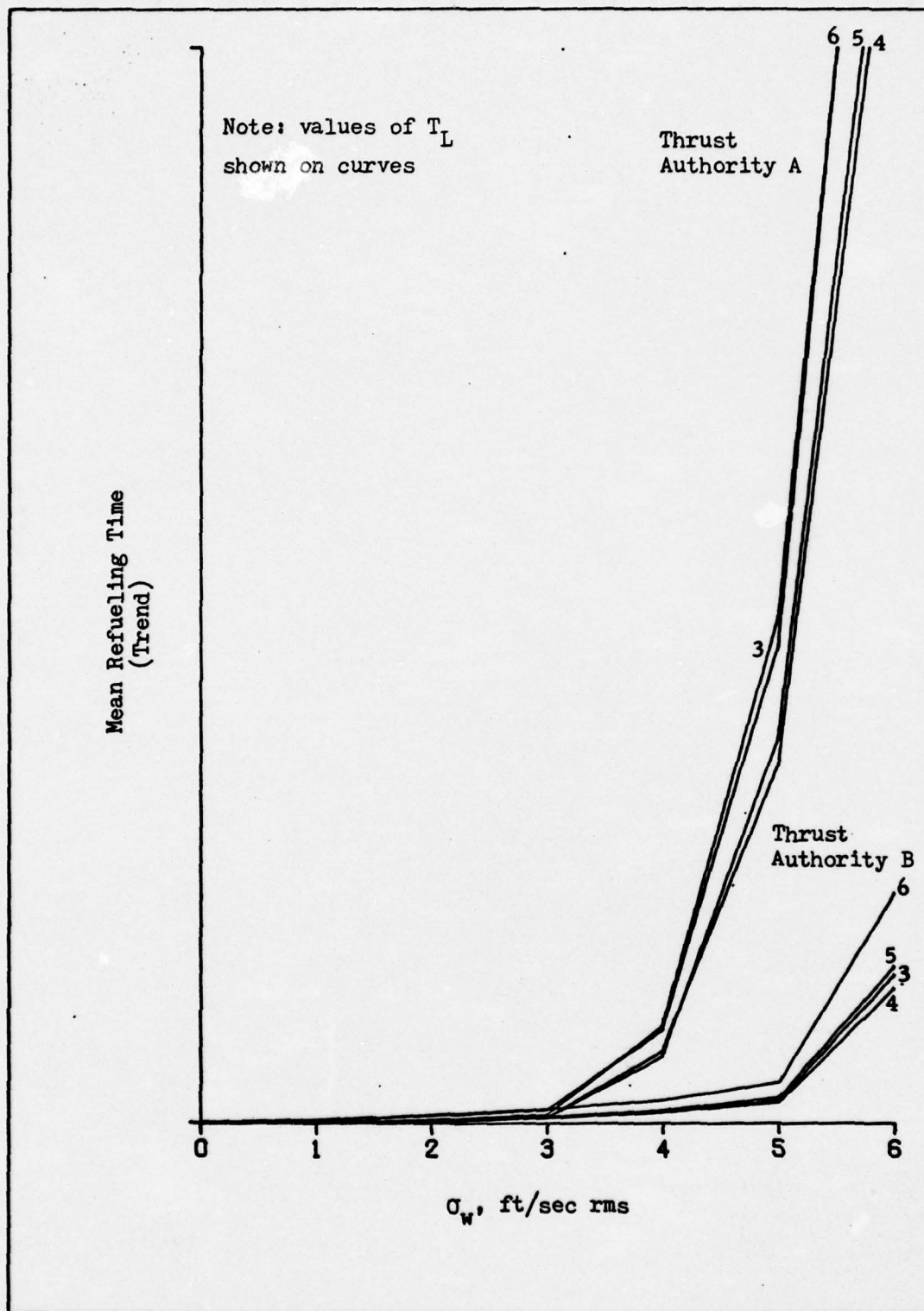


Figure 8. Mean Refueling Time vs. Gust Intensity for 500 Rads.



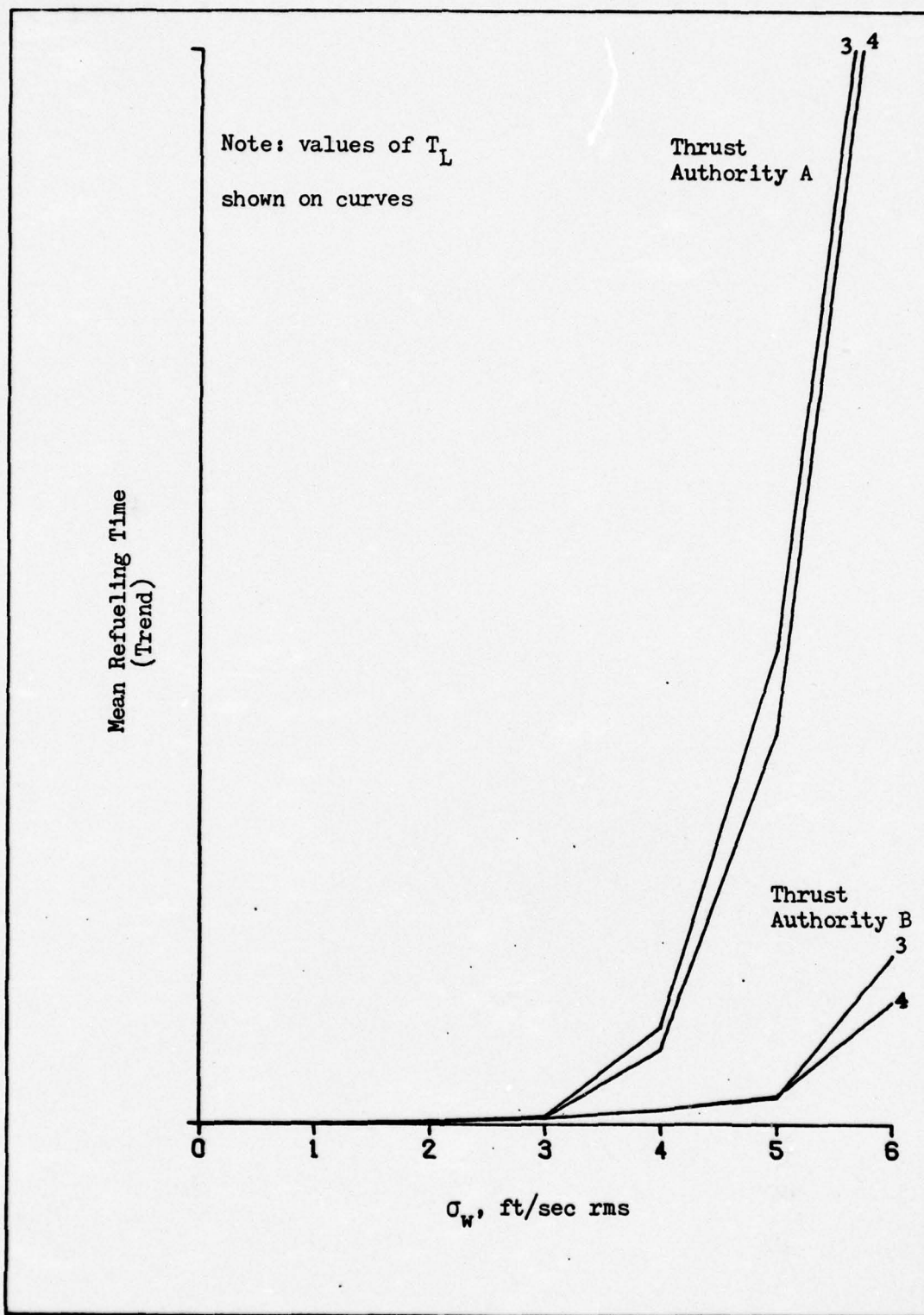


Figure 9. Mean Refueling Time vs. Gust Intensity for 1000 Rads.

#### Variation of Mean Refueling Time with Thrust Authority

Figures 7, 8, and 9 show that the thrust authority given the pilot model has a pronounced effect on the mean refueling time. As thrust authority is increased from level A to level B, as defined in Table VIII, the pilot model is able to perform the refueling in less time at the higher gust intensities.

#### Variation of Mean Refueling Time with $T_L$

Values of  $T_L$  are shown on each of the curves on Figures 7, 8, and 9. Figure 7 shows that the optimum  $T_L$  is 5 seconds for the non-irradiated pilot model operating under the restrictions of Thrust Authority A. For Thrust Authority B the optimum  $T_L$  appears to be 4 seconds. Figure 8 shows that  $T_L \approx 4$  sec is the optimum pilot lead for the case of a 500 rad radiation dose. This observation holds for both levels of thrust authority. Figure 9 indicates that the optimum  $T_L$  for 1000 rads also is 4 sec; however, in the case of Thrust Authority A, the gap between 4 sec and 3 sec appears to be closing somewhat. If that trend continues, 3 sec may well be the optimum value of pilot lead at radiation doses greater than 1000 rads.

#### Variation of Mean Refueling Time with Radiation Dose

Perhaps the most interesting effect on this model of the air refueling task is that of pilot irradiation as simulated by gain decrements. Examination of Figures 7, 8, and 9 shows that there is relatively little difference in mean refueling time as the simulated radiation dose is increased. Two other trends assume greater importance here. One of these trends--the shifting of the optimum  $T_L$

to a lower value as radiation dose increases--was discussed in the previous section. The other trend is clearly shown only by the plot for 1000 rads, Figure 9. The curves for  $T_L$ 's equal to 5 and 6 sec were not run because with  $T_L$  equal to 6 sec the pilot-aircraft system was unstable in the elevator control loop, and the refueling time data collected when  $T_L$  was set equal to 5 sec was erratic to the point of being unuseable. The values of  $K_{pE}$  used in these instances were .003281 and .003482 for  $T_L$  equal to 6 and 5, respectively. These pilot gains were derived by multiplying the non-irradiated pilot gains given in Table V by a gain factor of .83 (Table VI). Table V also shows that the minimum stable  $K_{pE}$  is .003404 for  $T_L = 6$  and .003403 for  $T_L = 5$  sec. Clearly, the value of  $K_{pE}$  used in conjunction with  $T_L = 6$  was in the unstable region while the value of  $K_{pE}$  used with  $T_L = 5$  was above but very close to the minimum stable value. This marginally stable aspect of the pilot-aircraft system having  $T_L$  equal to 5 sec accounts for its erratic behavior in the simulations.

#### Results of No-Downwash Simulations

Figure 10 depicts the trend of mean refueling time with increasing gust intensity for the model of the non-irradiated pilot with  $T_L = 5$  sec. The data for both levels of thrust authority show marked increases in refueling time over the corresponding curves with downwash that are presented in Figure 7. The conclusion may have been drawn from the comparisons of Tables III and IV that the downwash effects caused the refueling task to be more difficult due to decreasing the damping and increasing the frequency of the short period mode. These



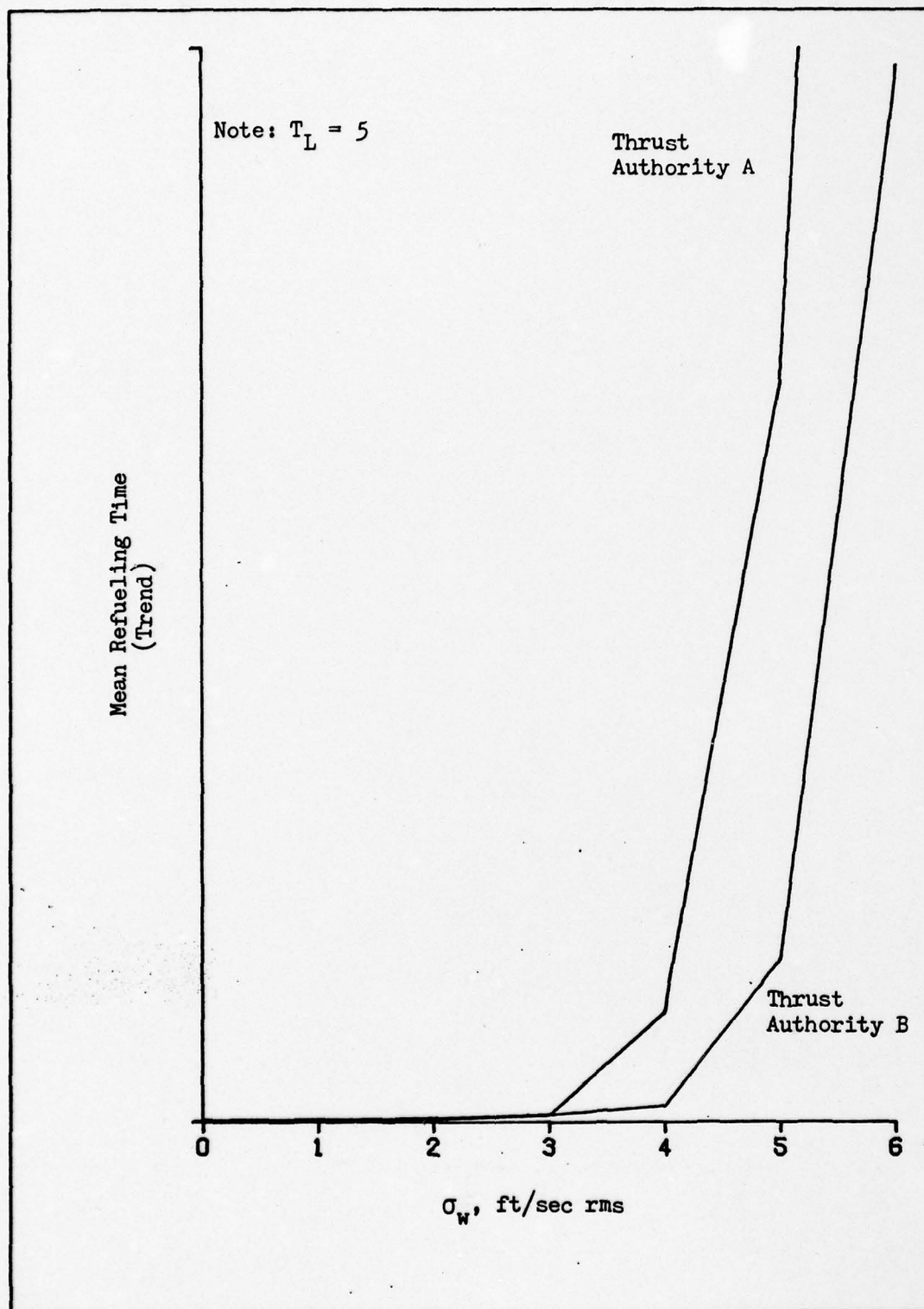


Figure 10. Mean Refueling Time vs. Gust Intensity for 0 Rads,  
No Downwash.

results indicate that the air refueling task is actually made less difficult by the introduction of the downwash. This phenomenon was not investigated further than to observe that the rise time of the system with downwash was shorter than that of the system without downwash. In any case, the no-downwash situation is not encountered in practice.

## VI. Conclusions and Recommendations

The preceding discussion showed that the trends displayed by the mean refueling time as gust intensity increased depended heavily on the limits of the pilot thrust authority imposed on the simulation. It is not clear at this point as to how much thrust authority can realistically be allowed the pilot model in the simulation of the air refueling task. It is recommended that this aspect of the problem be investigated in future work, to include simulator studies involving human subjects and the collection of field data during actual air refueling missions.

Simulation of the air refueling task at two levels of thrust authority provided some insight into the variation of  $T_L$  with difficulty of task. The data seemed to indicate that the optimum value of  $T_L$  tended to be lower for the runs with Thrust Authority B, the large range of thrust authority. Although this trend was subtle, one might assume that the optimum  $T_L$  decreases as the difficulty of the task decreases.

The conclusion that seems to be indicated by the results of the simulated pilot irradiation by means of gain decrements is: the pilot must decrease his  $T_L$  to maintain stability as his radiation dose increases. If the gain decrement causes  $K_{pE}$  to decrease below the minimum stable value, there is no recourse to the pilot except to lower his  $T_L$  to assure system stability.

Much work needs to be done to refine the model of the air refueling task. An important step would be the inclusion of the lateral equations of motion. This step would require the development of



additional pilot models and the simulation of the lateral downwash effects, which may prove to be quite significant.

### Bibliography

1. T.O. 1-1C-1-15, B-52G/H Flight Crew Air Refueling Procedures with KC-135, Change 13. Washington: Department of the Air Force, 15 April 1976.
2. Holloway, R. B. Critical Analysis of B-52 Stability Augmentation and Flight Control Systems for Improved Structural Life, Part V-C, Handling Qualities Evaluation of Proposed Configuration. D3-6453,. Wichita, Kansas: The Boeing Company, 30 August 1965.
3. Arnold, J. I. and G. O. Thompson. Stability Augmentation System Analysis--ECP 1195 Kit. D3-6950-1. Wichita, Kansas: The Boeing Company, 29 April 1970.
4. The Boeing Company. B-52G/H Propulsion Characteristics-Mission Simulators (U). Boeing Document No. D3-9776-3. Wichita, Kansas: The Boeing Company, December 1975.
5. The Boeing Company. B-52G/H Aerodynamic Characteristics-Mission Simulators (U). Boeing Document No. D3-9776-2. Wichita, Kansas: The Boeing Company, 1975.
6. Roskam, J. Flight Dynamics of Rigid and Elastic Airplanes (Parts One and Two). Lawrence, Kansas: Roskam Aviation and Engineering Corporation, 1972.
7. Chalk, C. R., T. P. Neal, T. M. Harris, F. E. Pritchard, and R. J. Woodcock. Background Information and User Guide for Mil-F-8785B(ASG), "Military Specification-Flying Qualities of Piloted Airplanes". Wright-Patterson Air Force Base, Ohio: Air Force Flight Dynamics Laboratory, 1969. AD 860856.
8. Gool, M. F. C. van and H. A. Mooij. "A Comparison of In-Flight and Ground-Based Pitch Attitude Tracking Experiments." NLR MP 76011 U. Paper presented at the Twelfth Annual Conference on Manual Control. National Aerospace Laboratory, May 1976.
9. McRuer, D. T., D. Graham, E. Krendel, and W. Reisener. Human Pilot Dynamics in Compensatory Systems. AFFDL-TR-65-15. Wright-Patterson Air Force Base, Ohio: Air Force Flight Dynamics Laboratory, July 1965. AD 470337.
10. D'Azzo, J. J. and C. H. Houpis. Linear Control System Analysis and Design: Conventional and Modern. New York: McGraw Hill, 1975.
11. Albanese, R. and J. E. Pickering. "Aircrew Vulnerability in Nuclear Encounters." Military Medicine, 139: 945-951 (1974).

Bibliography (Contd)

12. Albanese, R. Personal Communication. Brooks Air Force Base, Texas: United States Air Force School of Aerospace Medicine, 1976.
13. Engelken, E. J. Personal Communication. Brooks Air Force Base, Texas: United States Air Force School of Aerospace Medicine, 1976.



## APPENDIX A

### Linearization of Induced Effects Data by the Method of Least Squares

Table IX presents the induced effects of the KC-135 flow field (downwash) on the lift and moment coefficients of the B-52 in the refueling situation.

Table IX  
Induced Effects Data

<u><math>\hat{z}</math>, inches</u>	<u><math>\Delta C_{L1}</math></u>	<u><math>\Delta C_{m1}</math></u>
-39	-.080	.072
11	-.077	.067
61	-.072	.063
111	-.066	.058
161	-.061	.054
211	-.057	.050
261	-.052	.046
311	-.048	.042

(Ref 5: 2-79,4-95)

#### Method of Least Squares:

To fit the linear equation  $y = a_0 + a_1 x$  to a set of data  $(X_i, Y_i)$ ,  $i = 1, n$  it is necessary to solve for the constants  $a_0$  and  $a_1$  by means of the simultaneous equations:

$$\sum Y_i = a_0 n + a_1 \sum X_i \quad (59)$$

$$\sum X_i Y_i = a_0 \sum X_i + a_1 \sum X_i^2 \quad (60)$$

To find  $\Delta C_{L_1}$  as a function of  $\hat{z}$ :  $X_1 = \hat{z}_1$  (61)

$$Y_1 = (\Delta C_{L_1})_1 \quad (62)$$

$$n = 8 \quad (63)$$

The following simultaneous equations are formulated:

$$8a_0 + 1088a_1 = -0.513 \quad (64)$$

$$1088a_0 + 252968a_1 = -59.793 \quad (65)$$

Solving yields  $a_0 = 0.000095$  (66)

$$a_1 = -0.077045 \quad (67)$$

Therefore, the linear equation for  $\Delta C_{L_1}$  is

$$\Delta C_{L_1} = -0.077045 + 0.000095\hat{z} \quad (\hat{z} \text{ in inches}) \quad (68)$$

or  $\Delta C_{L_1} = -0.077045 + 0.00114\hat{z} \quad (\hat{z} \text{ in feet}) \quad (69)$

Similarly for  $\Delta C_{m_1}$ , the simultaneous equations are

$$8a_0 + 1088a_1 = 0.452 \quad (70)$$

$$1088a_0 + 252968a_1 = 52.522 \quad (71)$$

which yield  $a_0 = 0.0680835$  (72)

$$a_1 = -0.0000852 \quad (73)$$

The linear equation for  $\Delta C_{m_1}$  is

$$\Delta C_{m_1} = 0.0680835 - 0.0000852\hat{z} \quad (\hat{z} \text{ in inches}) \quad (74)$$

or  $\Delta C_{m_1} = 0.0680835 - 0.0010224\hat{z} \quad (\hat{z} \text{ in feet}) \quad (75)$

## APPENDIX B

### Calculation of Steady State Angle of Attack in Downwash

In the case of steady state flight with no downwash, the following equations are applicable:

$$C_{L_1} = C_{L_0} + C_{L_\alpha} \alpha_1 + C_{L_{\delta_E}} \delta_{E_1} + C_{L_{\delta_{stab}}} \delta_{stab_1} \quad (76)$$

$$C_{m_1} = 0 = C_{m_0} + C_{m_\alpha} \alpha_1 + C_{m_{\delta_E}} \delta_{E_1} + C_{m_{\delta_{stab}}} \delta_{stab_1} \quad (77)$$

If the aircraft subsequently is trimmed for steady state flight in a downwash flow field the steady state equations are

$$C_{L_1} = C_{L_0} + C_{L_\alpha} (\alpha_1 + \alpha_{DW}) + C_{L_{\delta_E}} \delta_{E_1} + C_{L_{\delta_{stab}}} (\delta_{stab_1} + \delta_{stab_{DW}}) + \Delta C_{L_1} \quad (78)$$

$$0 = C_{m_0} + C_{m_\alpha} (\alpha_1 + \alpha_{DW}) + C_{m_{\delta_E}} \delta_{E_1} + C_{m_{\delta_{stab}}} (\delta_{stab_1} + \delta_{stab_{DW}}) + \Delta C_{m_1} \quad (79)$$

where  $\delta_{stab_{DW}}$  is the horizontal stabilizer input which produces the additional angle of attack,  $\alpha_{DW}$ , required to trim out the downwash-induced changes in the lift and moment coefficients,  $C_{L_1}$  and  $C_{m_1}$ , respectively.

If the weight of the aircraft does not change, then  $C_{L_1}$  must remain the same before and after entering the downwash field. The moment coefficient,  $C_{m_1}$ , must also remain zero if the aircraft is in equilibrium level flight. Therefore

$$C_{L_\alpha} \alpha_{DW} + C_{L_{\delta_{stab}}} \delta_{stab_{DW}} + \Delta C_{L_1} = 0 \quad (80)$$

$$C_{m_\alpha} \alpha_{DW} + C_{m_{\delta_{stab}}} \delta_{stab_{DW}} + \Delta C_{m_1} = 0 \quad (81)$$



For trimmed flight at the center of the refueling envelope ( $\hat{z} = 0$ ) these equations are

$$(.0891) \alpha_{DW} + (.01079) \delta_{stab_{DW}} - .077 = 0 \quad (82)$$

$$(-.0151) \alpha_{DW} - (.0327) \delta_{stab_{DW}} + .068 = 0 \quad (83)$$

Solving yields

$$\alpha_{DW} = 0.65^\circ \quad (84)$$

$$\delta_{stab_{DW}} = 1.78^\circ \quad (85)$$

The steady state angle of attack required to maintain the B-52 in equilibrium flight at the center of the refueling envelope is

$$\alpha_1 \text{ (in downwash)} = 0.03^\circ + 0.65^\circ = \underline{0.68^\circ} \quad (86)$$

## APPENDIX C

### Details of the Derivation of the Controlled Elements

The required aircraft transfer functions are derived from Eq (44) by means of Cramer's Rule. The gust terms are ignored in these derivations. A and B continue to be used to represent the coefficients of  $\hat{z}$ , the downwash variable. The transfer functions which are needed for the derivation of the controlled elements are

$$\frac{\hat{z}}{\delta_E} = \frac{-8.143 s^3 - 5.3384 s^2 + 166.705s - .071184}{\text{C.E.}} \quad (87)$$

$$\frac{\theta}{\delta_E} = \frac{-.627 s^3 - .239 s^2 + (-.0025167 + .627A - 8.143B)s + (.003A - .036B)}{\text{C.E.}} \quad (88)$$

$$\frac{q}{\delta_E} = s \frac{\theta}{\delta_E} \quad (89)$$

$$\frac{u}{\delta_T} = \frac{.0000715 \{s^4 + 1.417 s^3 + (2.291 - A)s^2 + (-1.005A + 4.6B)s + (-1.9A + 290.6B)\}}{\text{C.E.}} \quad (90)$$

where C.E. is the general characteristic equation as given by Eq (45). Eqs (87) and (88) above, are then used to calculate  $\frac{\hat{z}'}{\delta_E}$  by the method of Eq (12). That calculation yields

$$\frac{\hat{z}'}{\delta_E} = \frac{25.7 s^3 + 7.6 s^2 + (166.8 - 34A + 440B)s + (-.0712 - .15A + 2B)}{\text{C.E.}} \quad (91)$$

By block diagram reduction of the B-52 pitch SAS control loop shown in Figure 2, the transfer function  $\frac{q}{\delta_{PE}}$  was found to be

$$\frac{q}{\delta_{PE}} = \frac{.9315 s(s+.15)(s+.25)(\theta/\delta_E)}{\Delta} \quad (92)$$

$$\text{where } \Delta = s^7 + 2.45s^6 + (3.14625 - A)s^5 + (.988 - 2.0A + 12.8B)s^4 + (.099 - 2.3A + 292.6B)s^3 \\ + (.0037 - .8A + 116.4B)s^2 + (.0003 - .074A + 10.9B)s + (-.00032A - .000057B) \quad (93)$$

Finally, the elevator controlled element is derived by substituting Eqs (89), (91), and (92) into Eq (48), yielding  $Y_{cE} = \frac{\hat{z}}{\delta_{pE}}$

$$= \frac{.93(s+.15)(s+.25)\{25.7s^3 + 7.6s^2 + (166.8 - 34A + 440B)s + (-.0712 - .15A + 2B)\}}{\Delta} \quad (94)$$

The throttle controlled element is derived by substituting Eqs (25) and (90) into Eq (49).

The controlled elements, with and without downwash, are presented below in factored form.

Without Downwash: A = B = 0

$$Y_{cE})_{\text{No DW}} = \frac{23.93(s+.15)(s+.25)(s+.1475+j2.54)(s-.0004)}{s(s+1.03+j1.11)(s+.0017+j.0593)(s+.2216)(s+.1673)} \quad (95)$$

$$Y_{cT})_{\text{No DW}} = \frac{.0000715}{(.25s+1)(s+.0017+j.0593)} \quad (96)$$

With Downwash: A = -.06471, B = -.002269

$$Y_{cE})_{\text{DW}} = \frac{23.93(s+.1474+j2.553)(s-.0004)}{(s+.9066+j1.158)(s+.631)(s-.3891)(s-.00105)} \quad (97)$$

$$Y_{cT})_{\text{DW}} = \frac{.0000715(s+.54945)(s-.40764)}{s(.25s+1)(s+.5484)(s-.402)(s-.00106)} \quad (98)$$

Bode magnitude and phase angle plots of the controlled elements without downwash are given in Figures C-1 and C-2. Bode plots of the controlled elements with downwash are shown in Figures C-3 and C-4.



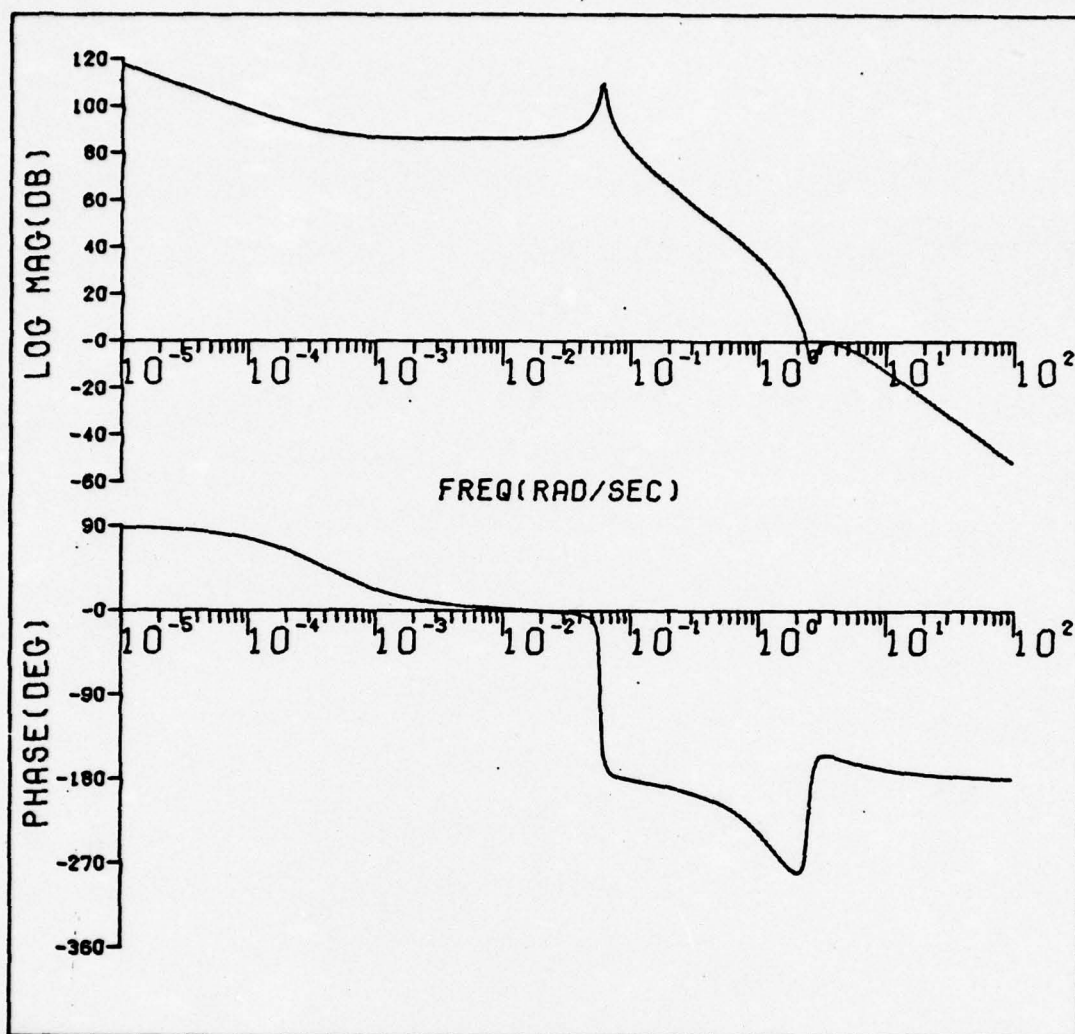


Figure C-1. Bode Plot of  $Y_{c_E}$  No DW.

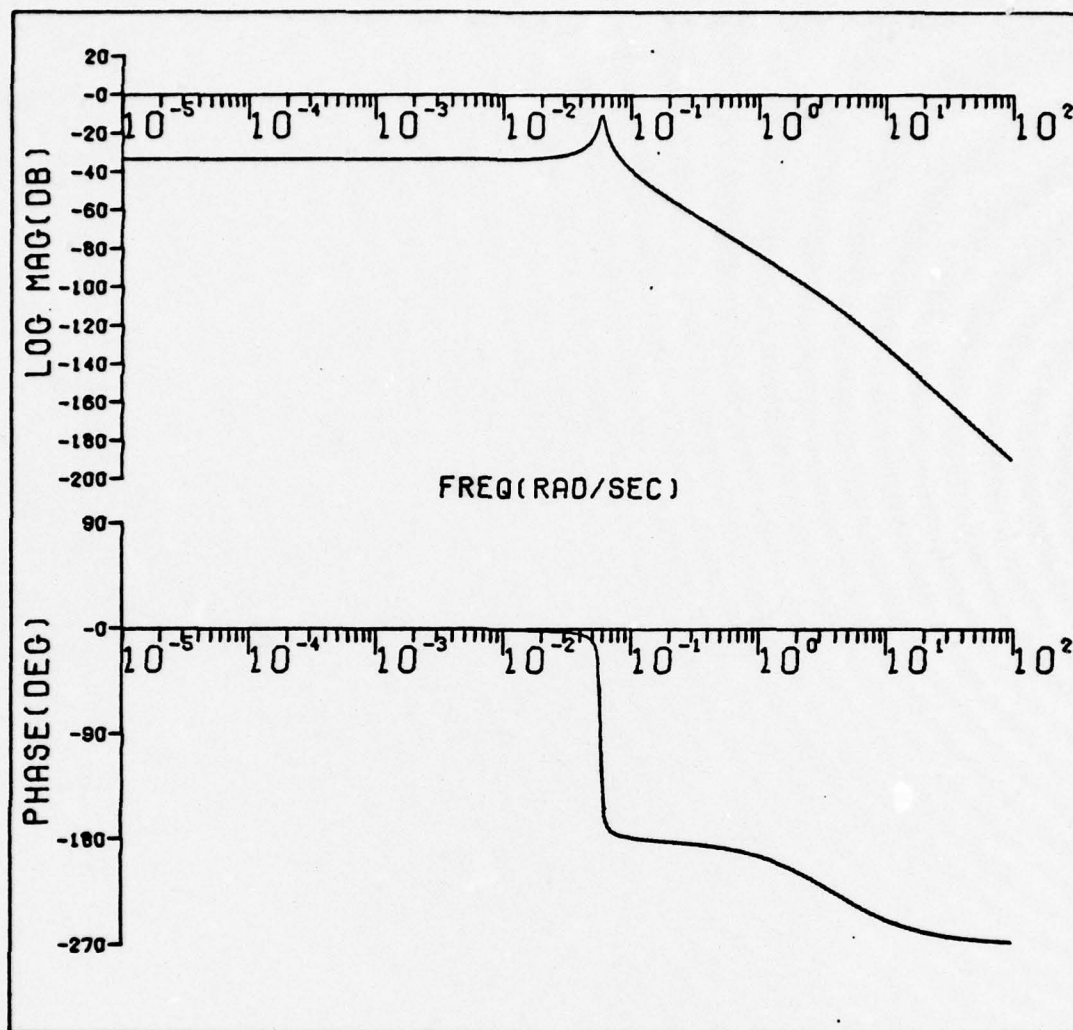


Figure C-2. Bode Plot of  $Y_{c_T})$  No DW.

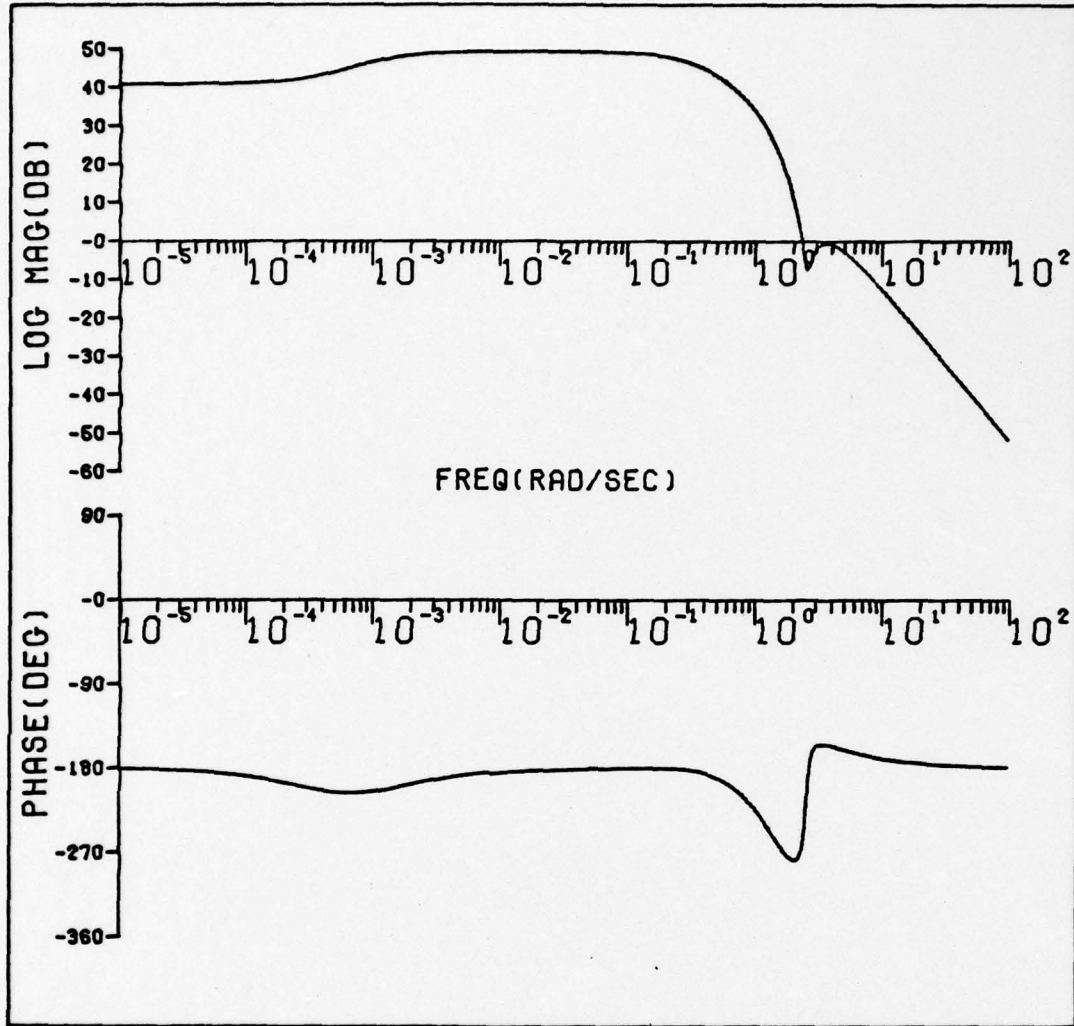


Figure C-3. Bode Plot of  $Y_{c_E})_{DW}$ .



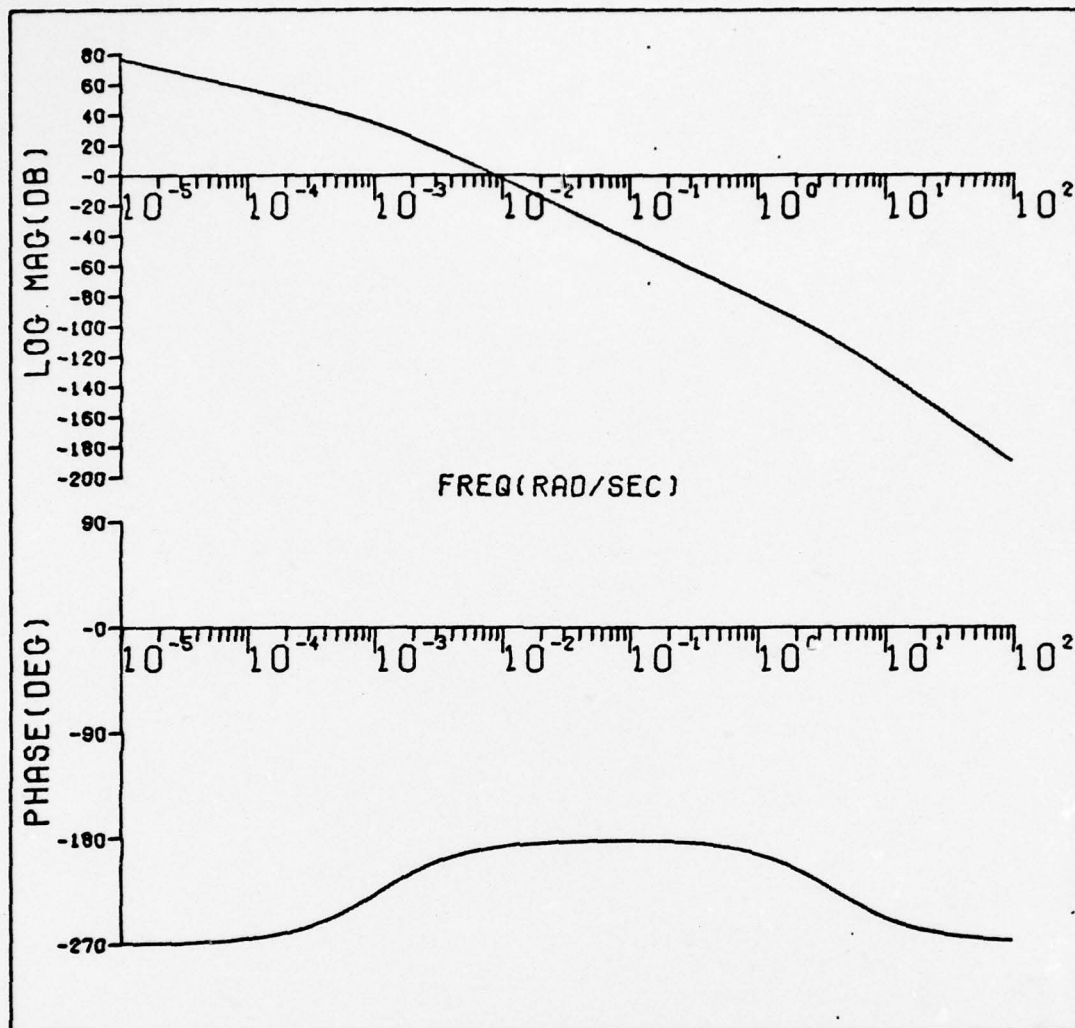


Figure C-4. Bode Plot of  $Y_{c_T})_{DW}$ .

## APPENDIX D

### Gust Model

Assume the Dryden spectral form

$$T_{w_g}(s) = \frac{w_g(s)}{\xi(s)} = \sigma_w \sqrt{\frac{L_w}{\pi U_1}} \frac{1 + \frac{\sqrt{3} L_w}{U_1} s}{(1 + \frac{L_w}{U_1} s)^2} \quad (99)$$

According to the Dryden scales for clear air turbulence,

$$L_w = 1750 \text{ ft}$$

Then,

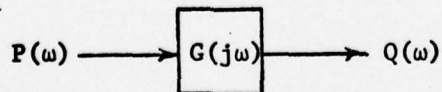
$$\begin{aligned} \frac{w_g(s)}{\xi(s)} &= \sigma_w \sqrt{\frac{1750}{\pi(706)}} \frac{1 + \frac{\sqrt{3} 1750}{706} s}{(1 + \frac{1750}{706} s)^2} \\ &= \sigma_w (.8883) \frac{1 + 4.29 s}{(1 + 2.48 s)^2} \end{aligned} \quad (100)$$

where  $\sigma_w$  is the rms gust intensity.

(Ref 7: 444-459)

### Calculation of Gain Needed to Compensate for Filter Loss

Assume the following system:



If  $P(\omega)$  and  $Q(\omega)$  are power density functions then a filter  $G(j\omega)$  will have the effect:

$$Q(\omega) = |G(j\omega)|^2 P(\omega) \quad (101)$$

Therefore, the total power in  $Q(\omega)$  across all frequencies is:

$$Q = \int_0^{\infty} Q(\omega) d\omega = \int_0^{\infty} |G(j\omega)|^2 P(\omega) d\omega \quad (102)$$

or

$$Q \approx \int_0^{\omega_d} |G(j\omega)|^2 P(\omega) d\omega \quad (103)$$

where  $\omega_d = 20$  db rolloff point of the filter or the 20 db rolloff point of  $P(\omega)$ , whichever is less. In the case of the gust filter,

$$G(j\omega) = \sqrt{\frac{\alpha}{\pi}} \sigma_w \frac{1 + \sqrt{3} \alpha j\omega}{(1 + \alpha j\omega)^2} \quad (104)$$

where  $\alpha = \frac{L_w}{U_1}$

Assume uniform power density to  $1.05 f_0$ , where  $f_0$  is the cutoff frequency of the noise generator.

$$\text{Then} \quad P(\omega) = \frac{P}{2\pi f_0(1.05)} = \frac{P}{2.1\pi f_0} = \frac{P}{\omega_d} \quad (105)$$

Now we have:

$$|G(j\omega)|^2 = \frac{\alpha}{\pi} \sigma_w^2 \frac{1 + 3 \alpha^2 \omega^2}{(1 + \alpha^2 \omega^2)^2} \quad (106)$$

and

$$Q = \frac{\alpha \sigma_w^2}{\pi} \frac{P}{\omega_d} \int_0^{\omega_d} \frac{1 + 3 \alpha^2 \omega^2}{(1 + \alpha^2 \omega^2)^2} d\omega \quad (107)$$

$$Q = \frac{\alpha}{\pi} \frac{P}{\omega_d} \sigma_w^2 (\Omega) \quad (108)$$



where

$$\Omega = \int_0^{\omega_d} \frac{1 + 3\alpha^2 \omega^2}{(1 + \alpha^2 \omega^2)^2} d\omega \quad (109)$$

or

$$\begin{aligned} \Omega &= \int_0^{\omega_d} \frac{d\omega}{(1 + \alpha^2 \omega^2)^2} + 3\alpha^2 \int_0^{\omega_d} \frac{\omega^2}{(1 + \alpha^2 \omega^2)^2} d\omega \\ &= \Omega_1 + 3\alpha^2 \Omega_2 \end{aligned} \quad (110)$$

Integrating yields

$$\Omega_1 = \frac{\omega_d}{2(1 + \alpha^2 \omega_d^2)} + \frac{1}{2\alpha} \arctan (\alpha \omega_d) \quad (111)$$

$$\Omega_2 = \frac{1}{2\alpha^2} \left( \frac{-\omega_d}{1 + \alpha^2 \omega_d^2} + \frac{1}{\alpha} \arctan (\alpha \omega_d) \right) \quad (112)$$

For a cutoff frequency,  $f_o$ , equal to 1.5 Hz,

$$\omega_d = 2.1\pi f_o = 9.896 \text{ rad/sec} \quad (113)$$

Substituting the numerical values for  $L_w$  and  $U_1$  yields

$$\alpha = 1750/706 = 2.48 \quad (114)$$

Then  $\Omega_1$  and  $\Omega_2$  are found to be

$$\Omega_1 = 0.3166 \quad (115)$$

$$\Omega_2 = 0.0488 \quad (116)$$

Substituting the values of  $\Omega_1$  and  $\Omega_2$  into Eqs (110) and (108) yields

$$\begin{aligned} Q &= \frac{2.48}{\pi} \frac{P}{9.896} \sigma_w^2 \{ 0.3166 + 3(2.48)^2(0.0488) \} \\ &= .09708 \sigma_w^2 P \end{aligned} \quad (117)$$

$$\sqrt{Q} = \sqrt{.09708} \sigma_w \sqrt{P} \quad (118)$$

Therefore, the gain needed to make up for the filter loss is

$$K_F = \frac{1}{\sqrt{.09708}} = \underline{3.209} \quad (119)$$

$K_F$  is applied to the gust model as an additional factor in the gain, so that Eq (100) becomes

$$\frac{w_g(s)}{\xi(s)} = 2.85 \sigma_w \frac{4.29 s + 1}{(2.48 s + 1)^2} \quad (120)$$

which is the gust model (Ref 13).

A bode plot of Eq (120) is shown in Figure D-1.

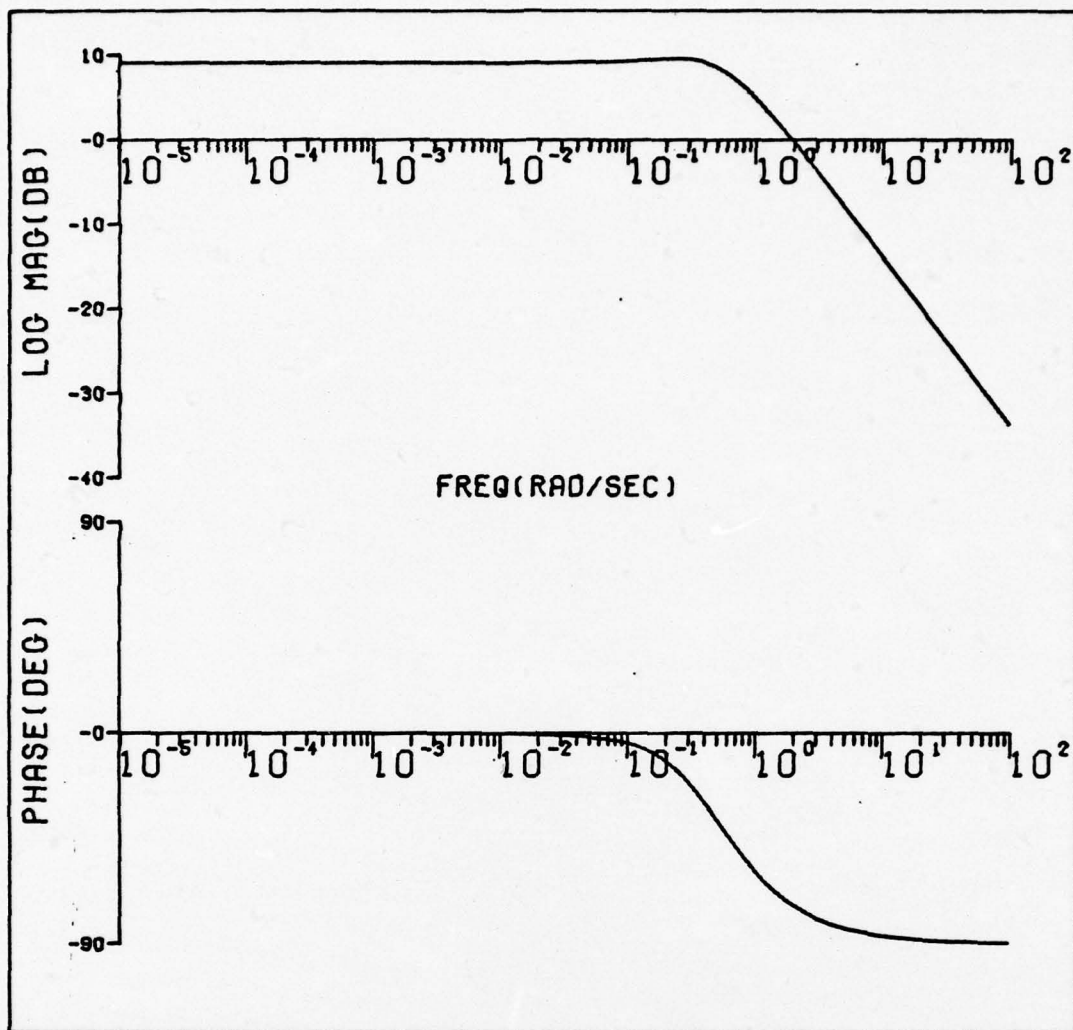


Figure D-1. Bode Plot of Gust Model.



## APPENDIX E

### Bode and Polar Plots of the Open-Loop Pilot-Aircraft Transfer Functions Without Downwash

Bode and polar plots of  $Y_{PE} Y_{CE}$ ) No DW and  $Y_{PT} Y_{CT}$ ) No DW are shown for values of  $T_L$  starting with  $T_L = 8$  and decreasing to  $T_L = 1$ . These transfer functions are given by Eqs (52) and (53). Pilot gains used in calculating these plots are given in Table V.

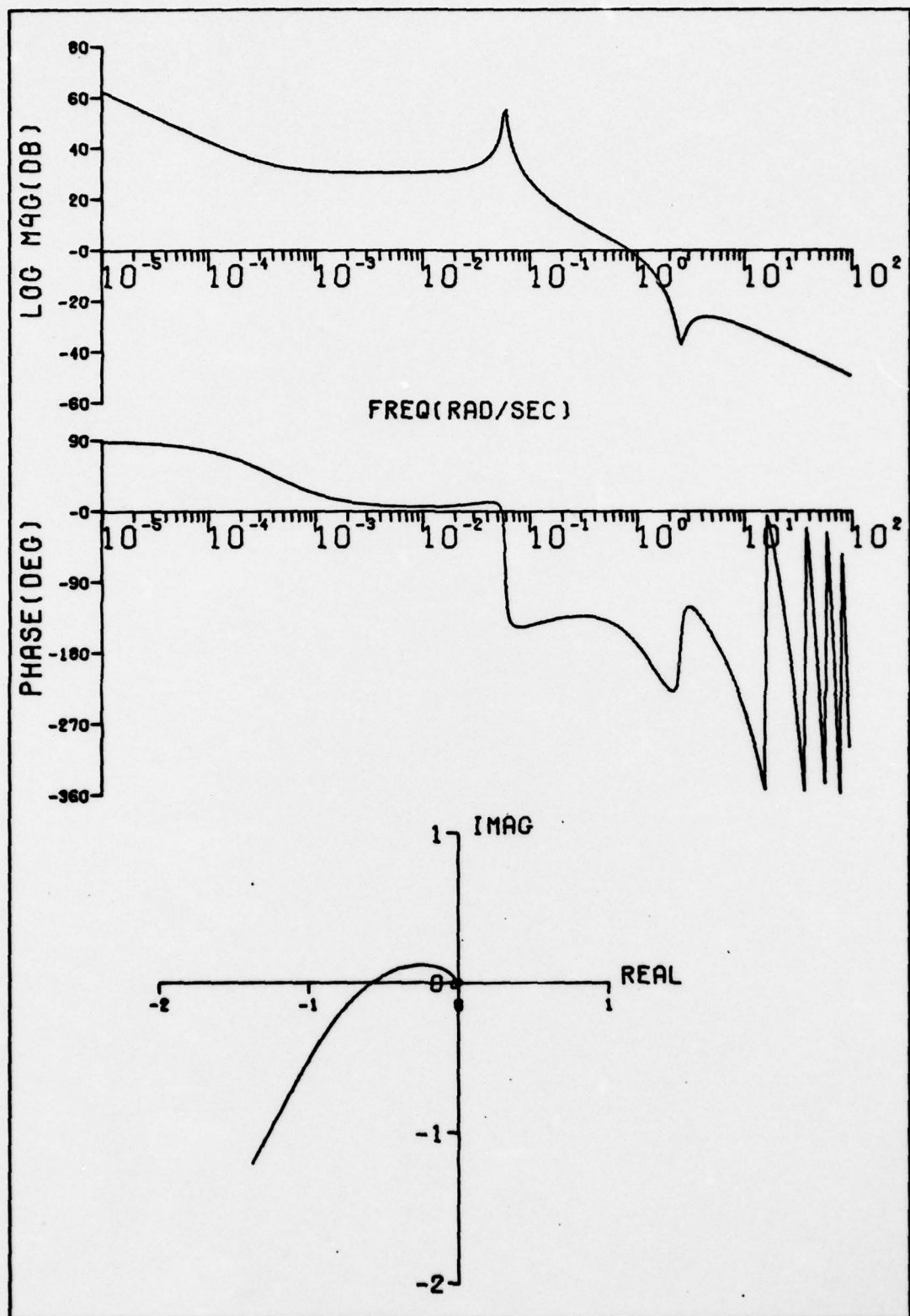


Figure E-1. Bode and Polar Plots of  $Y_{PE} Y_{c_E}$  No DW,  $T_L = 8$ .

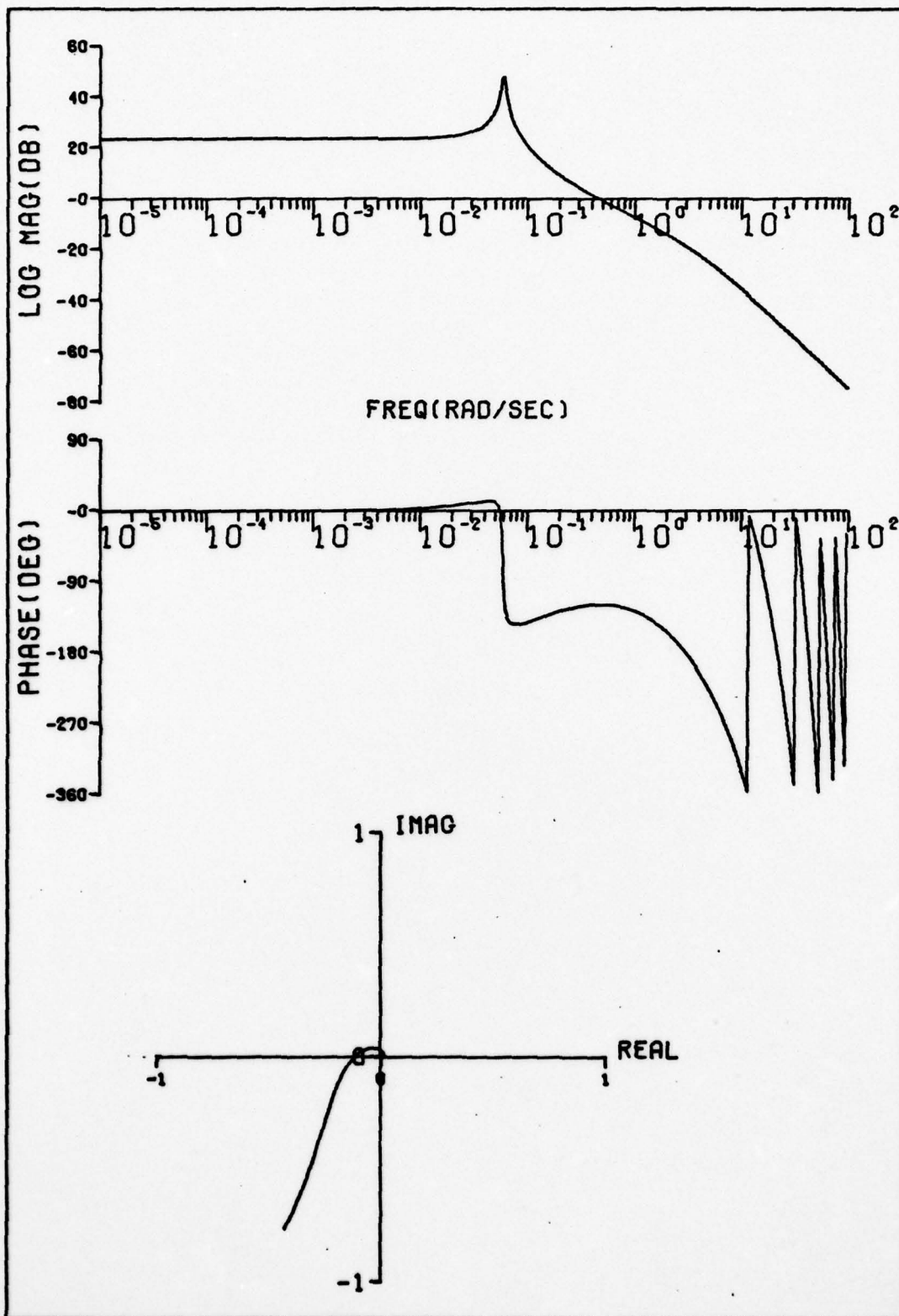


Figure E-2. Bode and Polar Plots of  $Y_{P_T c_T}$  No DW,  $T_L = 8$ .



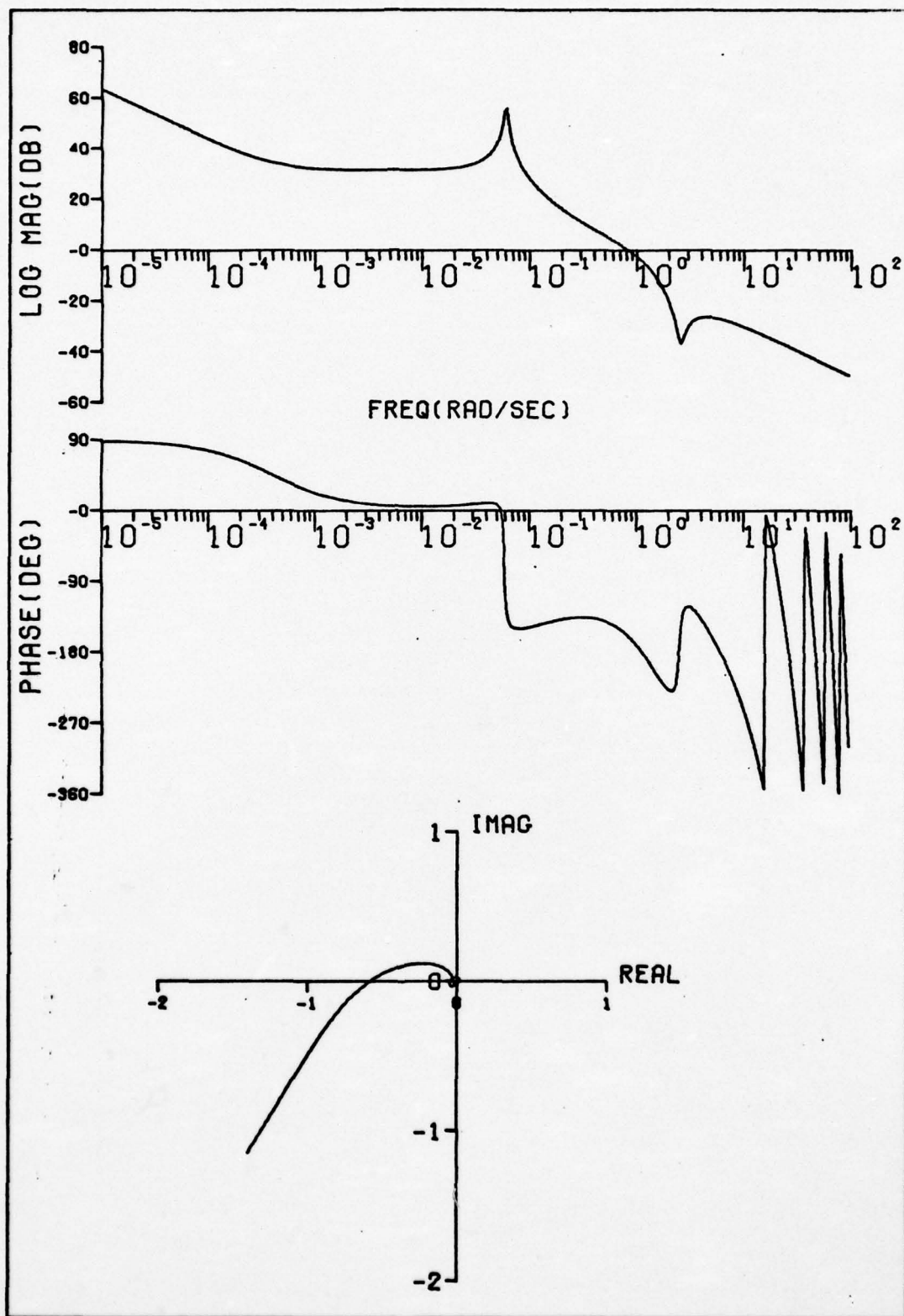


Figure E-3. Bode and Polar Plots of  $Y_{PE} Y_{cE}$  No DW,  $T_L = 7$ .

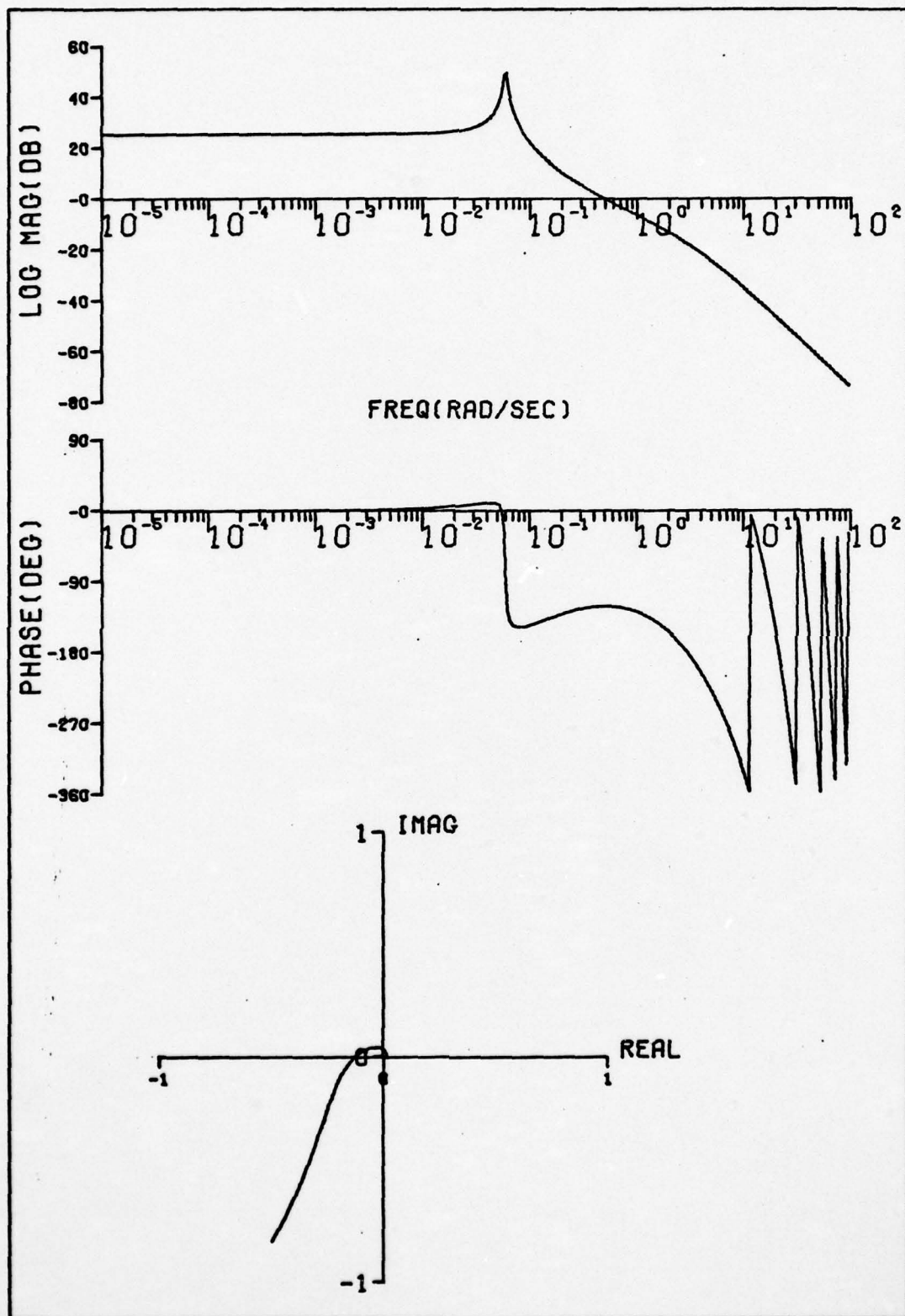


Figure E-4. Bode and Polar Plots of  $Y_{P_T c_T}$  No DW,  $T_L = 7$ .

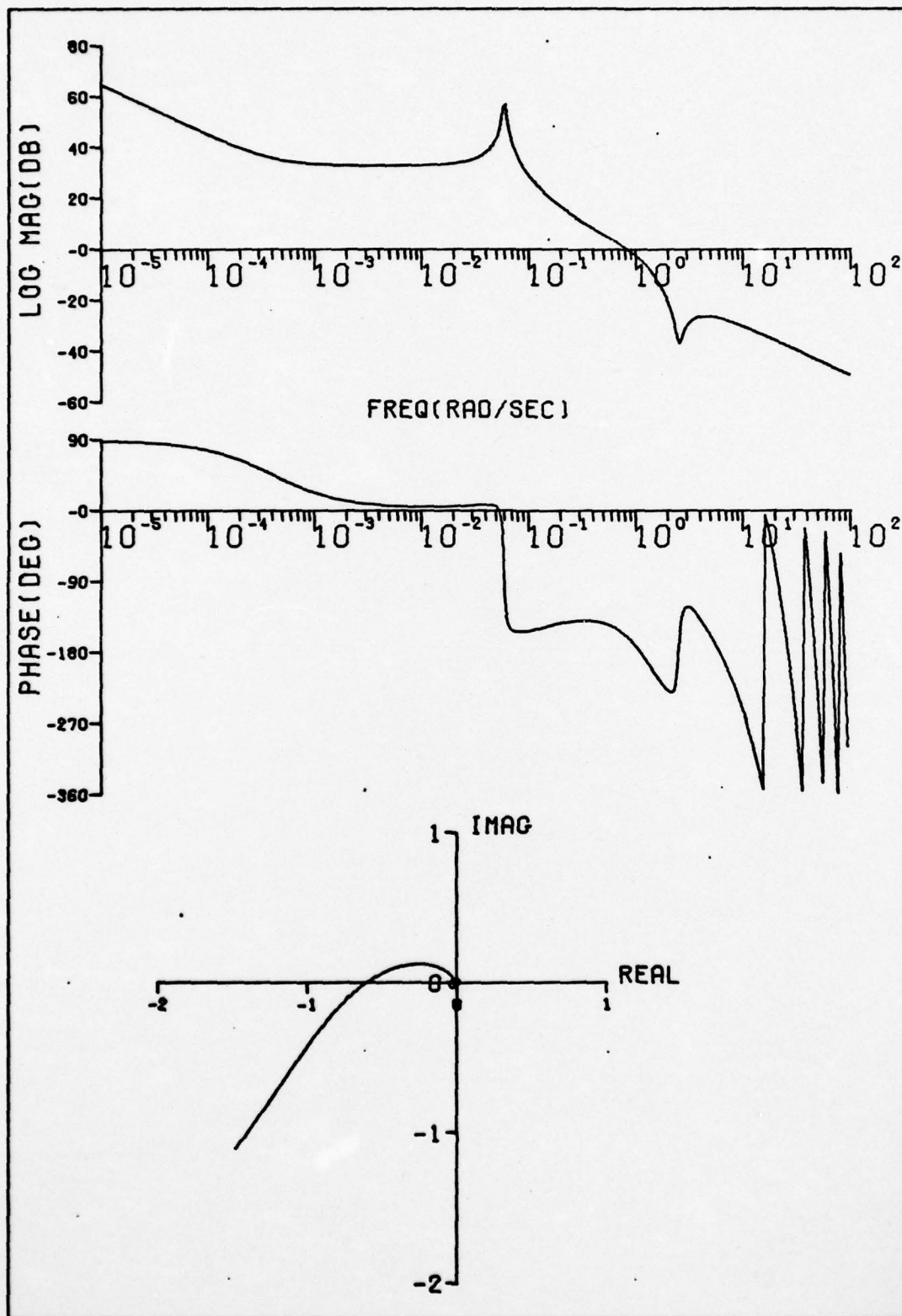


Figure E-5. Bode and Polar Plots of  $Y_{PE} Y_{cE})$  No DW,  $T_L = 6$ .

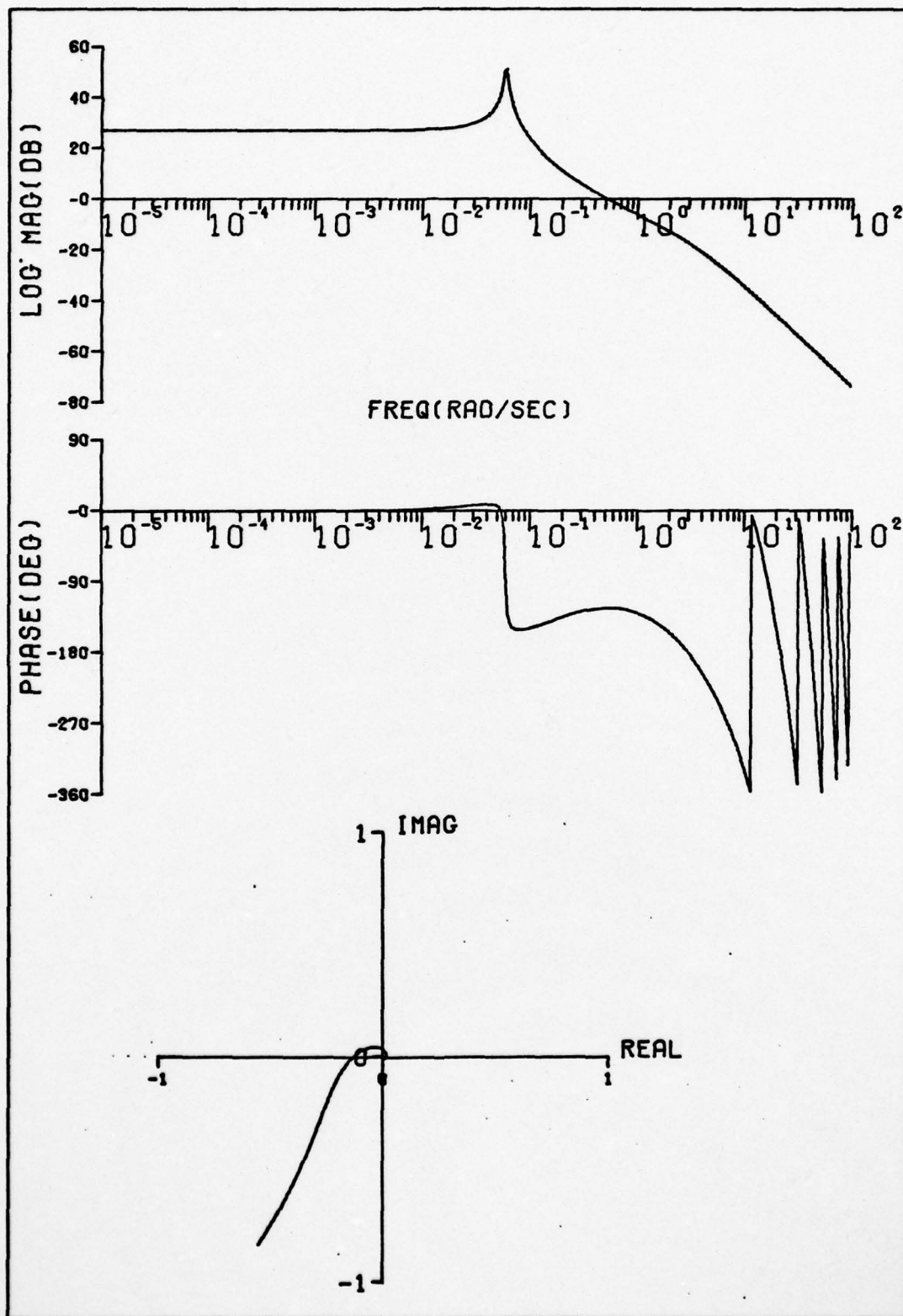


Figure E-6. Bode and Polar Plots of  $Y_{P_T Y_{c_T}} No DW, T_L = 6$ .



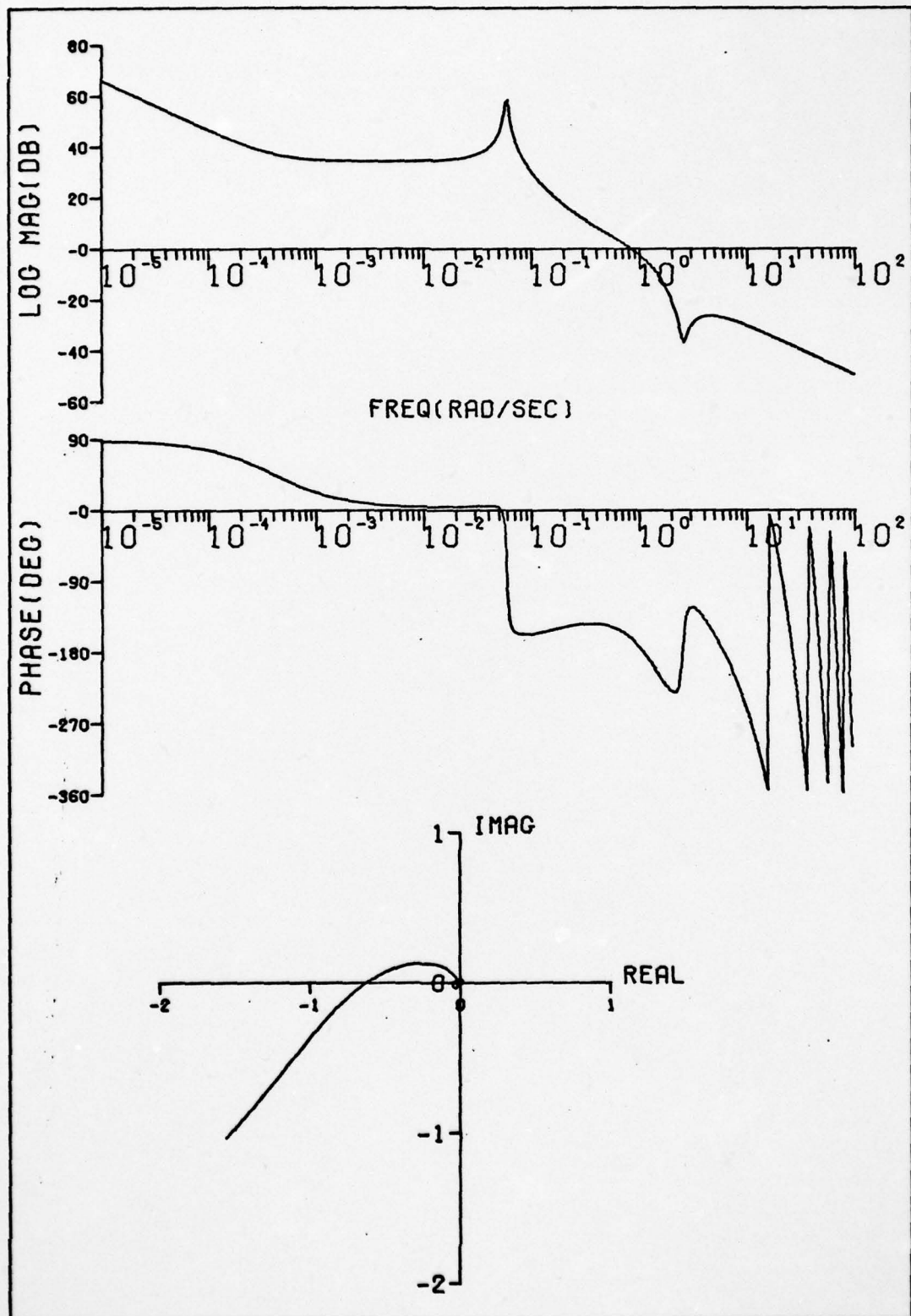


Figure E-7. Bode and Polar Plots of  $Y_{PE} Y_{CE}$  No DW,  $T_L = 5$ .

AD-A034 946 AIR FORCE INST OF TECH WRIGHT-PATTERSON AFB OHIO SCH--ETC F/G 1/2  
A CONTROL THEORETIC STUDY OF THE NUCLEAR VULNERABILITY OF THE A--ETC(U)  
DEC 76 J T MERRIFIELD  
UNCLASSIFIED GA/MC/76D-10 NL

AIR FORCE INST OF TECH WRIGHT-PATTERSON AFB OHIO SCH--ETC F/G 1/2  
A CONTROL THEORETIC STUDY OF THE NUCLEAR VULNERABILITY OF THE A--ETC(U)  
DEC 76 J T MERRIFIELD  
GA/MC/76D-10 NL

NL

2 of 2  
ADA034946

ADA034946

1000

END

DATE  
FILMED  
3 - 77

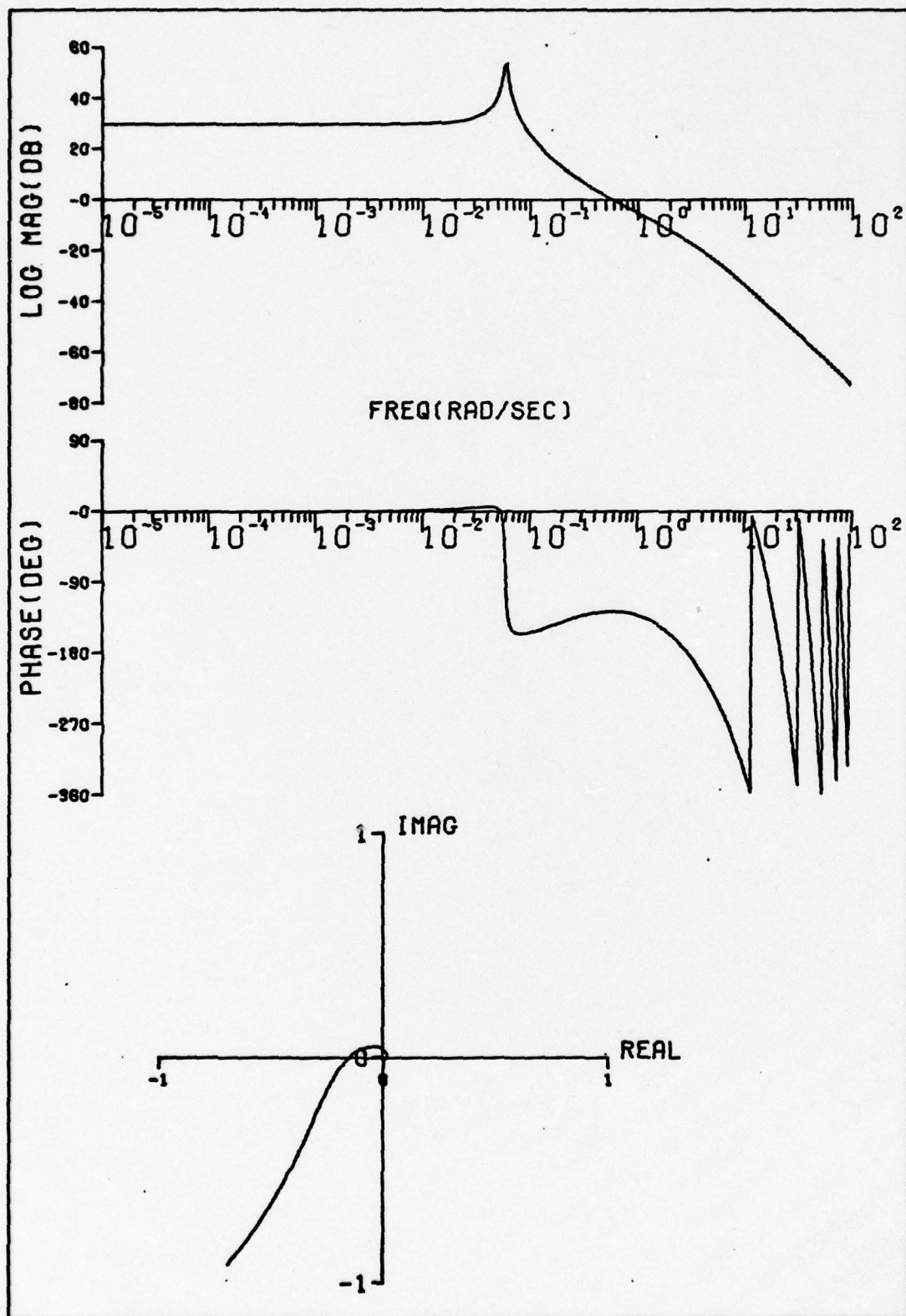


Figure E-8. Bode and Polar Plots of  $Y_{P_T C_T}$  No DW,  $T_L = 5$ .

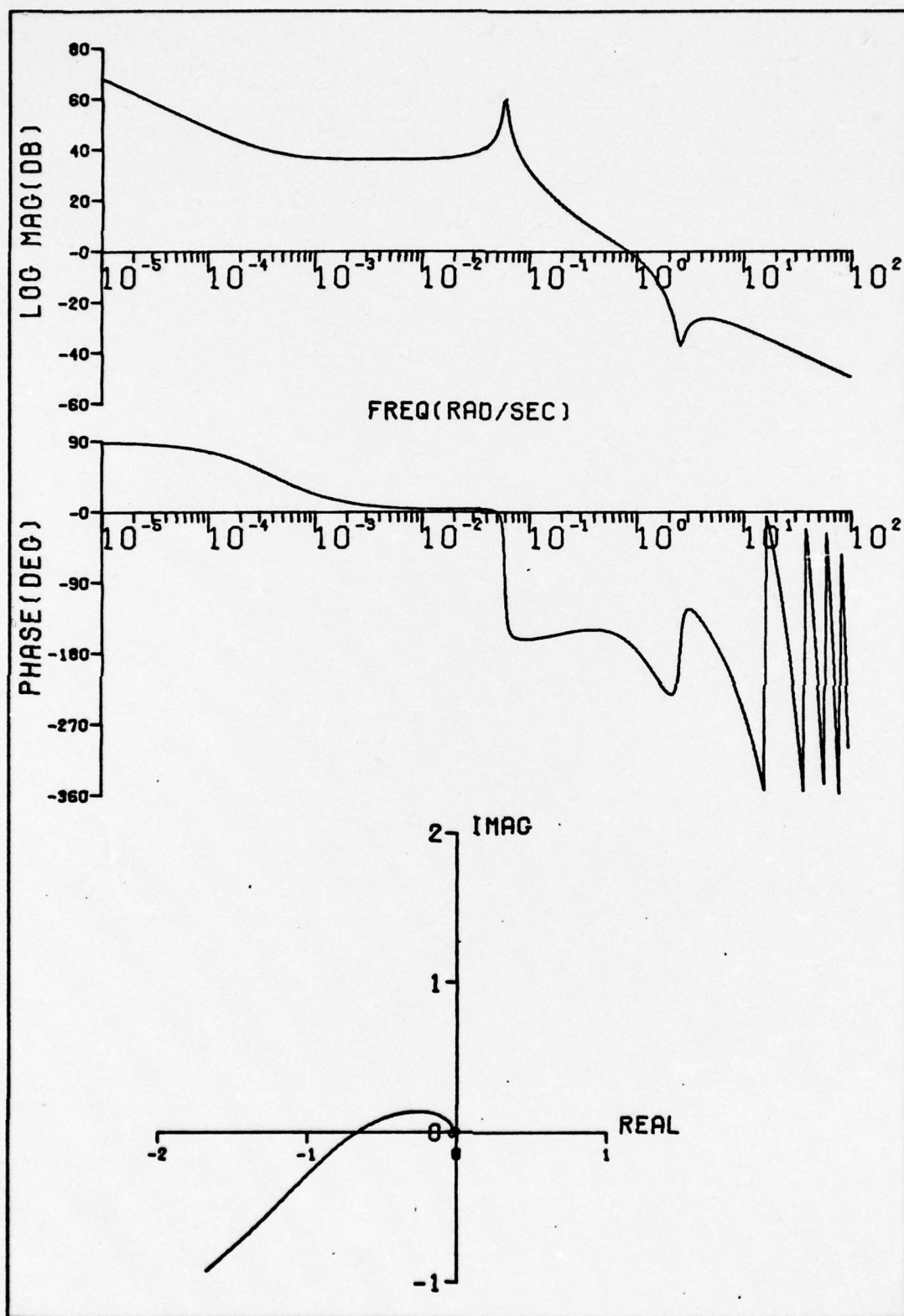


Figure E-9. Bode and Polar Plots of  $Y_{PE} Y_{CE}$  No DW,  $T_L = 4$ .



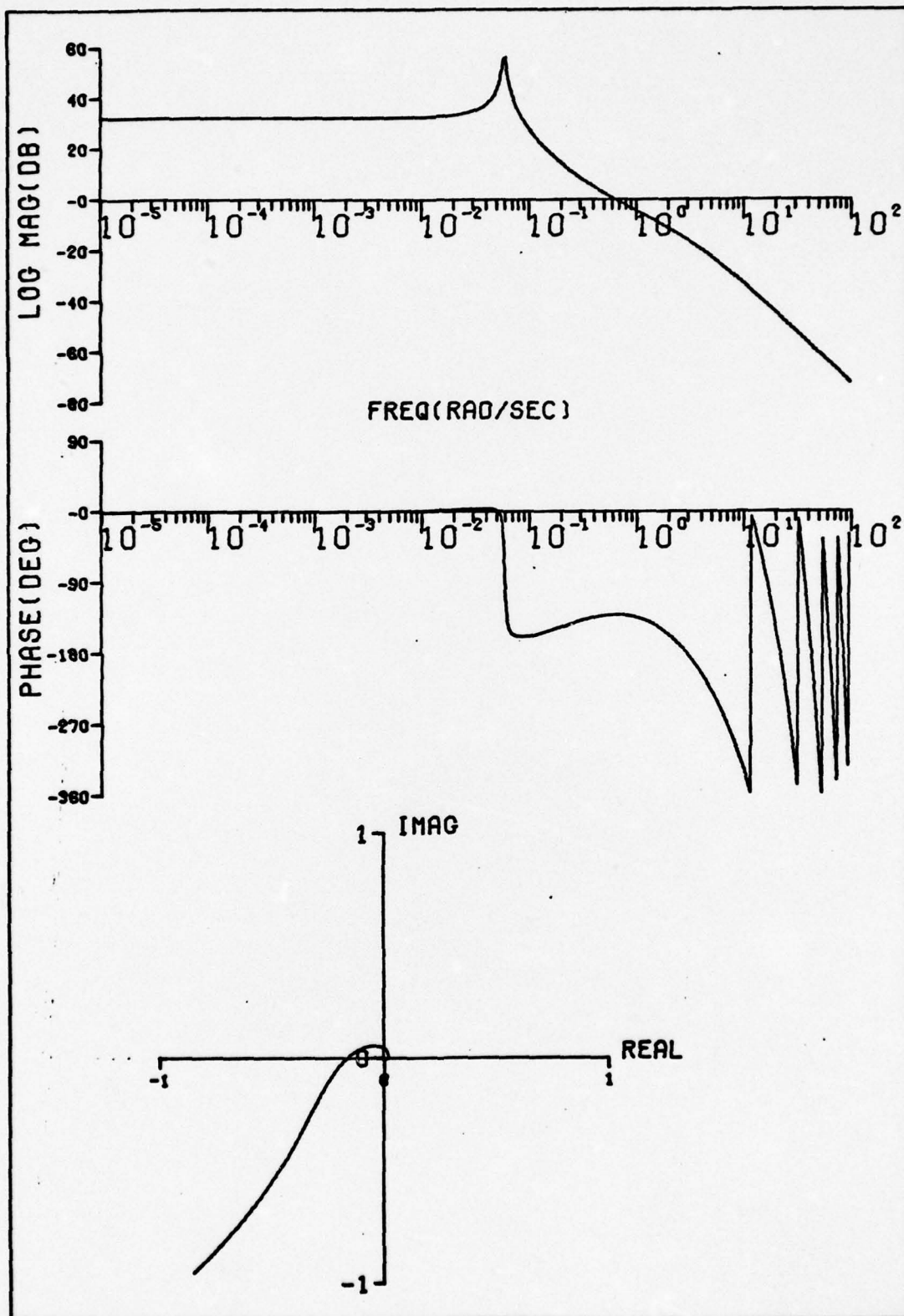


Figure E-10. Bode and Polar Plots of  $Y_{P_T c_T}$  No DW,  $T_L = 4$ .

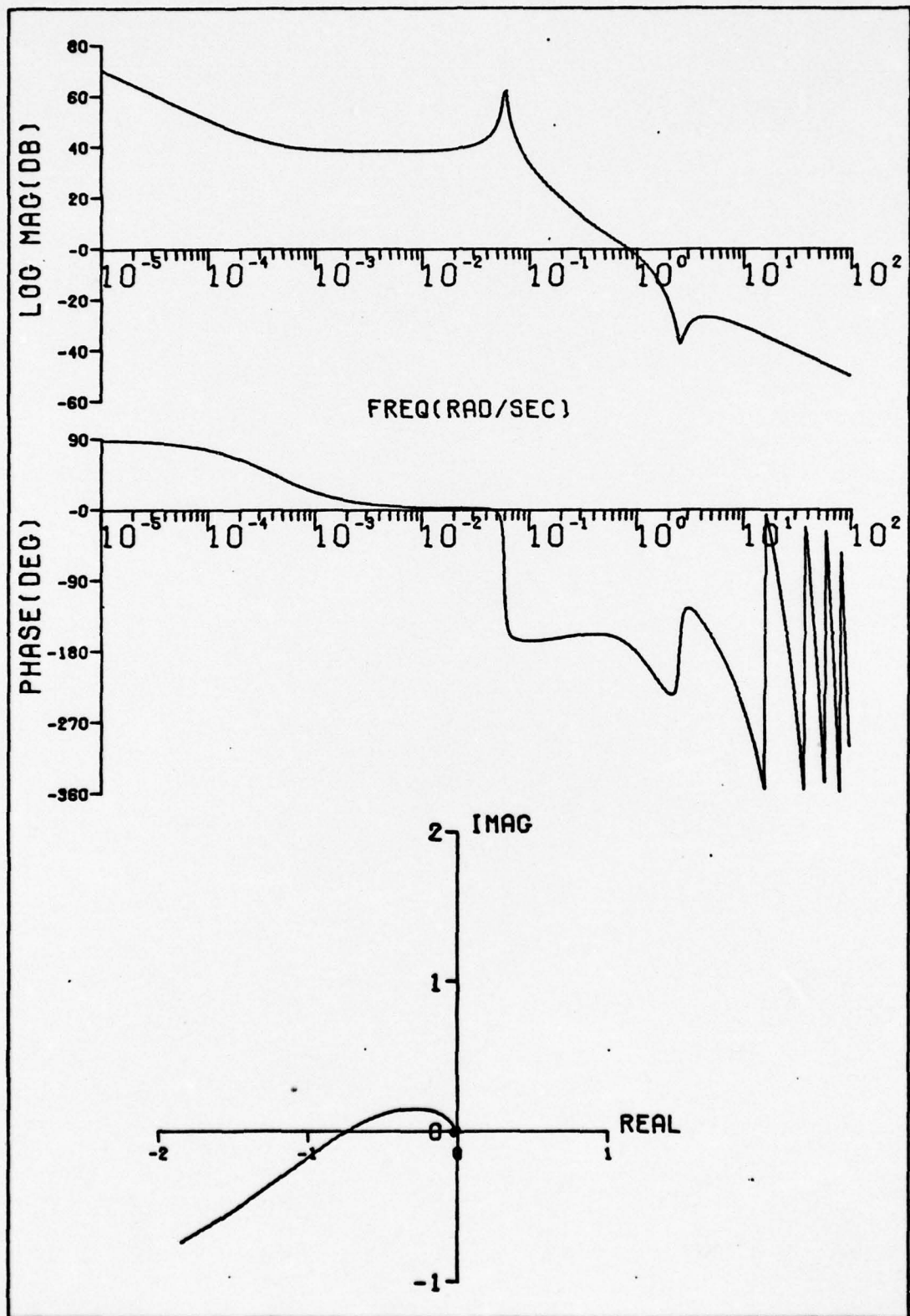


Figure E-11. Bode and Polar Plots of  $Y_{PE} Y_{c_E}$  No DW,  $T_L = 3$ .

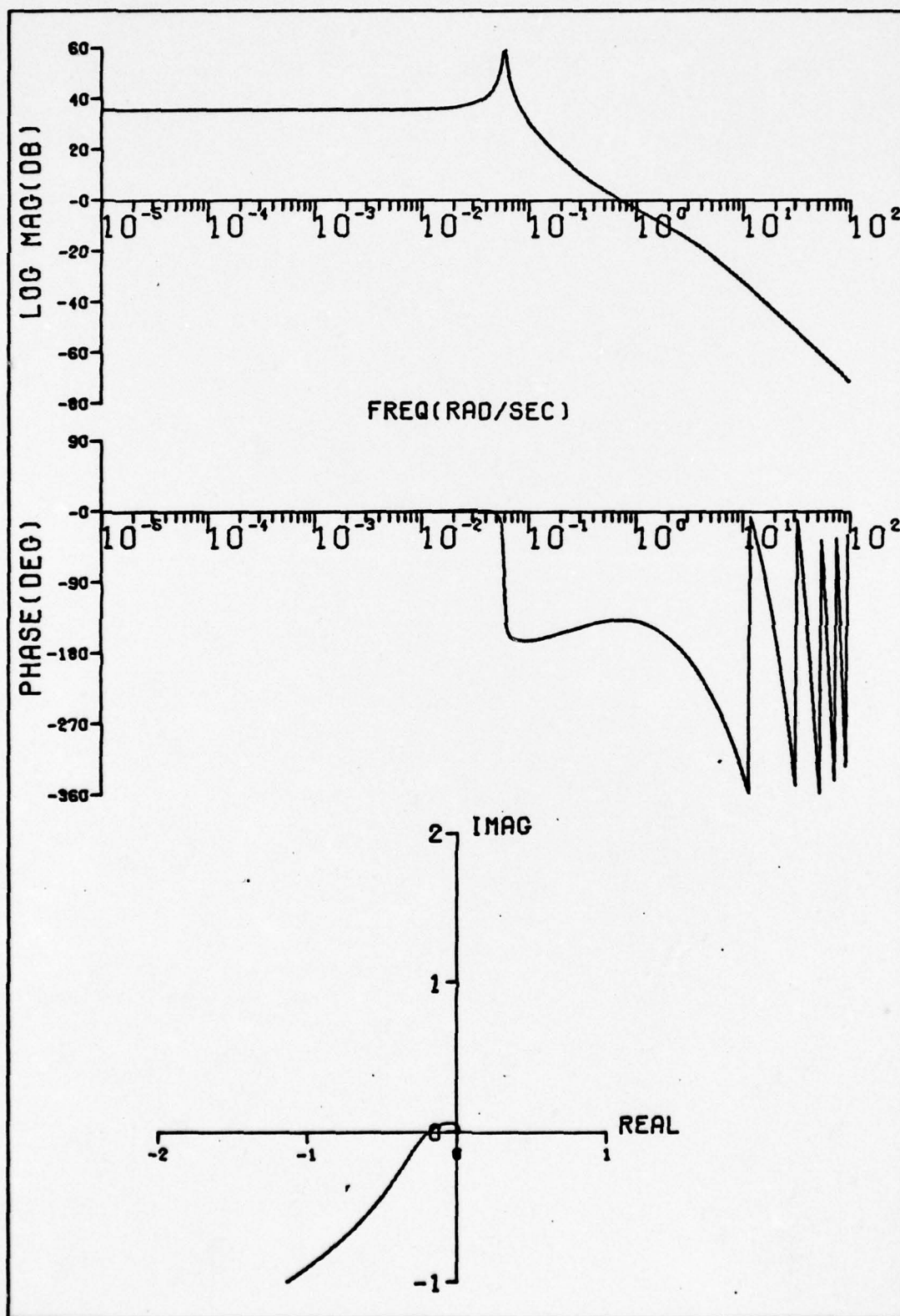


Figure E-12. Bode and Polar Plots of  $Y_{PT, C_T}$  No DW,  $T_L = 3$ .

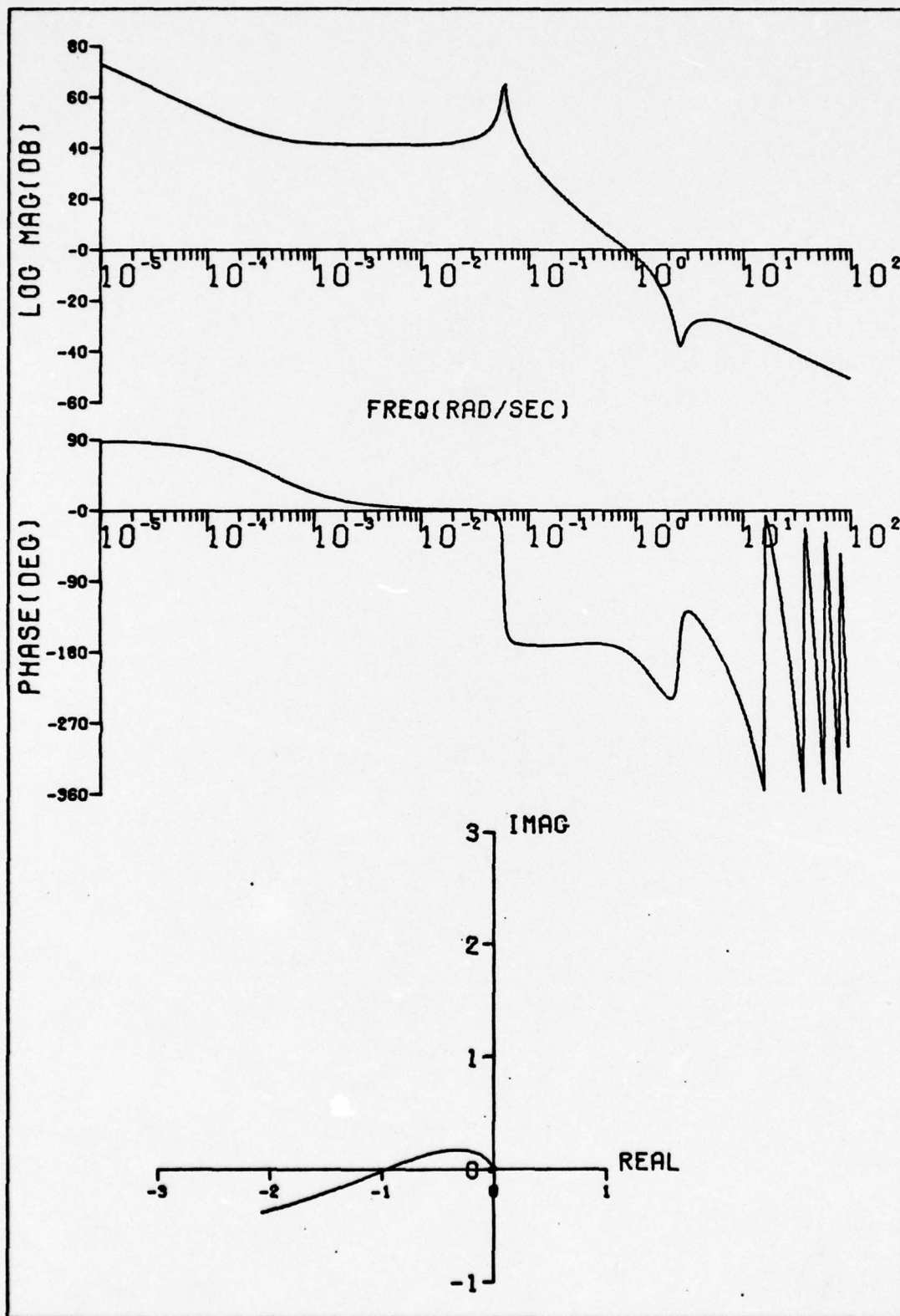


Figure E-13. Bode and Polar Plots of  $Y_{PE} Y_{CE}$  No DW,  $T_L = 2$ .



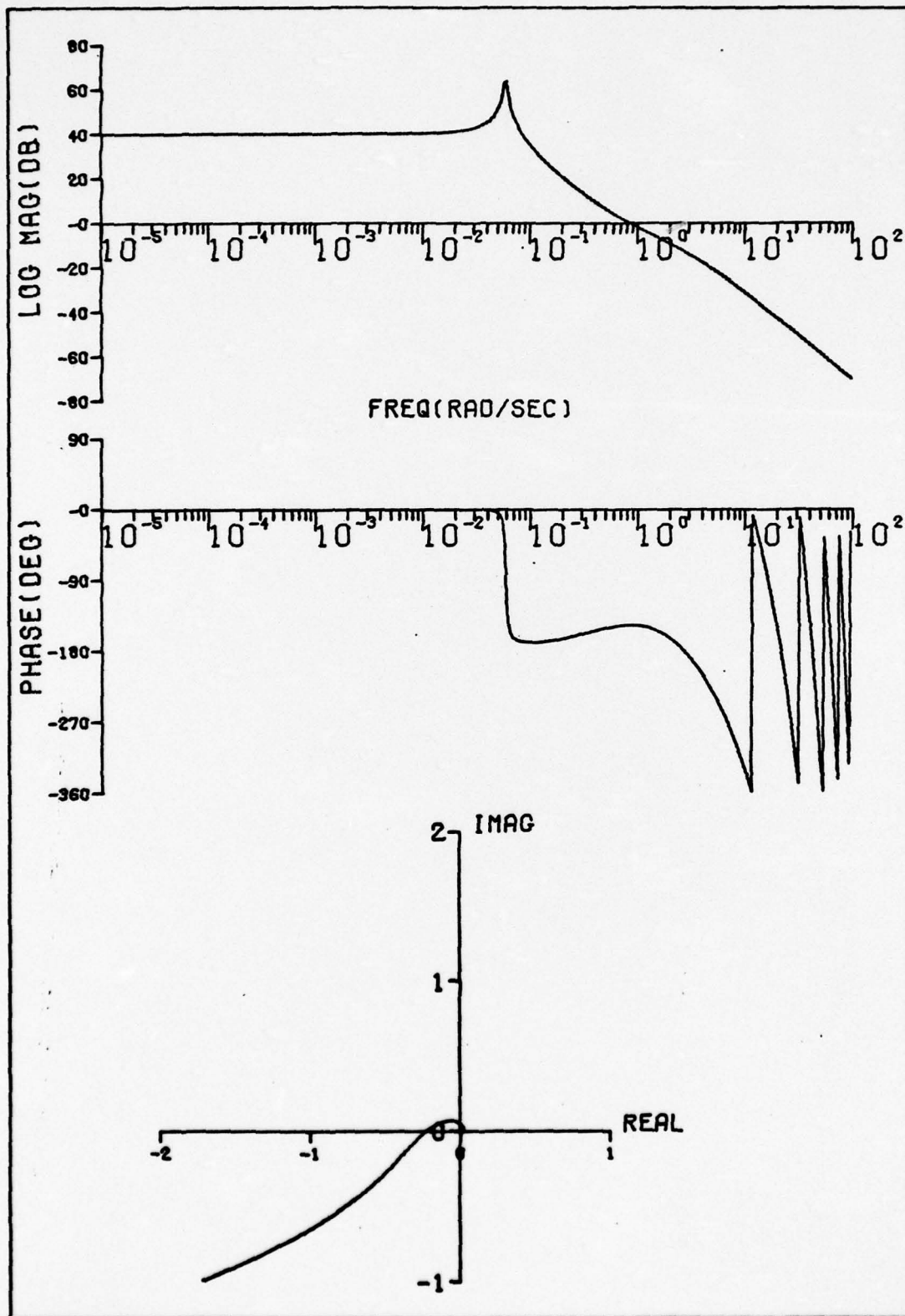


Figure E-14. Bode and Polar Plots of  $Y_{PT} Y_{c_T}$  No DW,  $T_L = 2$ .

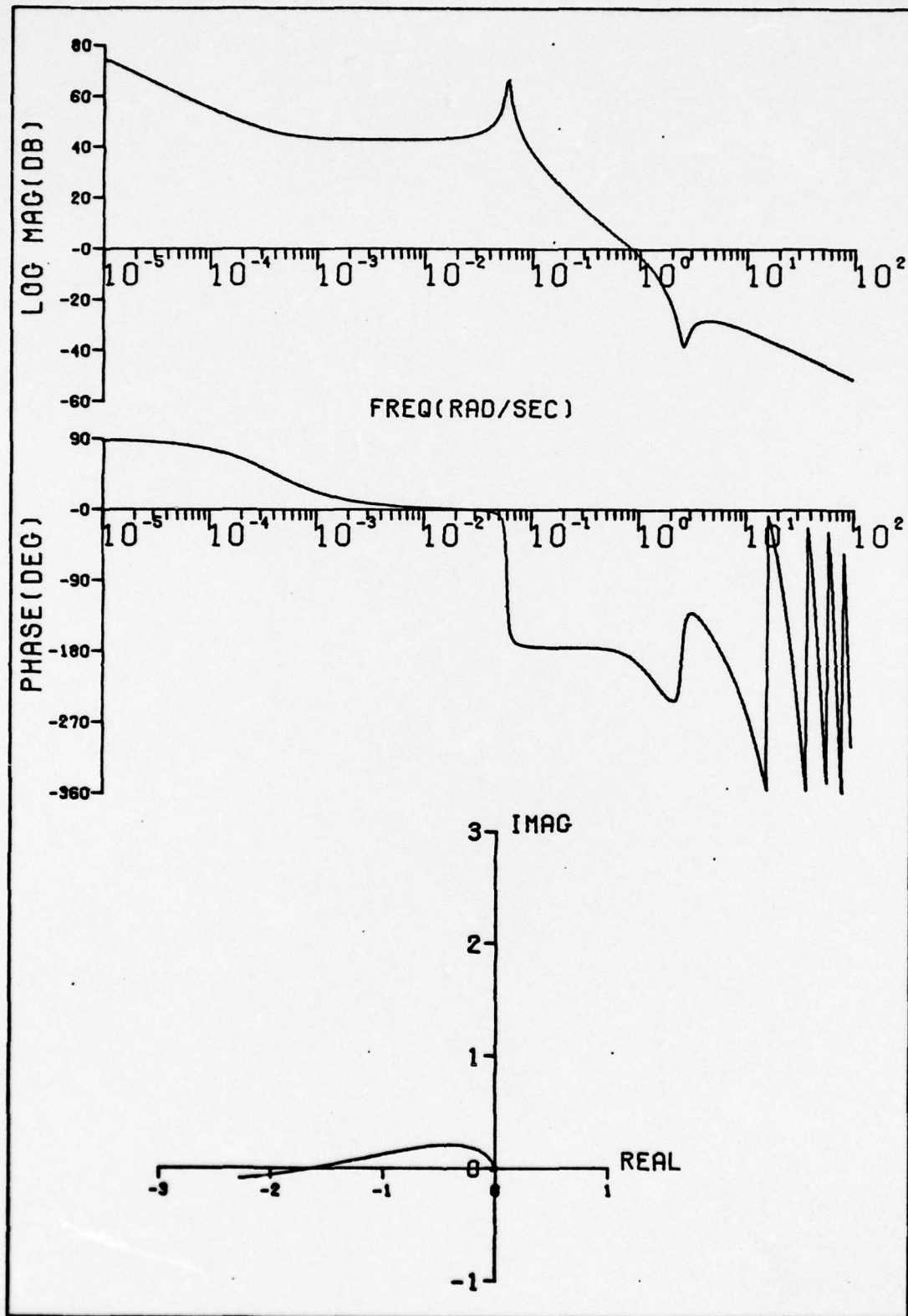


Figure E-15. Bode and Polar Plots of  $Y_{PE} Y_{CE})$  No DW,  $T_L = 1.5$ .

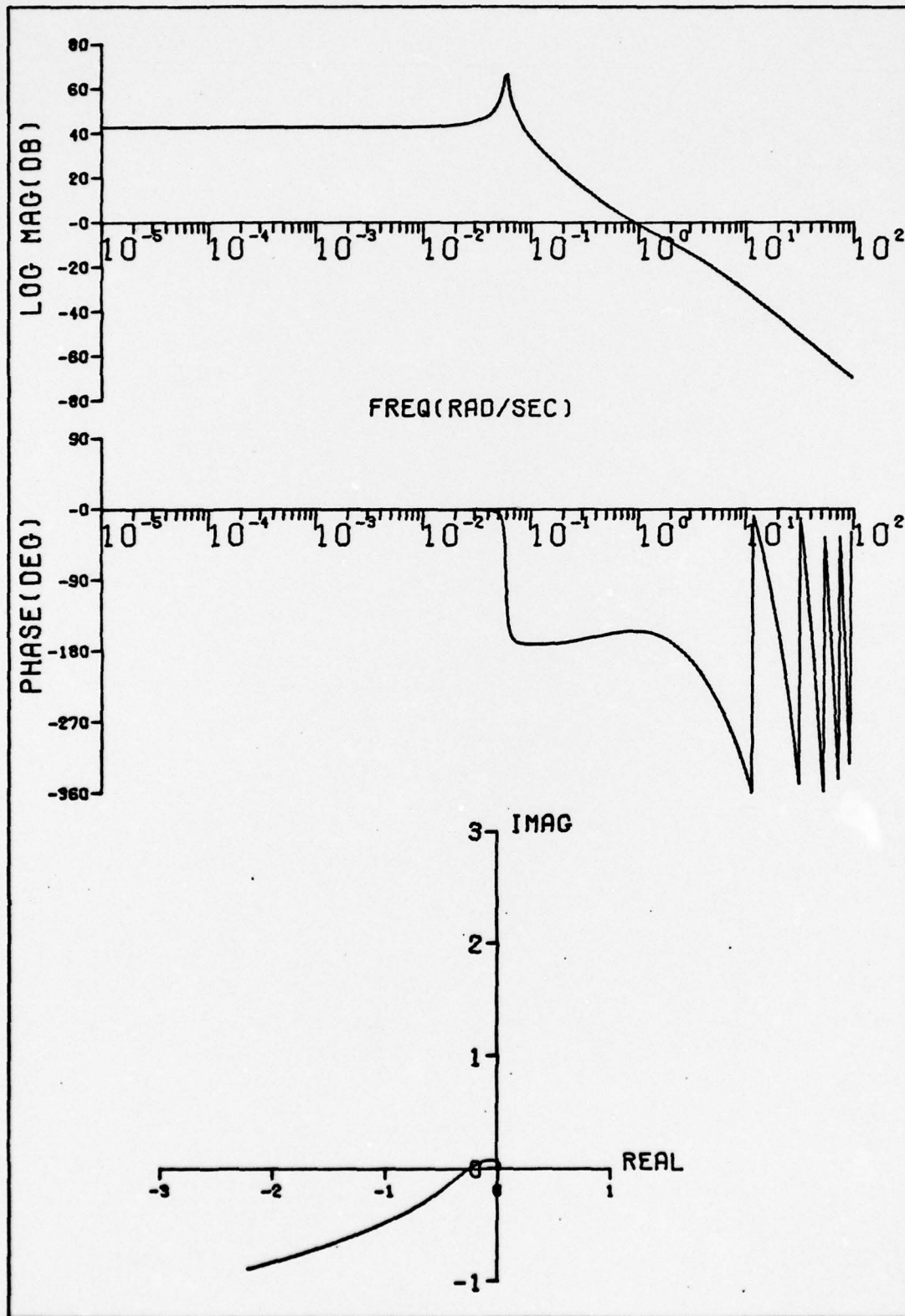


Figure E-16. Bode and Polar Plots of  $Y_{PT} Y_{CT}$  No DW,  $T_L = 1.5$ .

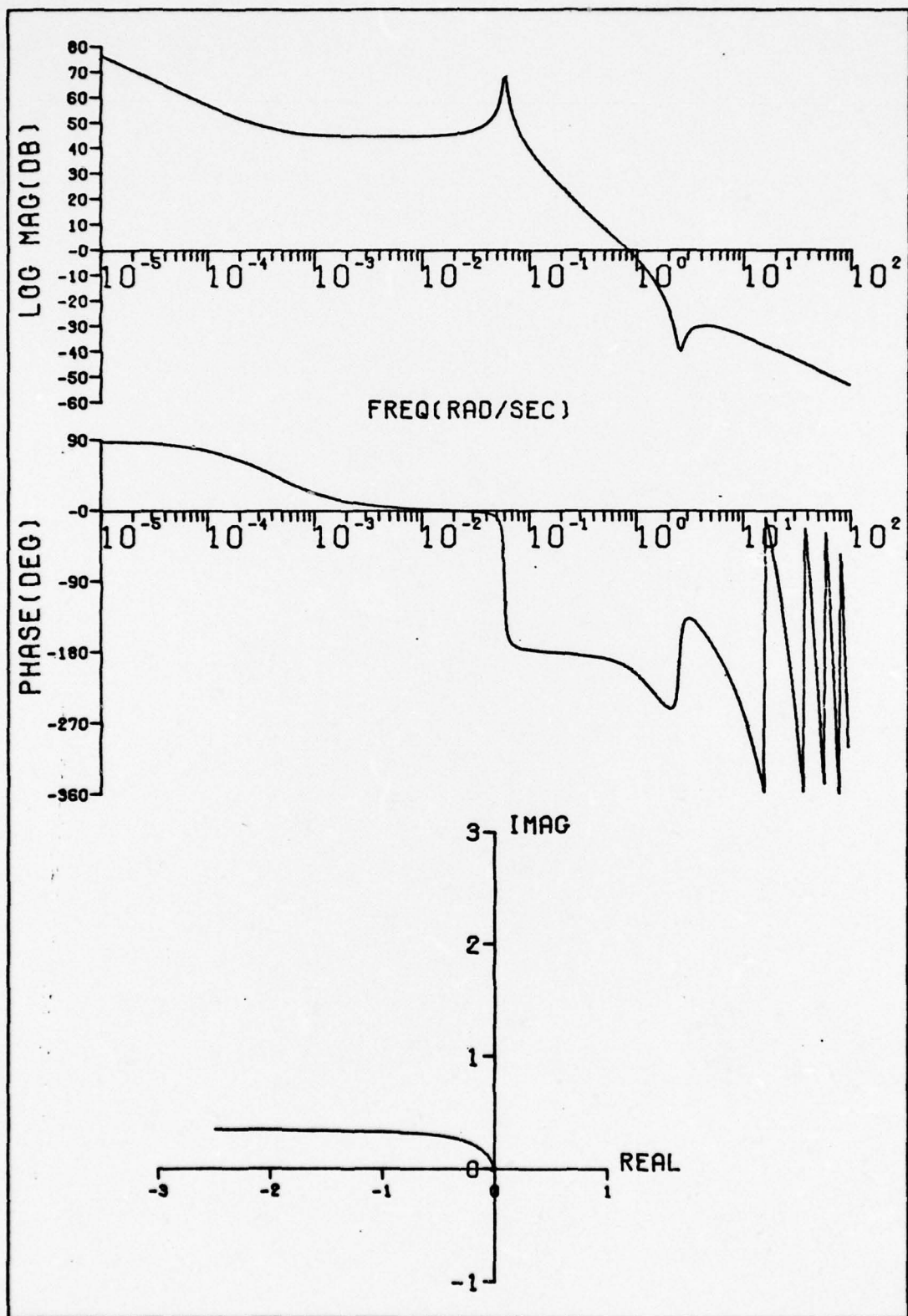


Figure E-17. Bode and Polar Plots of  $Y_{PE} Y_{CE}$  No DW,  $T_L = 1$ .



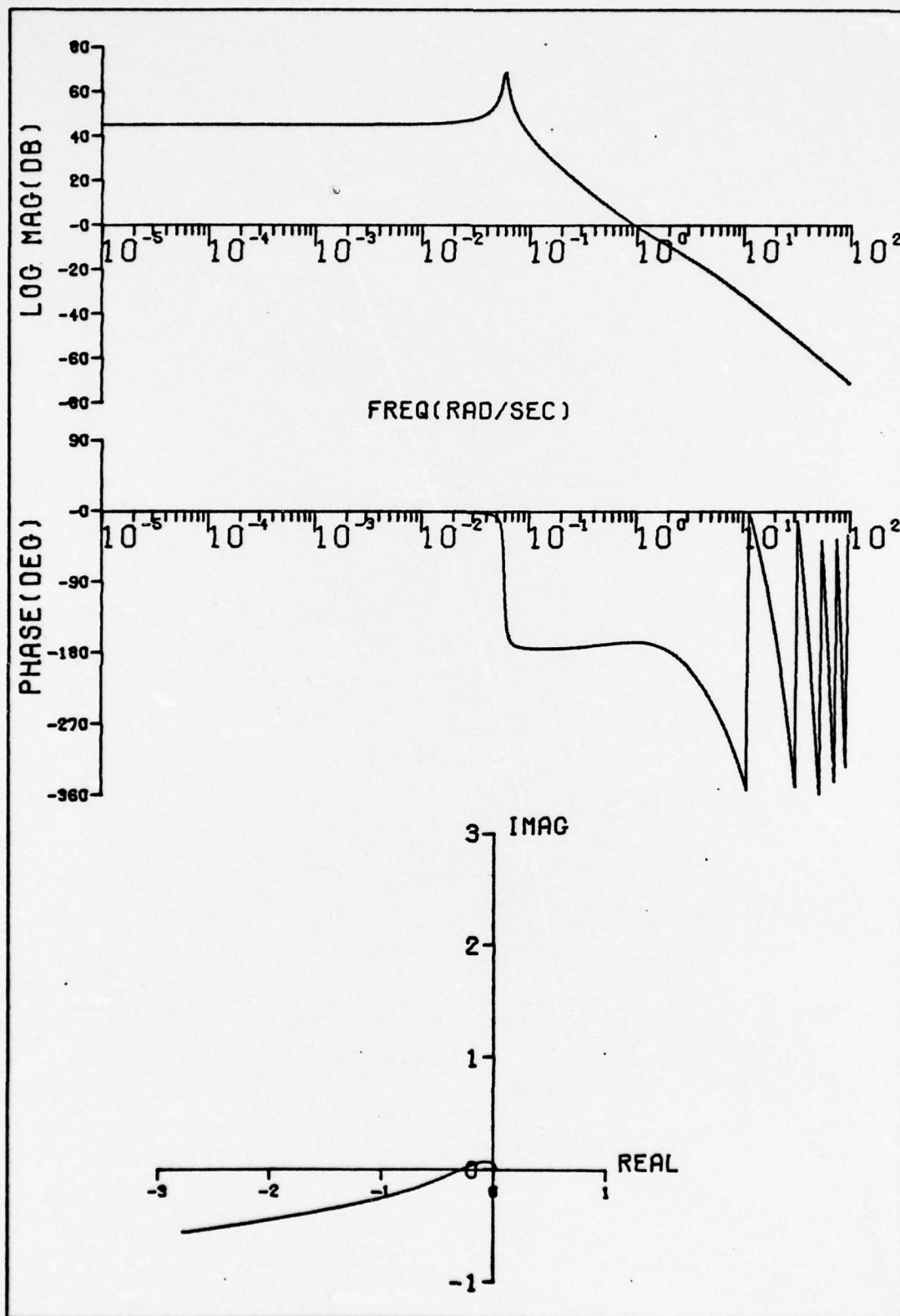


Figure E-18. Bode and Polar Plots of  $Y_{P_T c_T}$  No DW,  $T_L = 1$ .

## APPENDIX F

### Bode and Polar Plots of the Open-Loop Pilot-Aircraft Transfer Functions with Downwash

The figures contained herein present the Bode and polar plots of  $Y_{p_E} Y_{c_E})_{DW}$  and  $Y_{p_T} Y_{c_T})_{DW}$  as  $T_L$  is varied from 8 to 1. The transfer functions are given by Eqs (54) and (55). The values of  $K_{p_E}$  used in Eq (54) are listed in Table V. The plots of  $Y_{p_T} Y_{c_T})_{DW}$  were calculated by setting  $K_{p_T}$  equal to  $1/.06857 = 14.58$  in Eq (55) in order to show more detail in the  $-1 + j0$  regions of the polar plots.

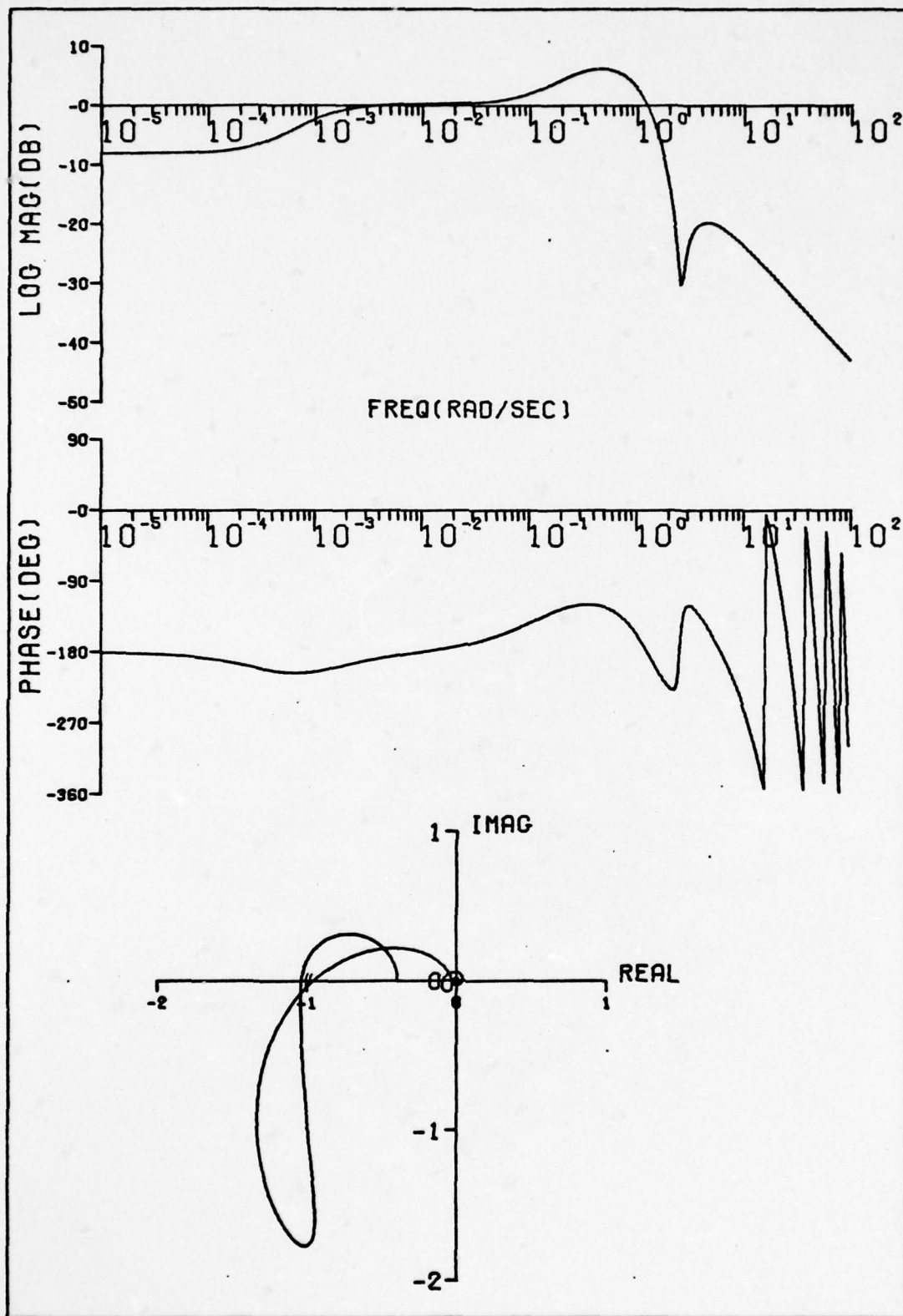


Figure F-1. Bode and Polar Plots of  $Y_{PE c_E} Y_{DW}, T_L = 8$ .

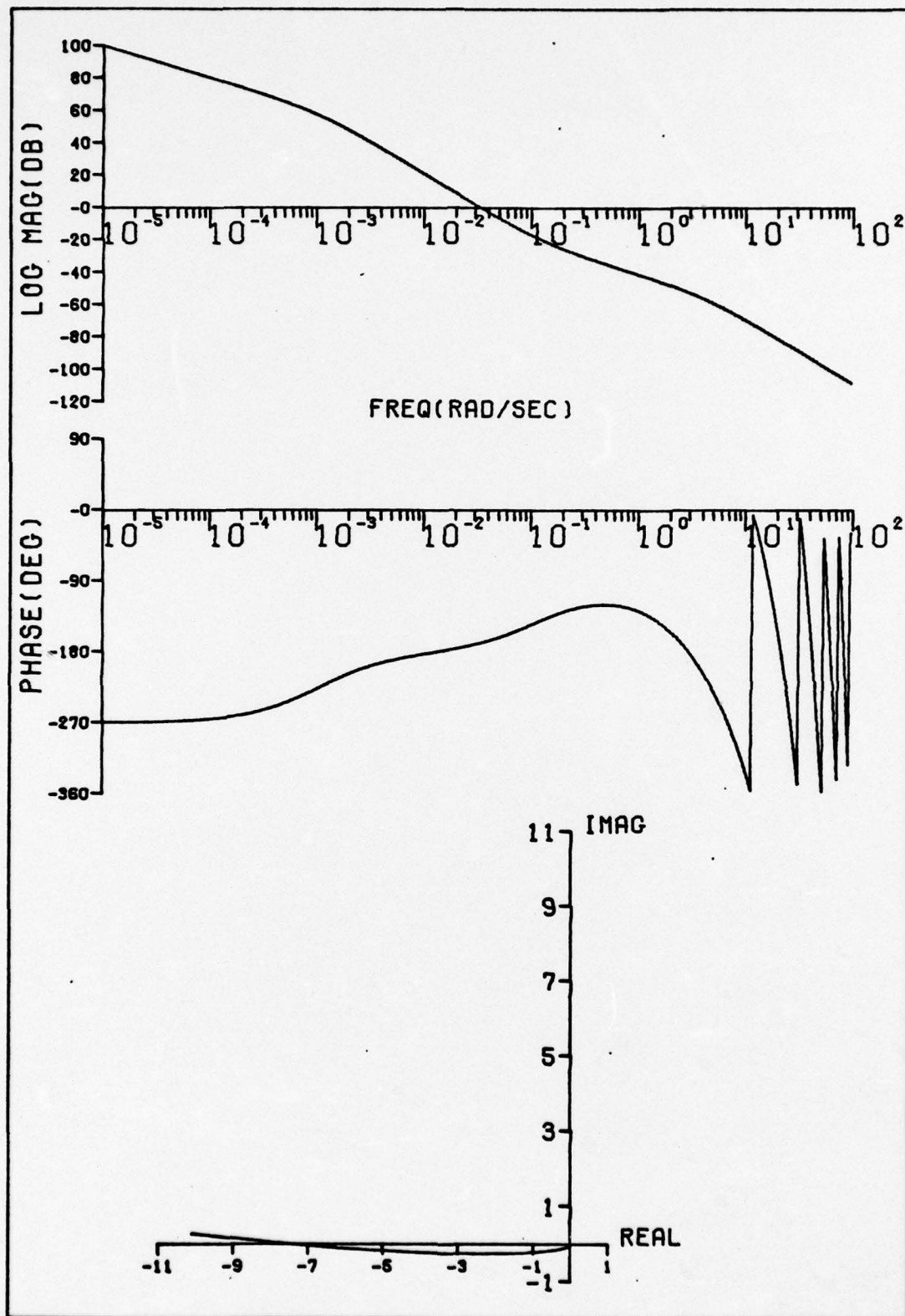


Figure F-2. Bode and Polar Plots of  $Y_{P_T Y_{C_T}}_{DW}, T_L = 8$ .



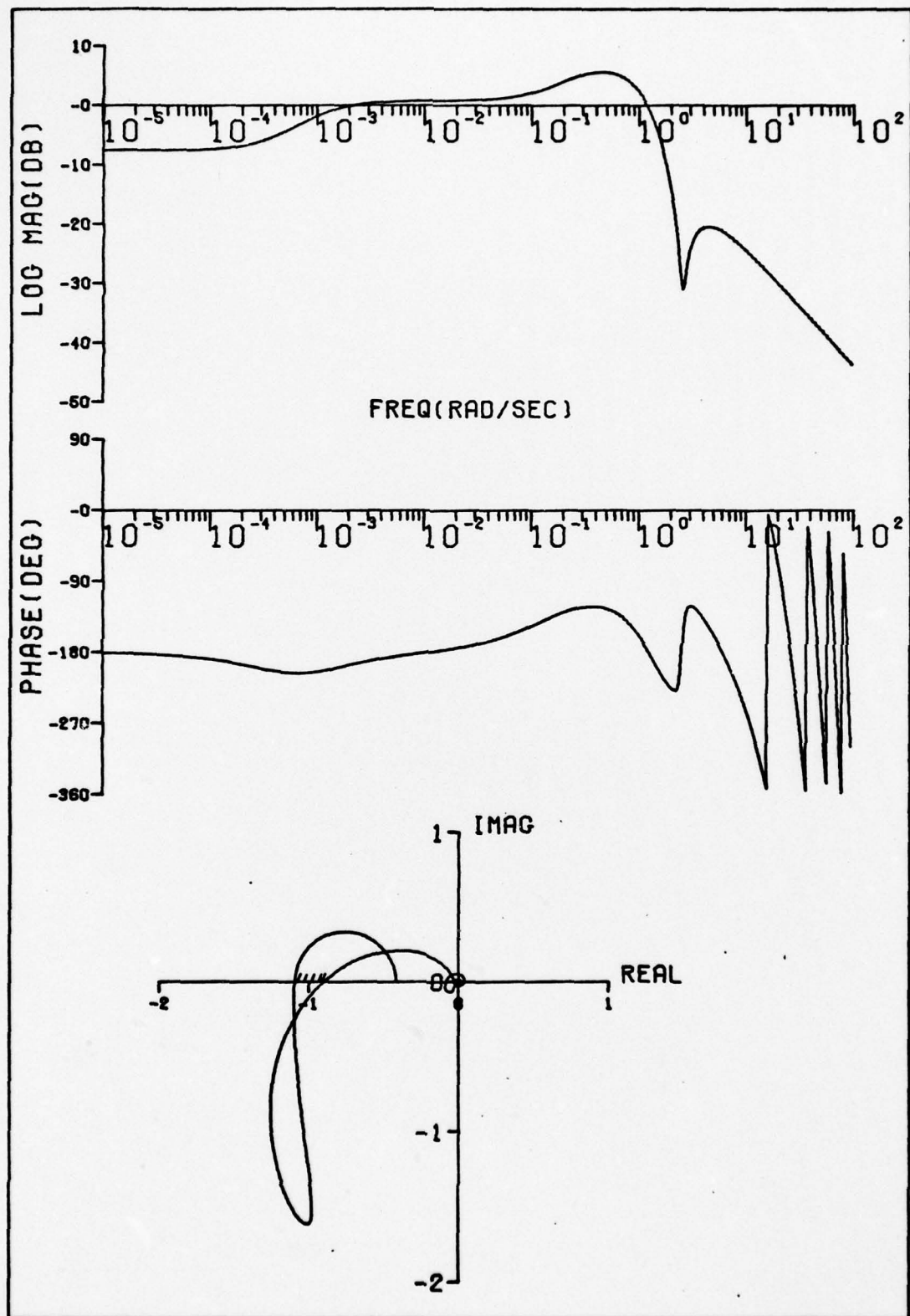


Figure F-3. Bode and Polar Plots of  $Y_{PE} Y_{cE})_{DW, T_L = 7}$ .

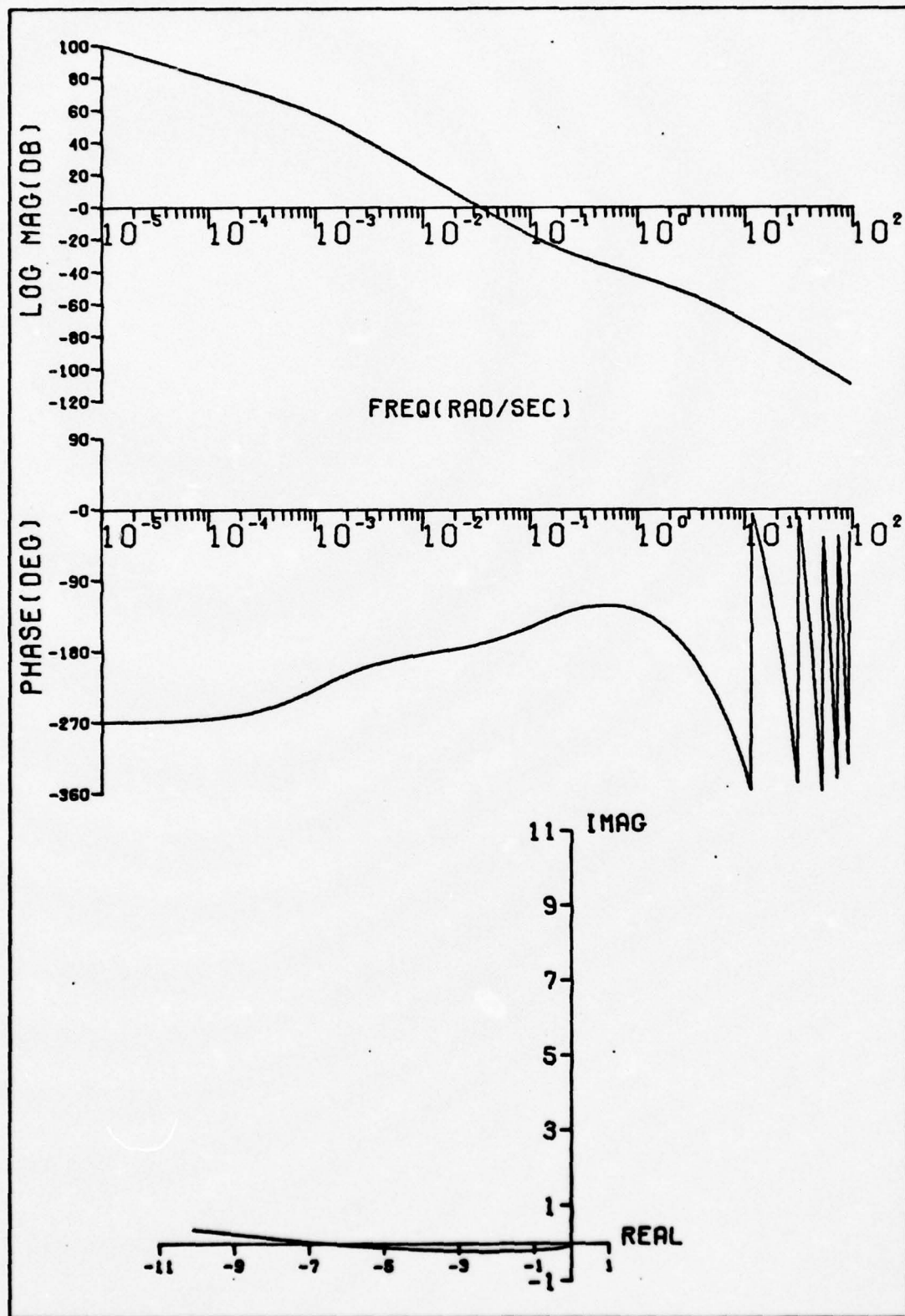


Figure F-4. Bode and Polar Plots of  $Y_{p_T c_T})_{DW, T_L = 7}$ .

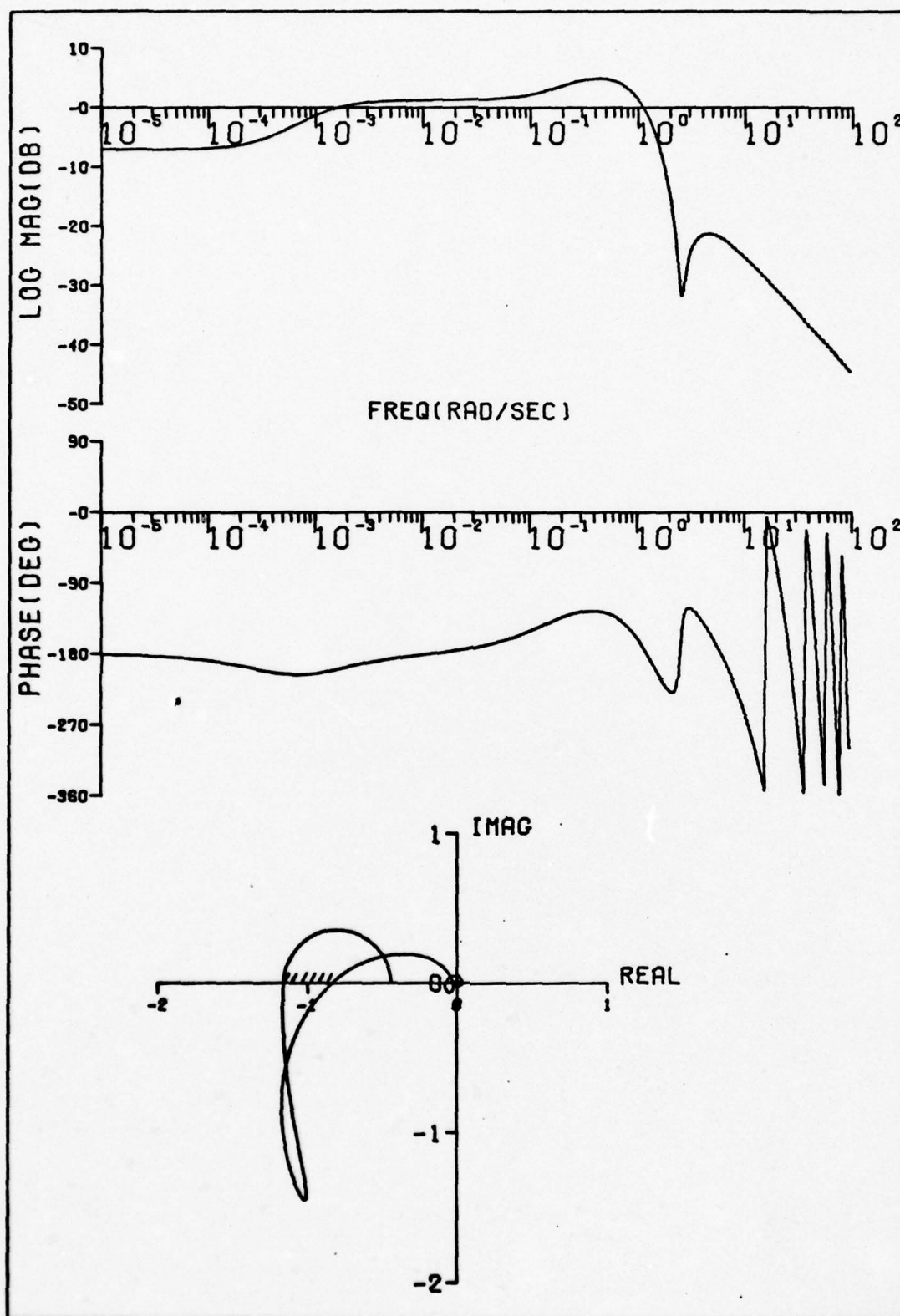


Figure F-5. Bode and Polar Plots of  $Y_{p_E c_E}^{Y_{DW}}$ ,  $T_L = 6$ .

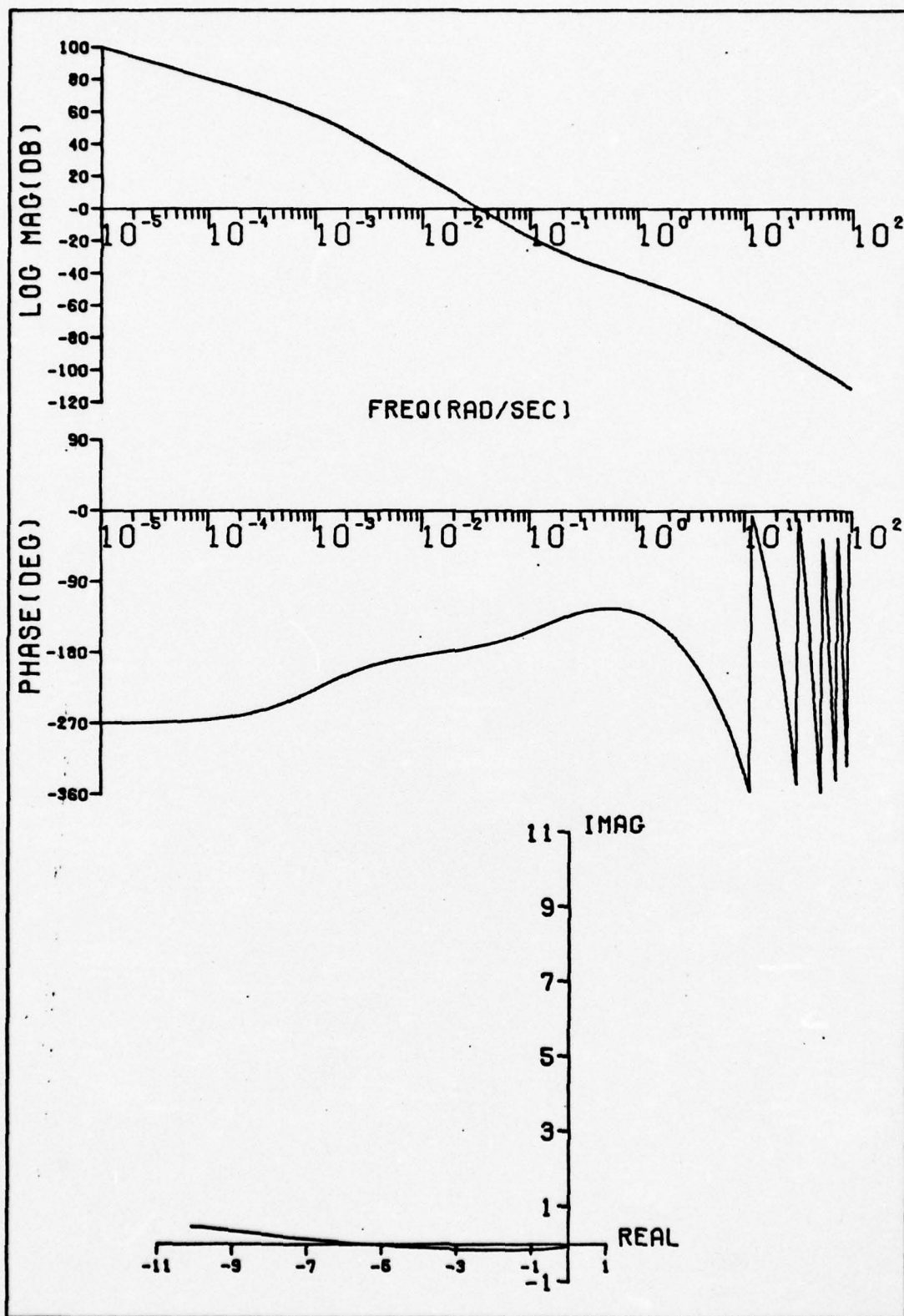


Figure F-6. Bode and Polar Plots of  $Y_{PT} Y_{c_T})_{DW, T_L = 6}$ .



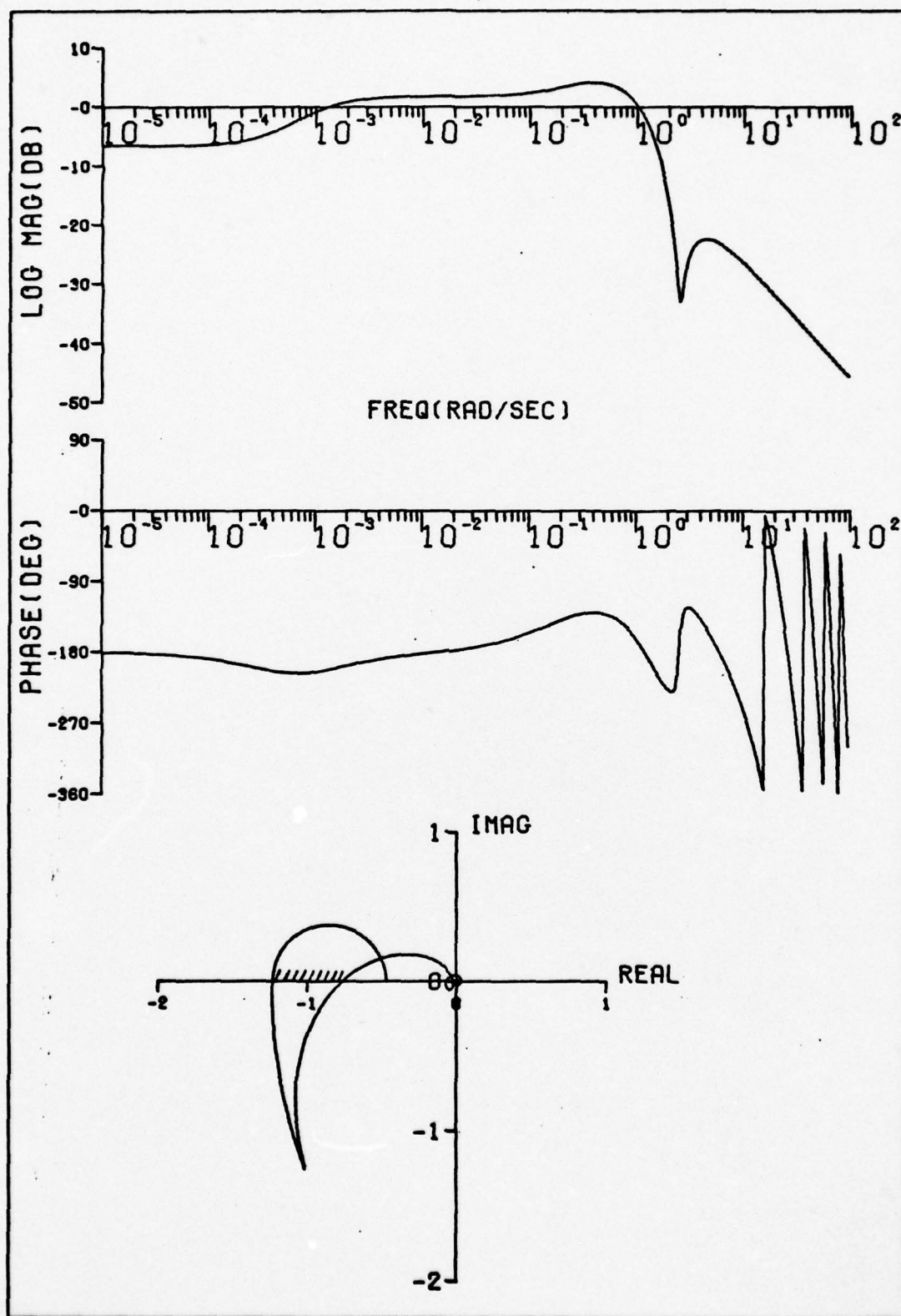


Figure F-7. Bode and Polar Plots of  $Y_{PE} Y_{CE})_{DW}, T_L = 5$ .

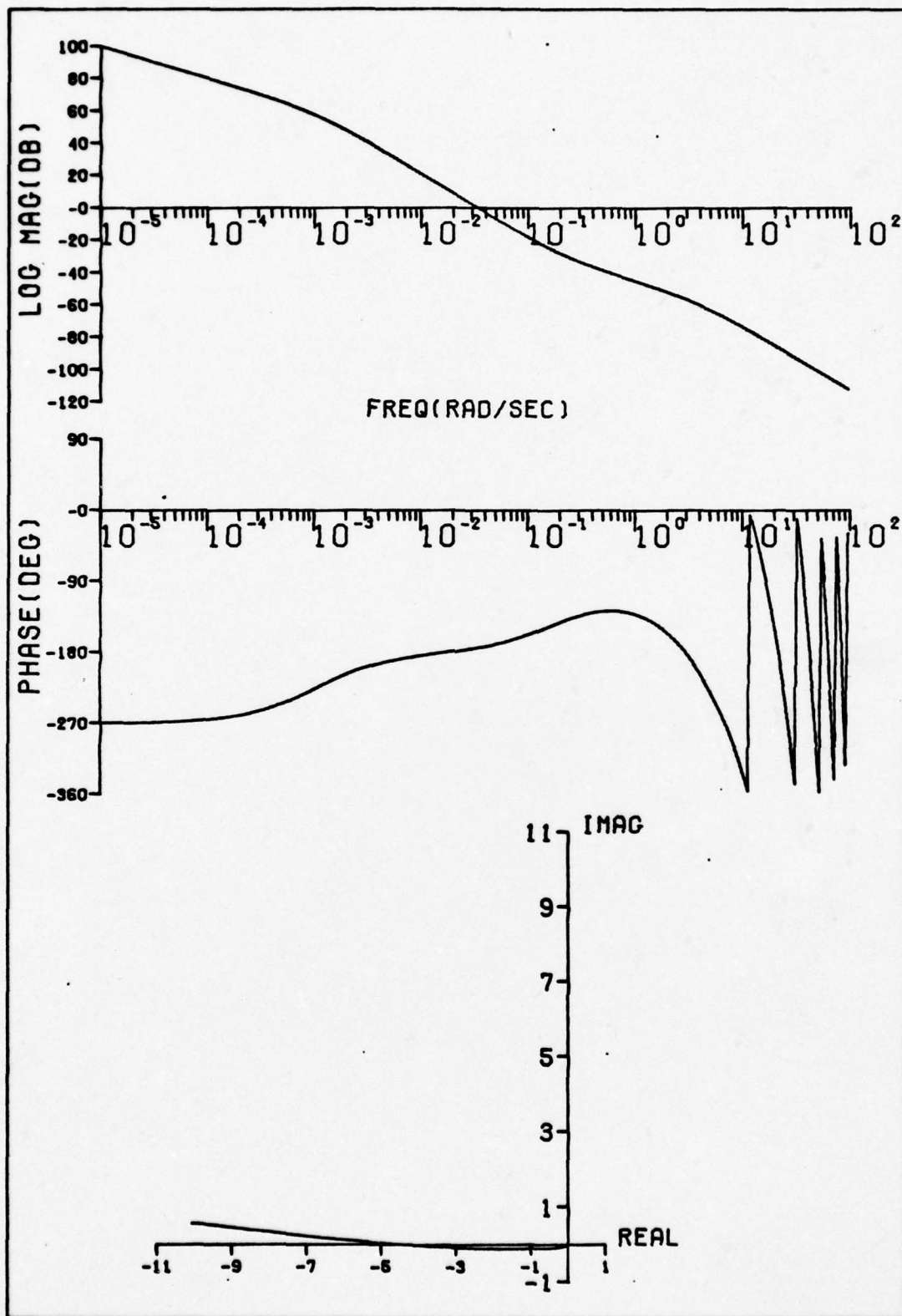


Figure F-8. Bode and Polar Plots of  $Y_{PT c_T}^{Y_{DW}}$ ,  $T_L = 5$ .

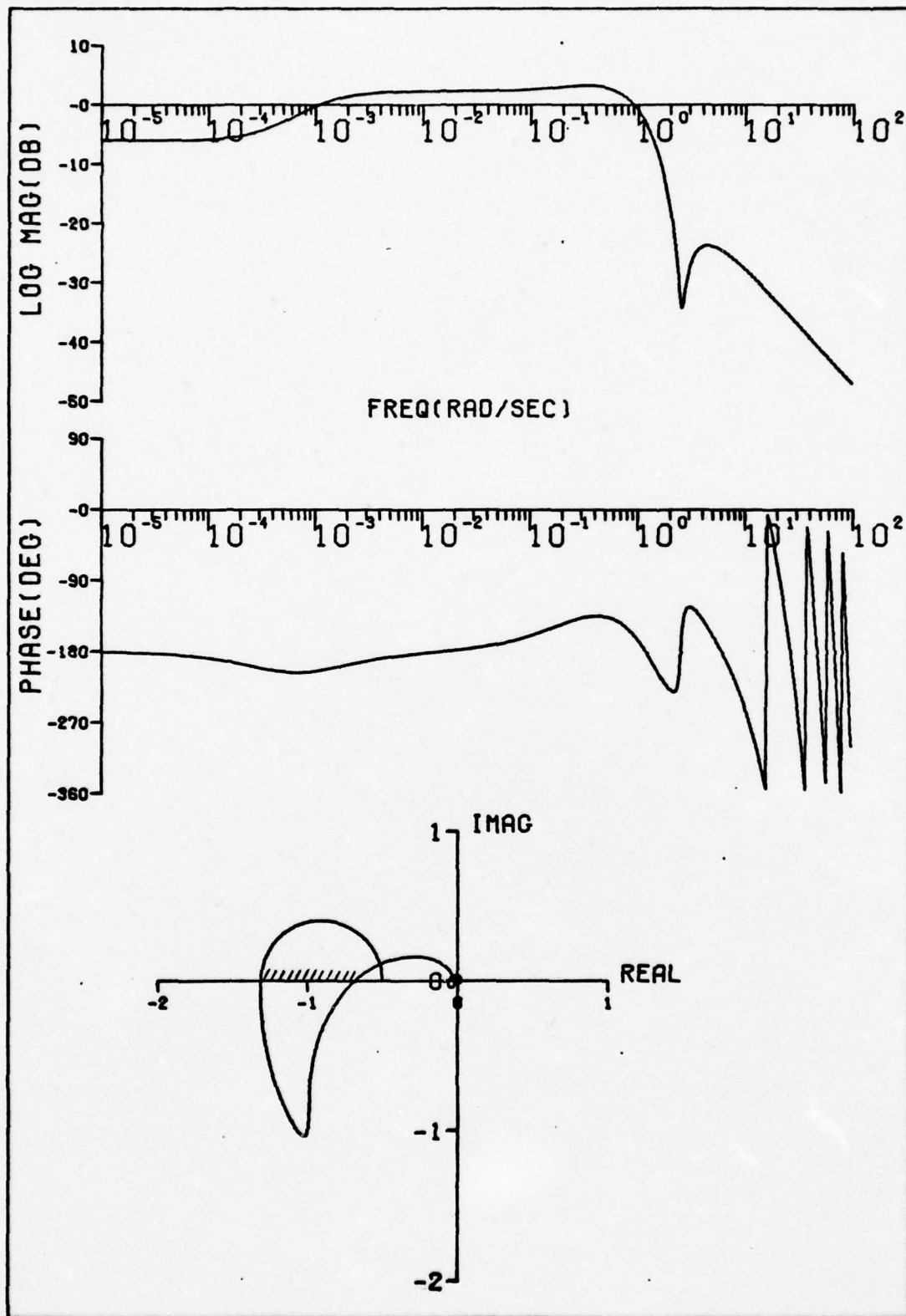


Figure F-9. Bode and Polar Plots of  $Y_{PE} Y_{CE})_{DW}, T_L = 4$ .

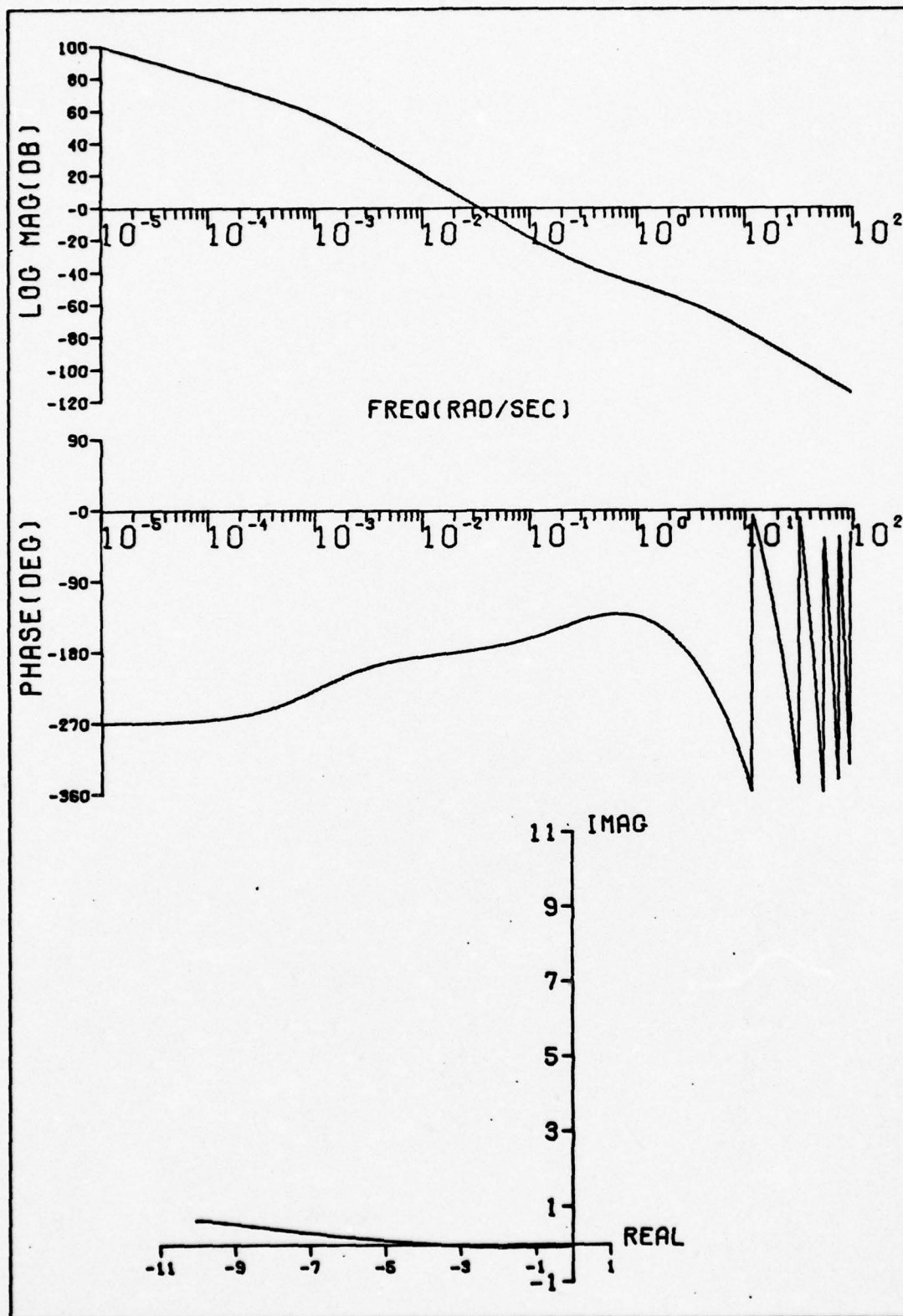


Figure F-10. Bode and Polar Plots of  $Y_{PT C_T DW}$ ,  $T_L = 4$ .



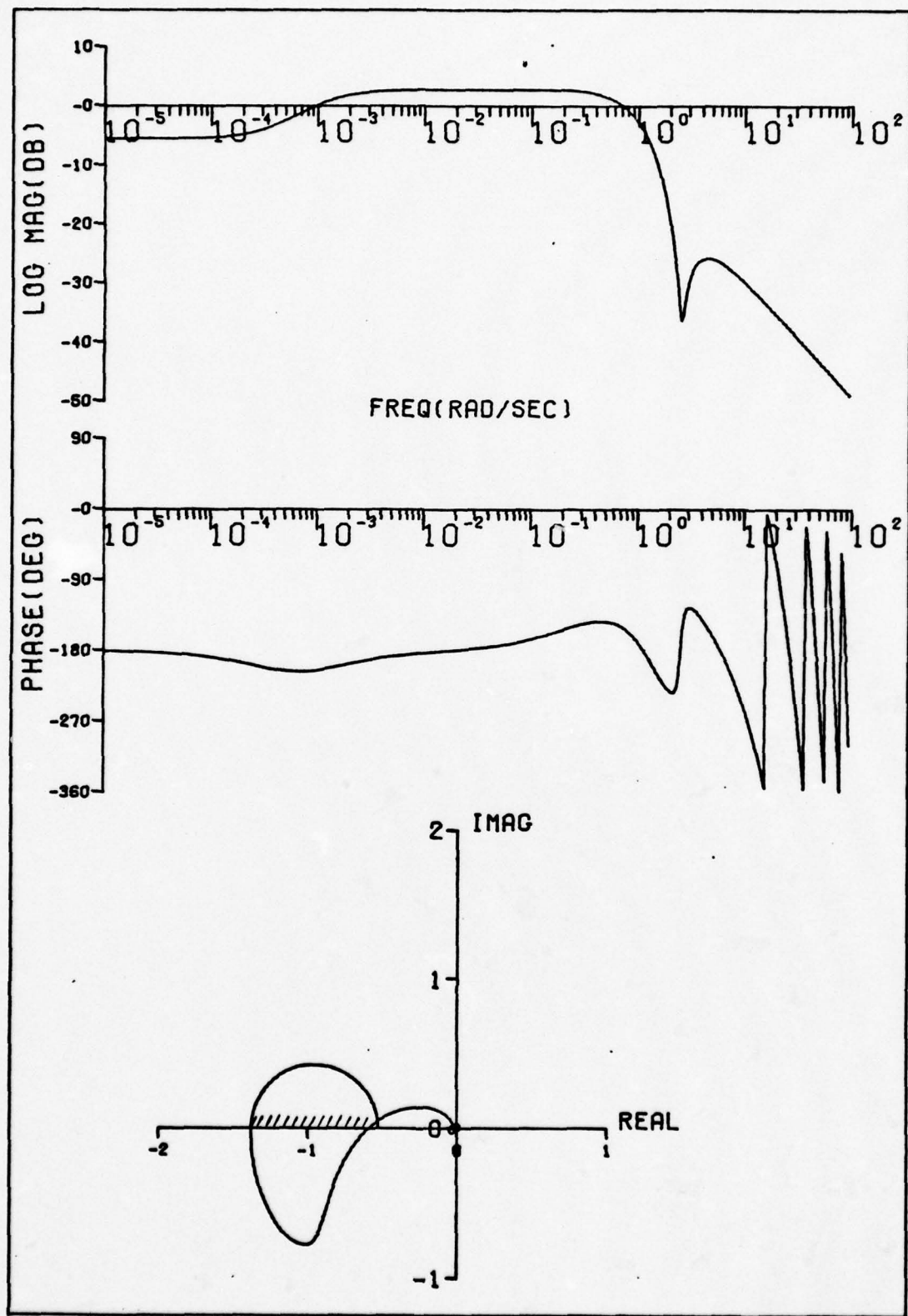


Figure F-11. Bode and Polar Plots of  $Y_{PE} Y_{c_E})_{DW}, T_L = 3$ .

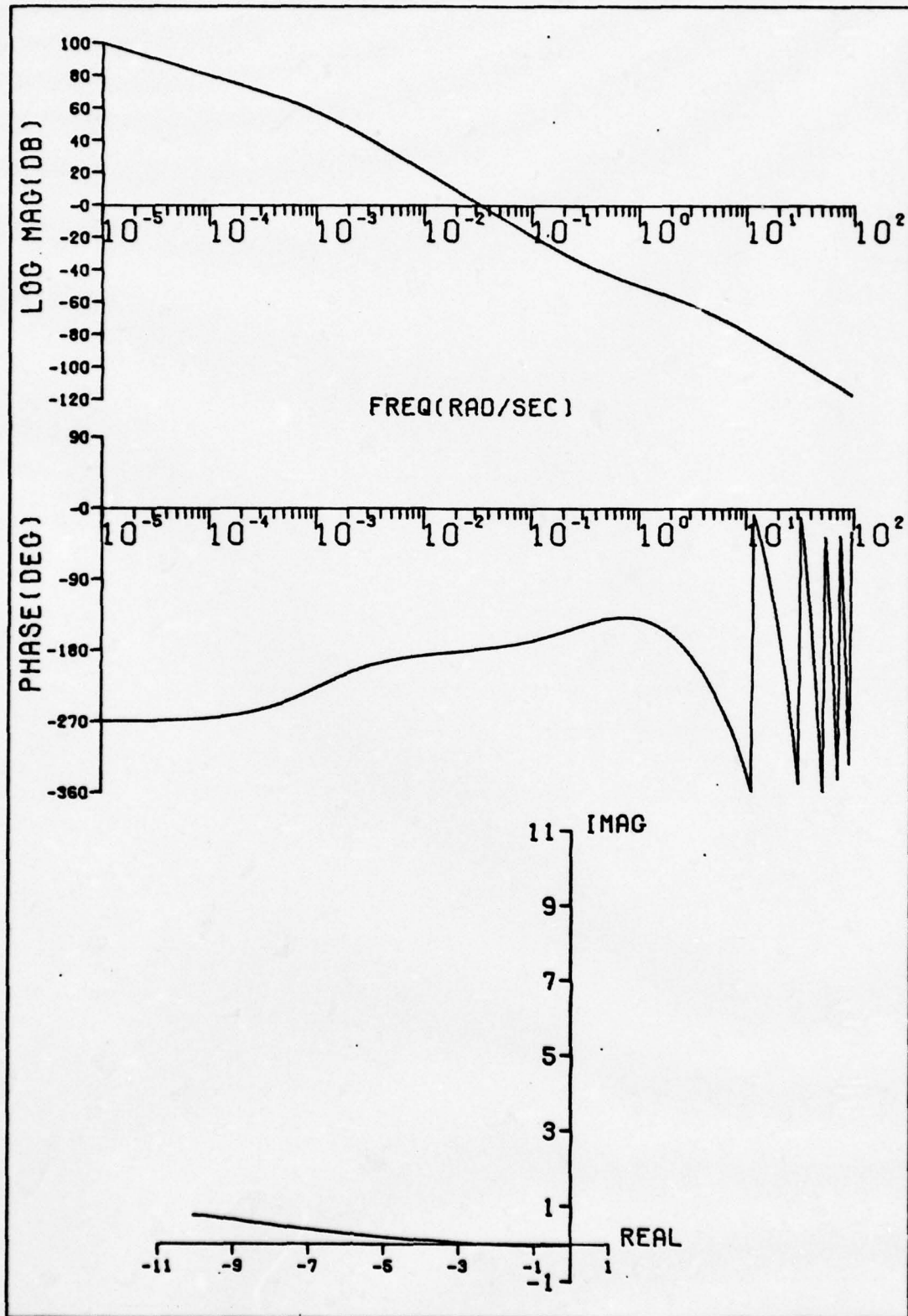


Figure F-12. Bode and Polar Plots of  $Y_{PT} Y_{c_T})_{DW, T_L = 3}$ .

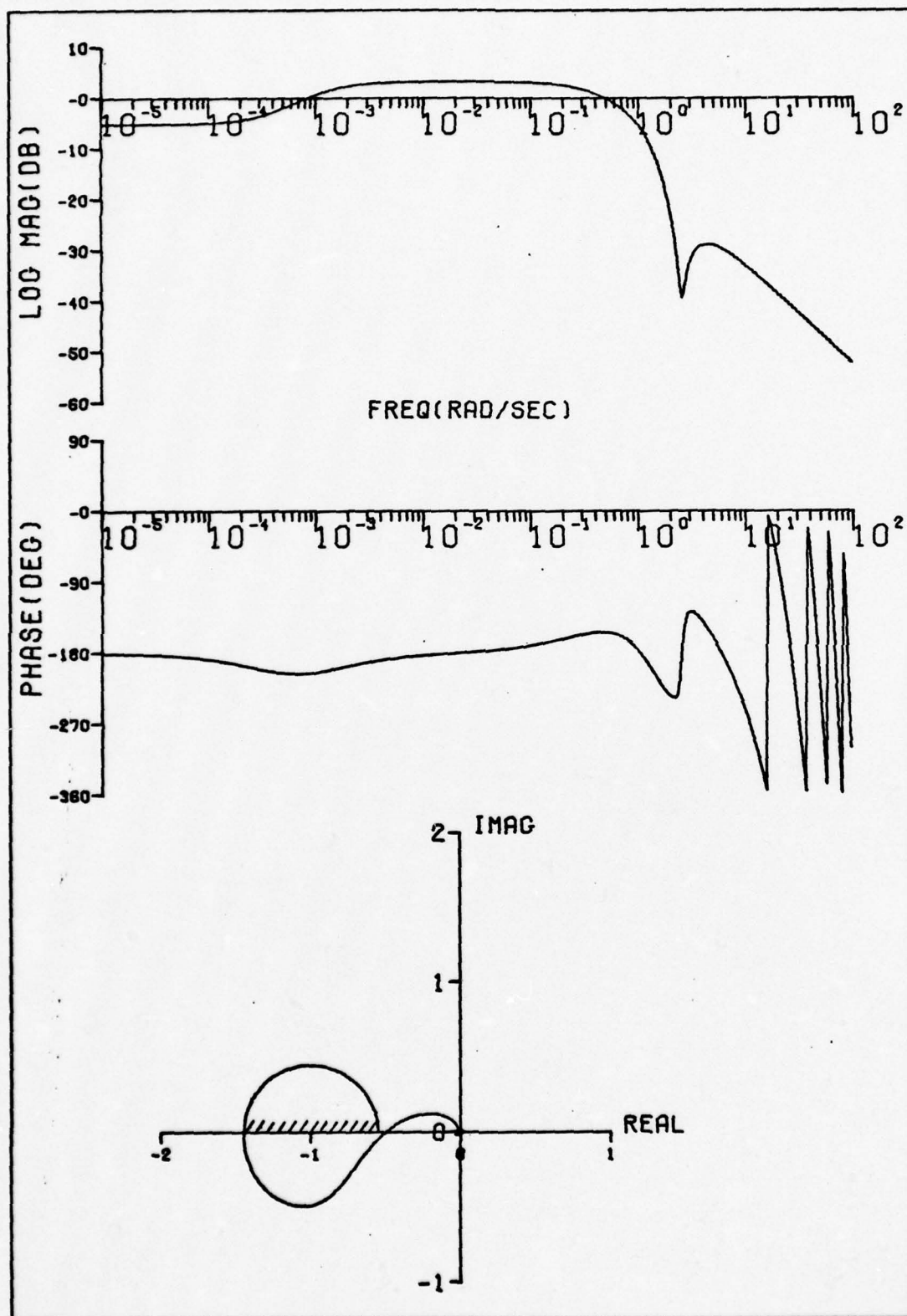


Figure F-13. Bode and Polar Plots of  $Y_{PE C_E}^{(DW)} T_L = 2$ .

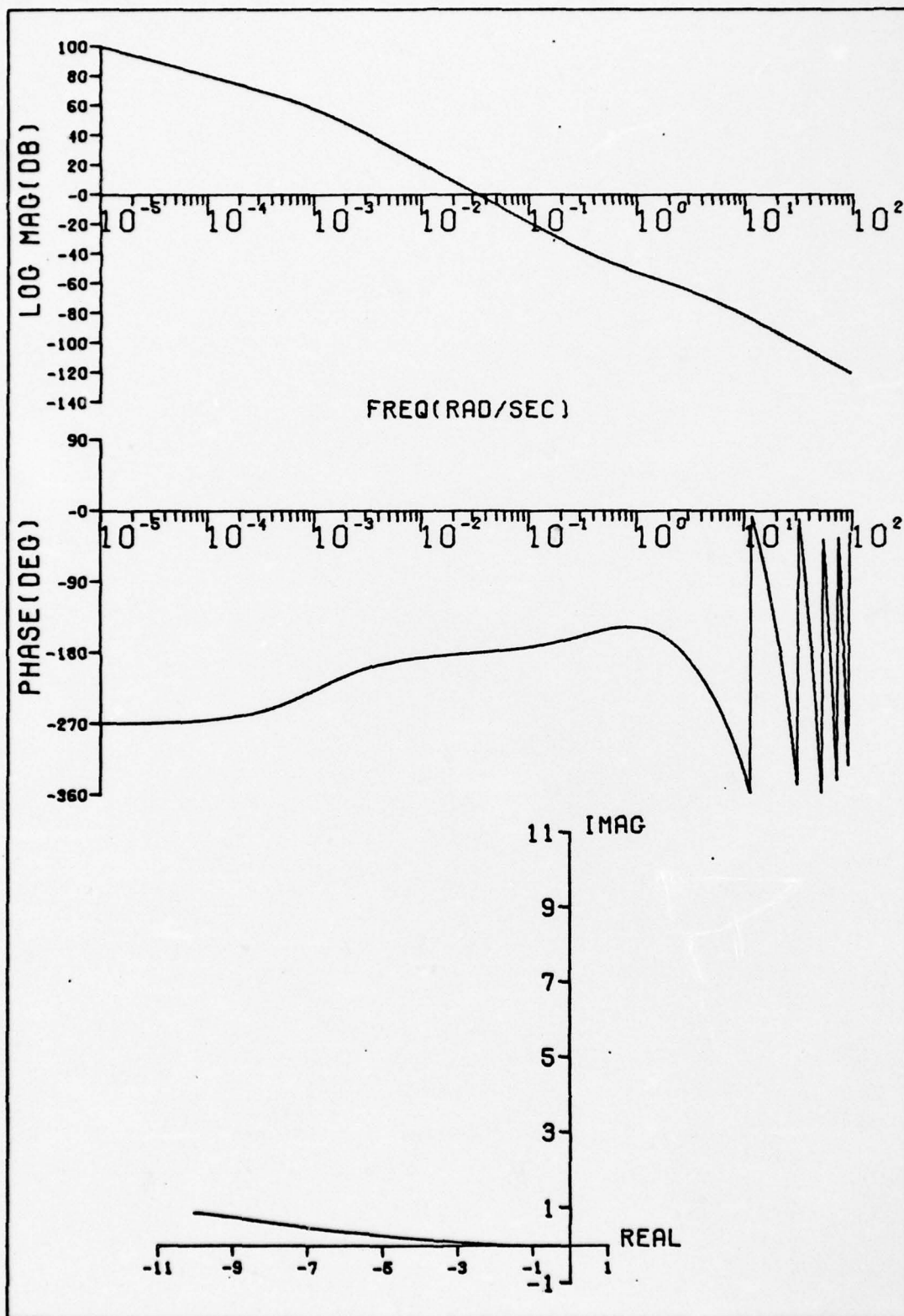


Figure F-14. Bode and Polar Plots of  $Y_{PT} Y_{CT} )_{DW, T_L = 2}$ .



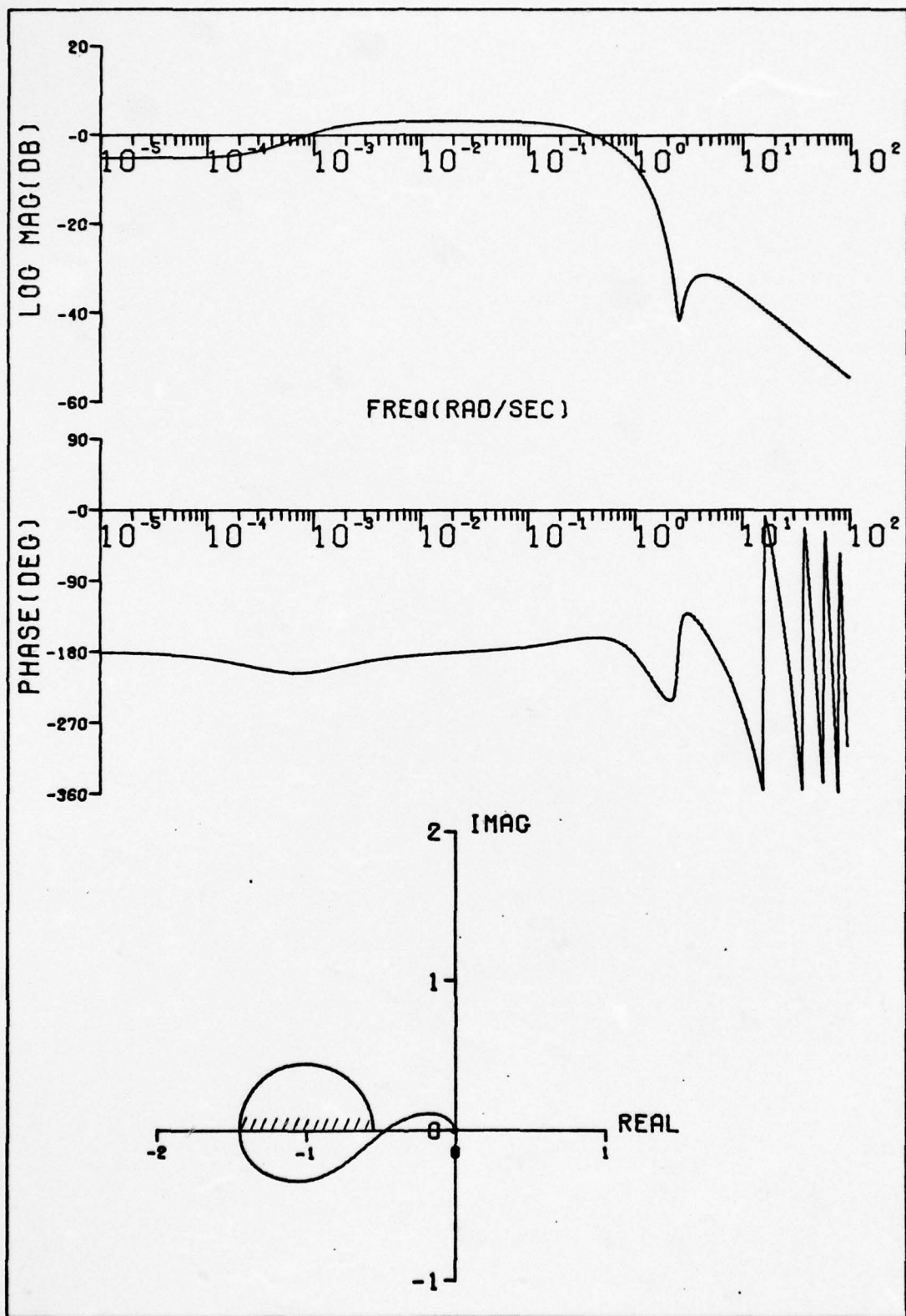


Figure F-15. Bode and Polar Plots of  $Y_{PE c_E} Y_{DW}$ ,  $T_L = 1.5$ .

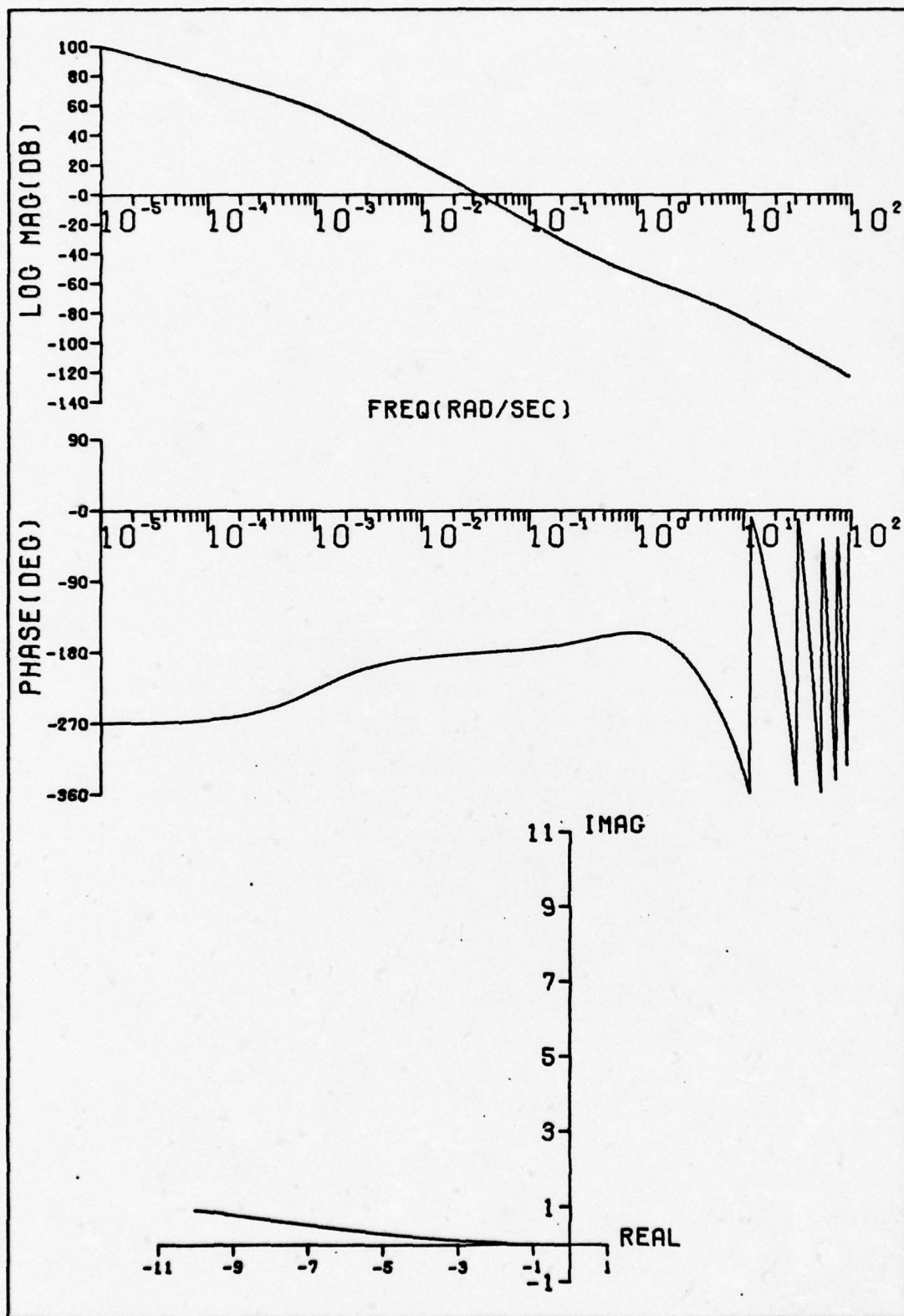


Figure F-16. Bode and Polar Plots of  $Y_{PT} Y_{CT})_{DW, T_L = 1.5}$ .

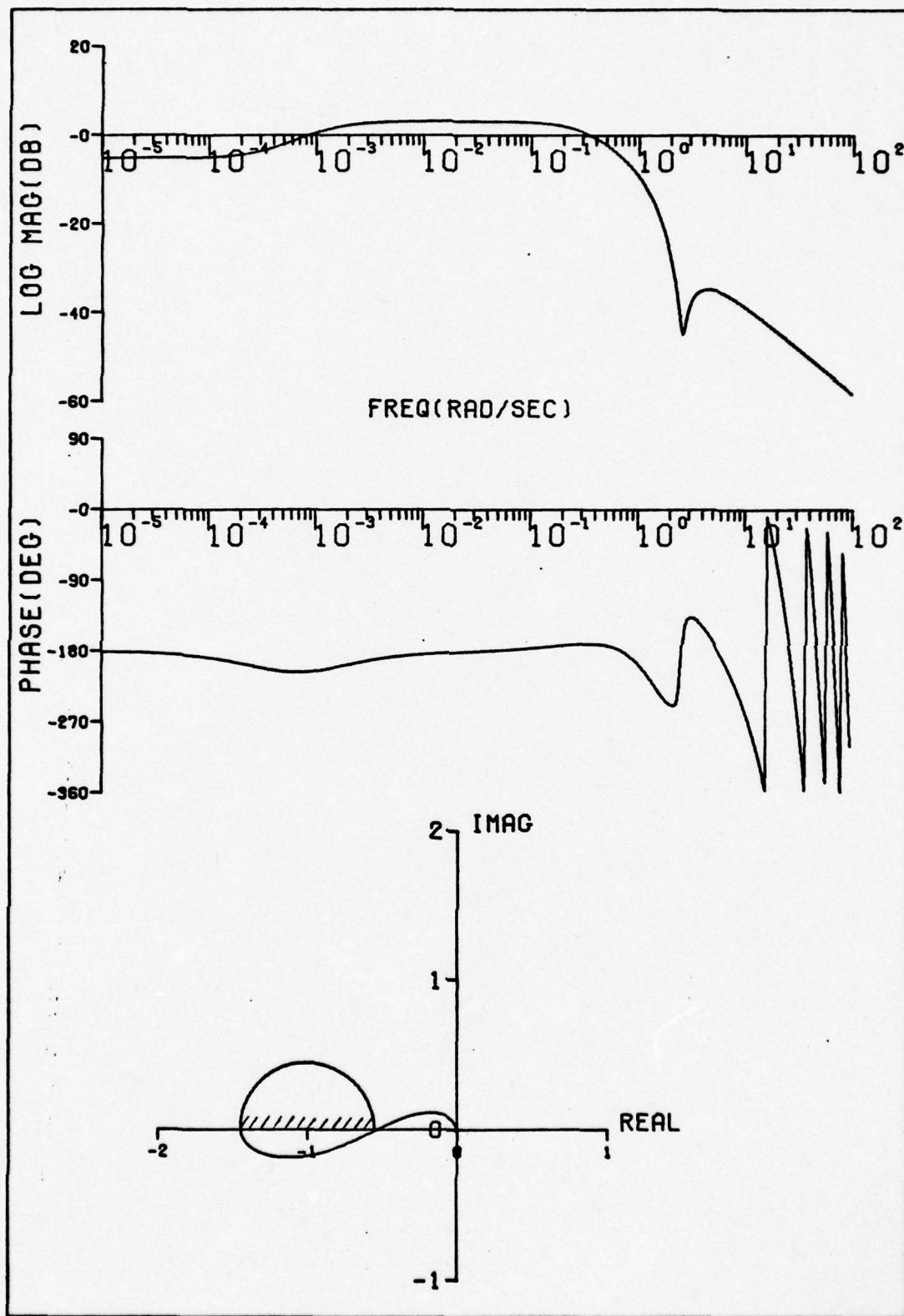


Figure F-17. Bode and Polar Plots of  $Y_{PE} Y_{c_E})_{DW}, T_L = 1$ .

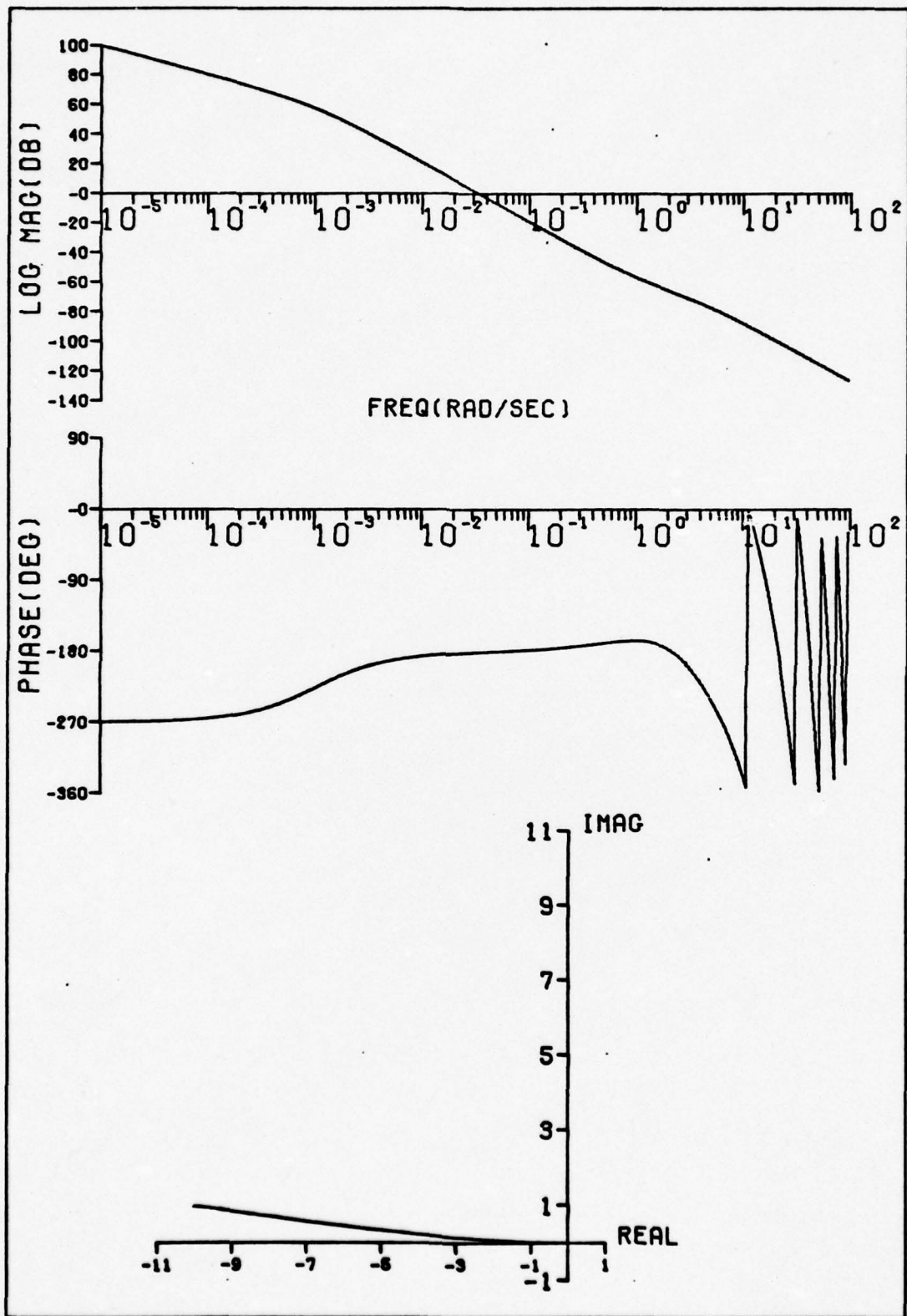


Figure F-18. Bode and Polar Plots of  $Y_{PT c_T}^{Y_{DW}}$ ,  $T_L = 1$ .



## APPENDIX G

### Analog Patching Diagram

The scaled analog patching diagram is shown in Figure G-1.  
Table X lists the potentiometer settings.

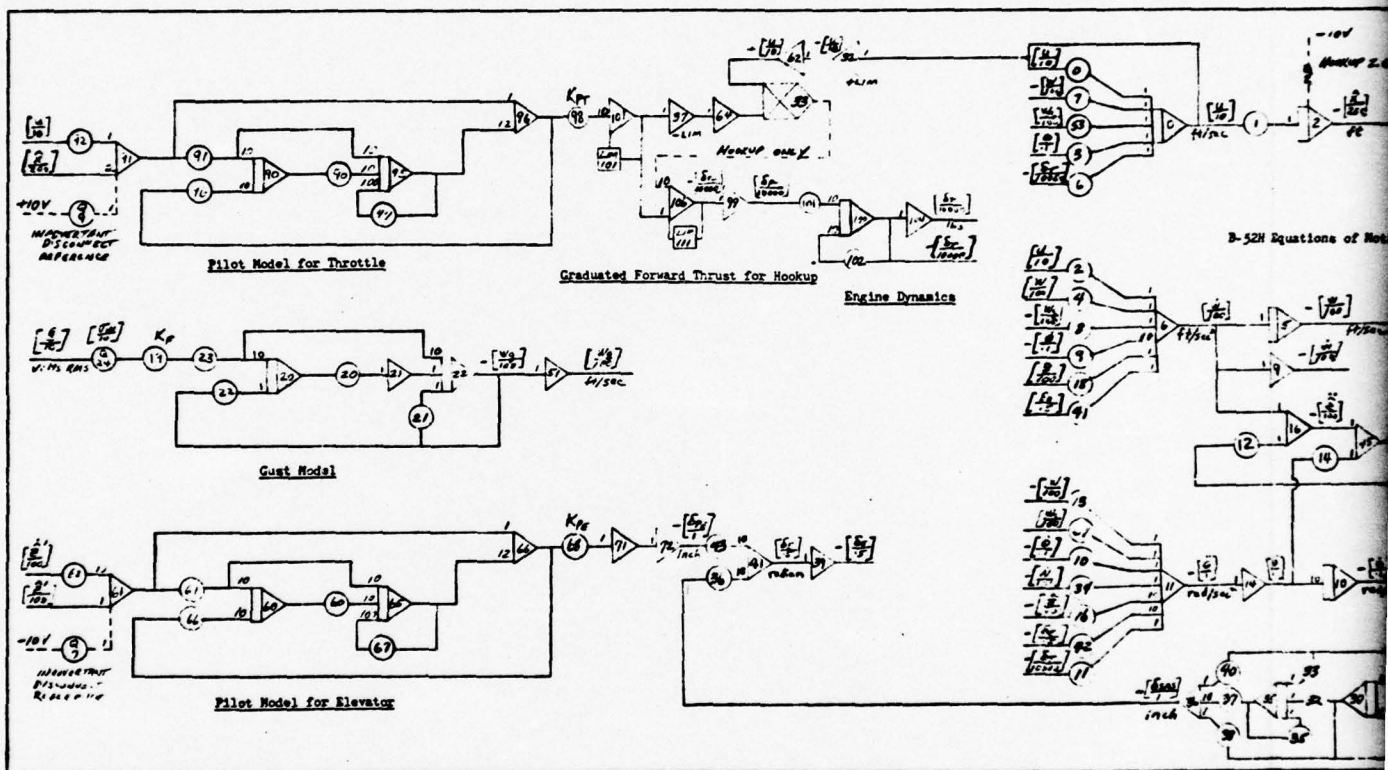


Figure G-1. Analog Patching Diagram.

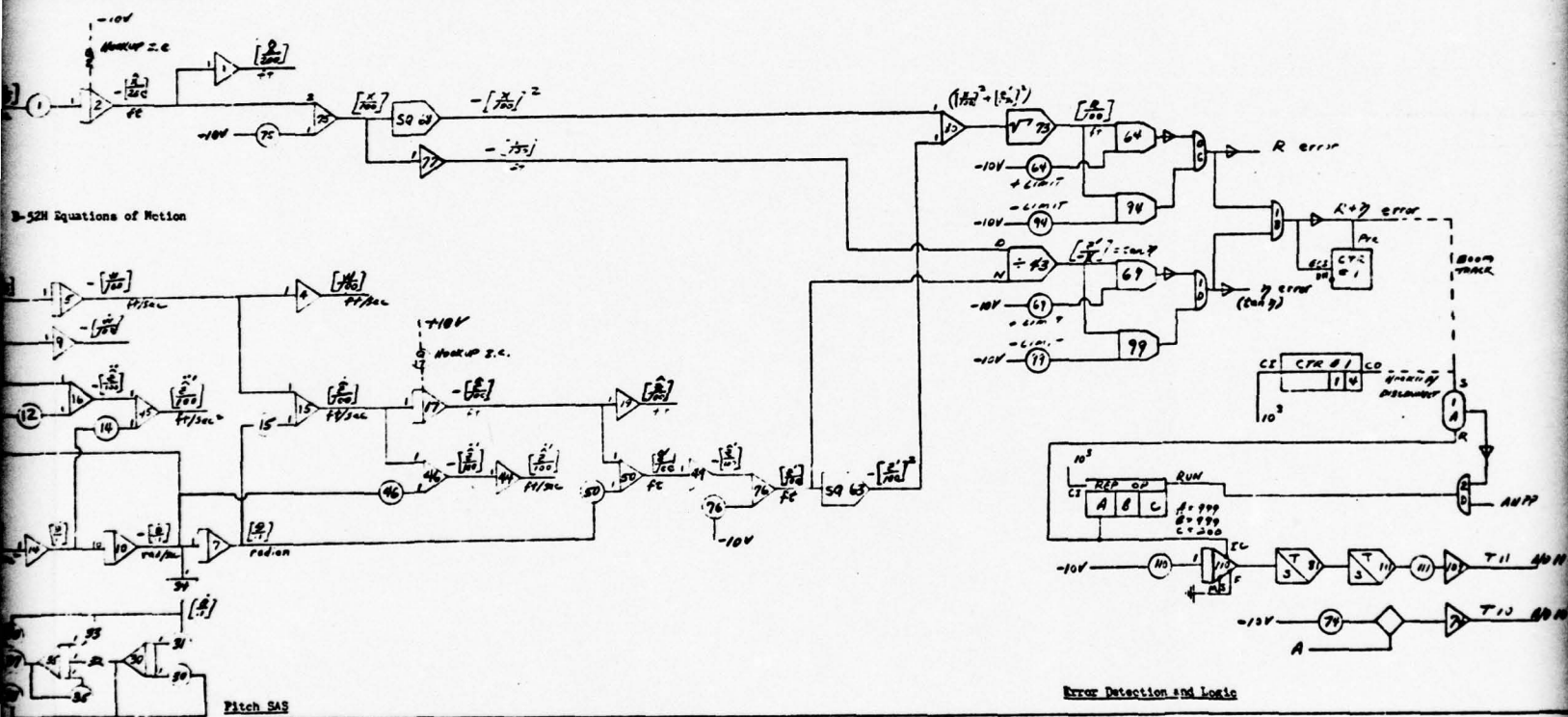


Table X  
Analog Potentiometer Settings

<u>Pot</u>	<u>Setting</u>	<u>Pot</u>	<u>Setting</u>	<u>Pot</u>	<u>Setting</u>
0	.0045	32	.2500	74	.1000
1	.0500	33	.2500	75	.3447
2	.0091	34	.0141	76	.1990
3	.3220	35	.2500	90	.3333
4	.4117	36	.1863	91	.3333
6	.0715	37	.0108	92	$T_L/10$
7	.2548	38	.1082	94	.3779 hookup .3367 boom track .8500 disconnect
8	.4117	40	.1082		
9	.0701	41	.0407	96	.3333
10	.0906	42	.0314	97	.2000
11	.0034	43	.1863	98	$K_{PT}/10000$
12	.7060	46	.0540	99	.4663 hookup .3640 boom track .2679 disconnect
13	.2734	50	.0540		
14	.5400	51	.2734	101	.4000
15	.7060	53	.2548	102	.4000
16	.0228	60	.3333	103	.1000
18	.0647	61	.3333	110	.5000
19	.3209	62	$T_L/10$	111	.1414
20	.2331	64	.4179 hookup .4592 boom track .9500 disconnect	Q2	.2500
21	.8065			Q7	.1000
22	.6975	66	.3333	Q9	.2500
23	.6196	67	.2000	Q17	.1000
30	.1500	68	$100 K_{PE}$	Q24	$\sigma_w/10$
31	.1500	69	.7002 hookup .8391 boom track .4663 disconnect		



## APPENDIX H

### Plots of Components of Mean Refueling Time

The components of mean refueling time--hookup time, time-on-boom, and inadvertant disconnect time-- are presented here as functions of gust intensity with  $T_L$ , radiation dose, and thrust authority as additional parameters. The plots of inadvertant disconnect times depict sketchy information due to the fact that the inadvertant disconnect procedure usually was simulated only when required for Eq (58).

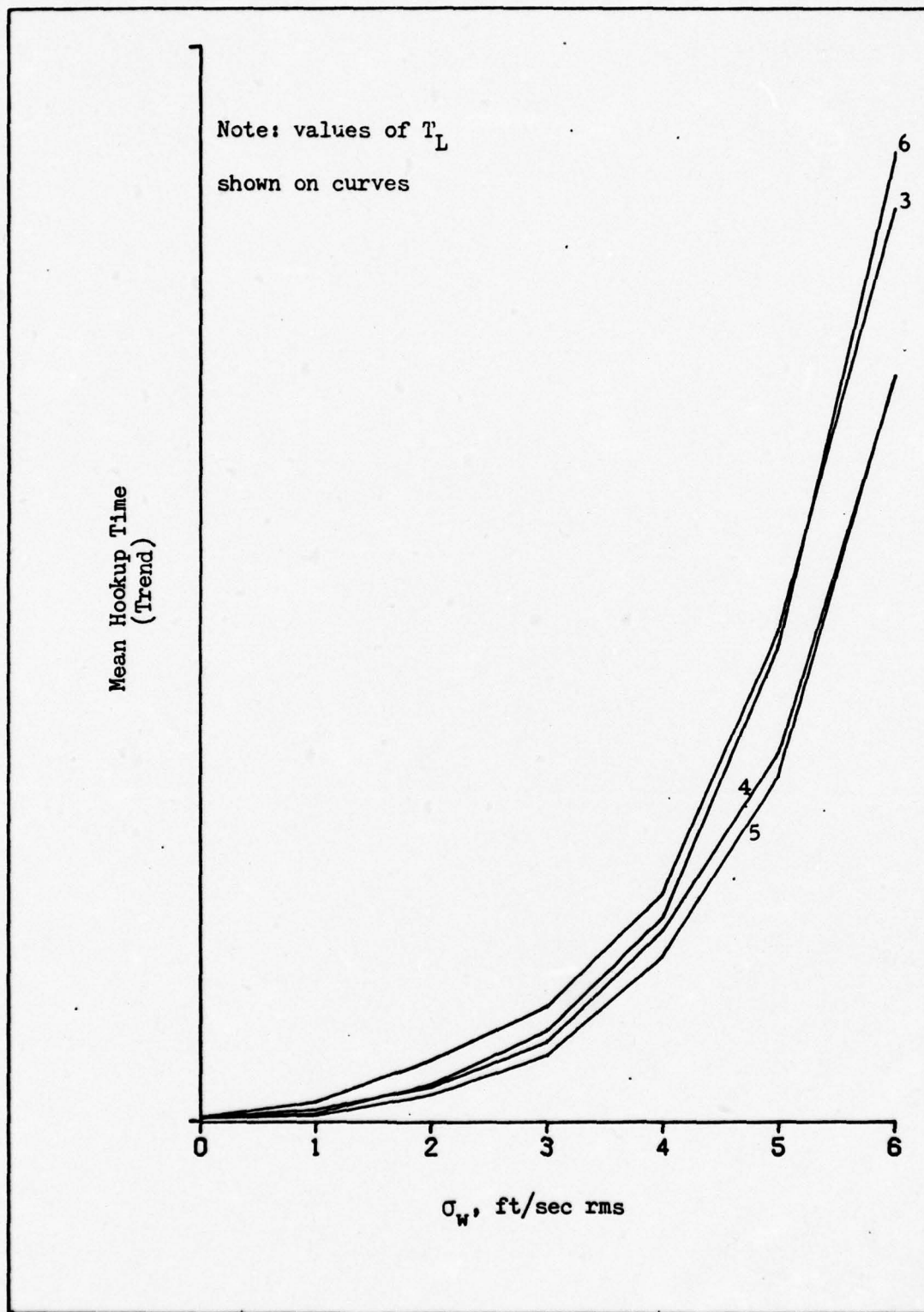


Figure H-1. Mean Hookup Time vs. Gust Intensity for 0 Rads, Thrust Authority A.

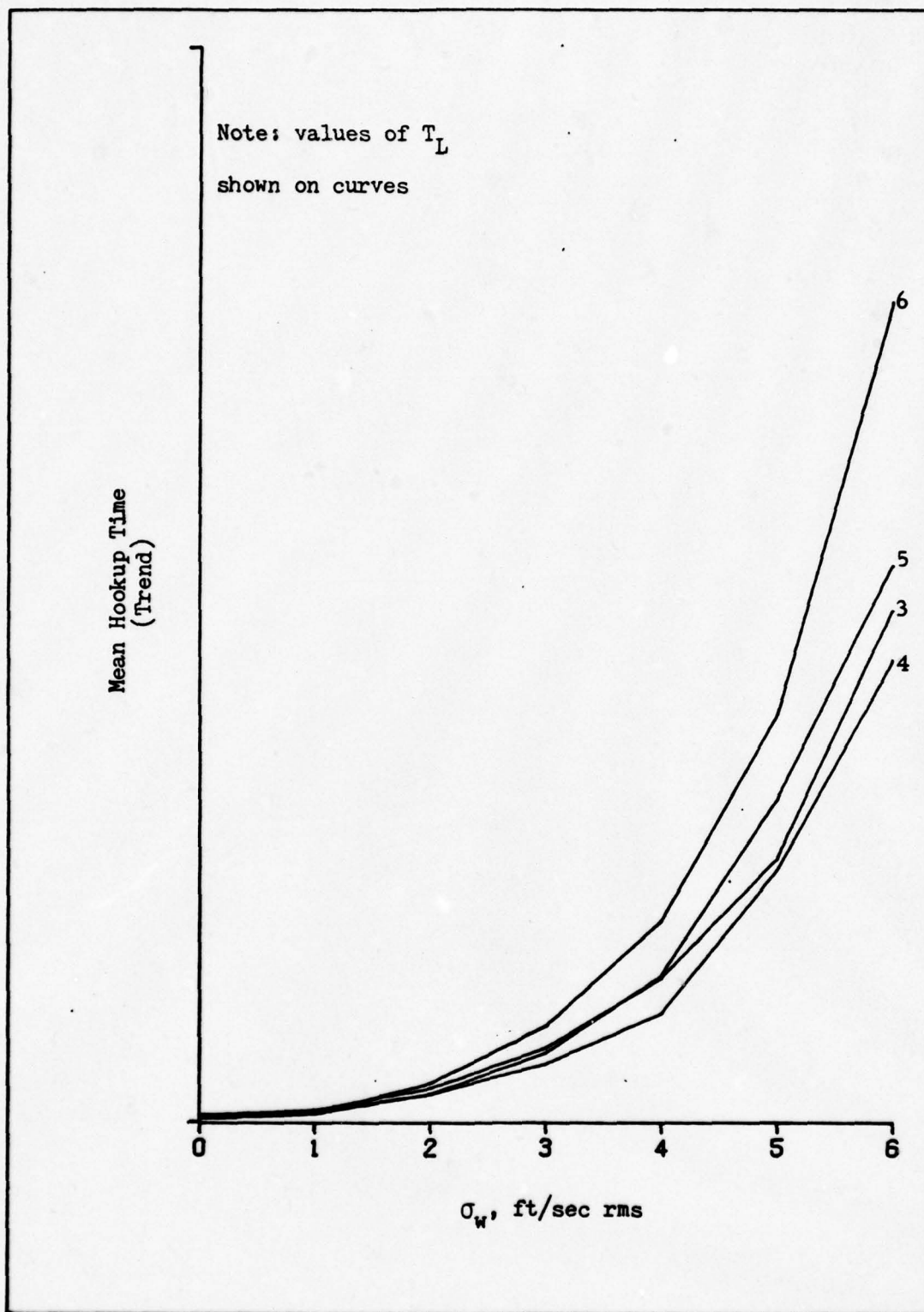


Figure H-2. Mean Hookup Time vs. Gust Intensity for 0 Rads, Thrust Authority B.

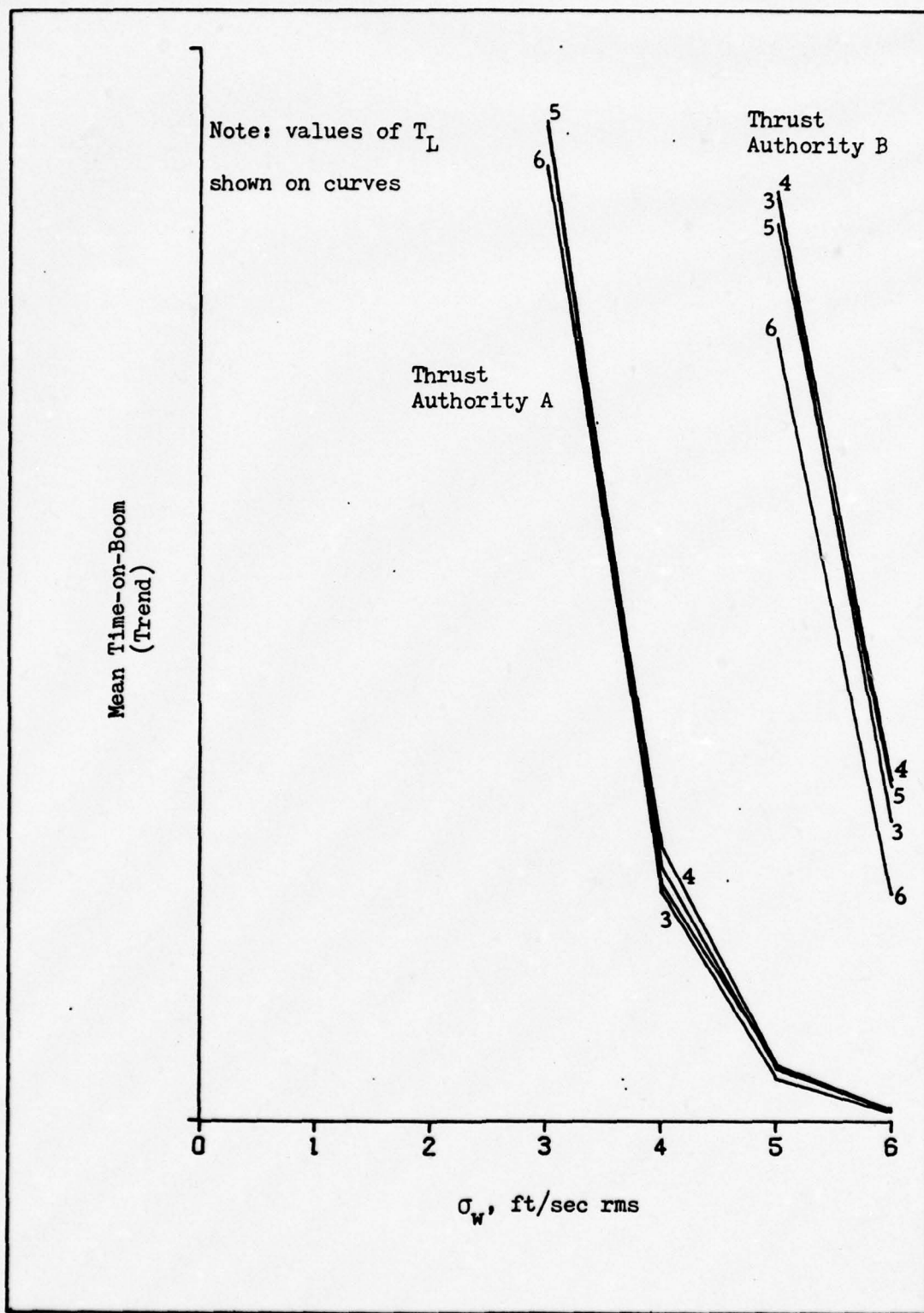


Figure H-3. Mean Time-on-Boom vs. Gust Intensity for 0 Rads.



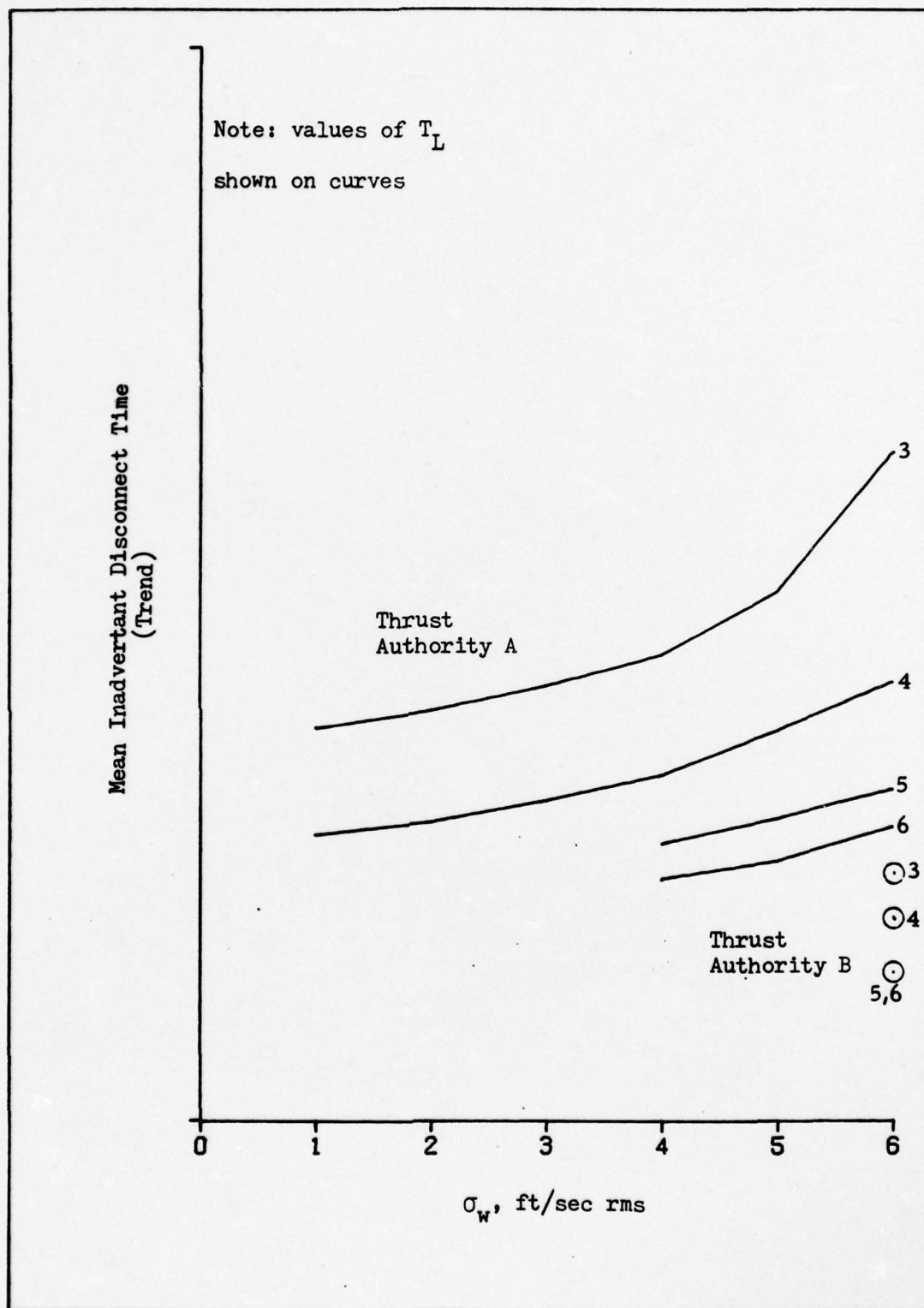


Figure H-4. Mean Inadvertant Disconnect Time vs. Gust Intensity for 0 Rads.

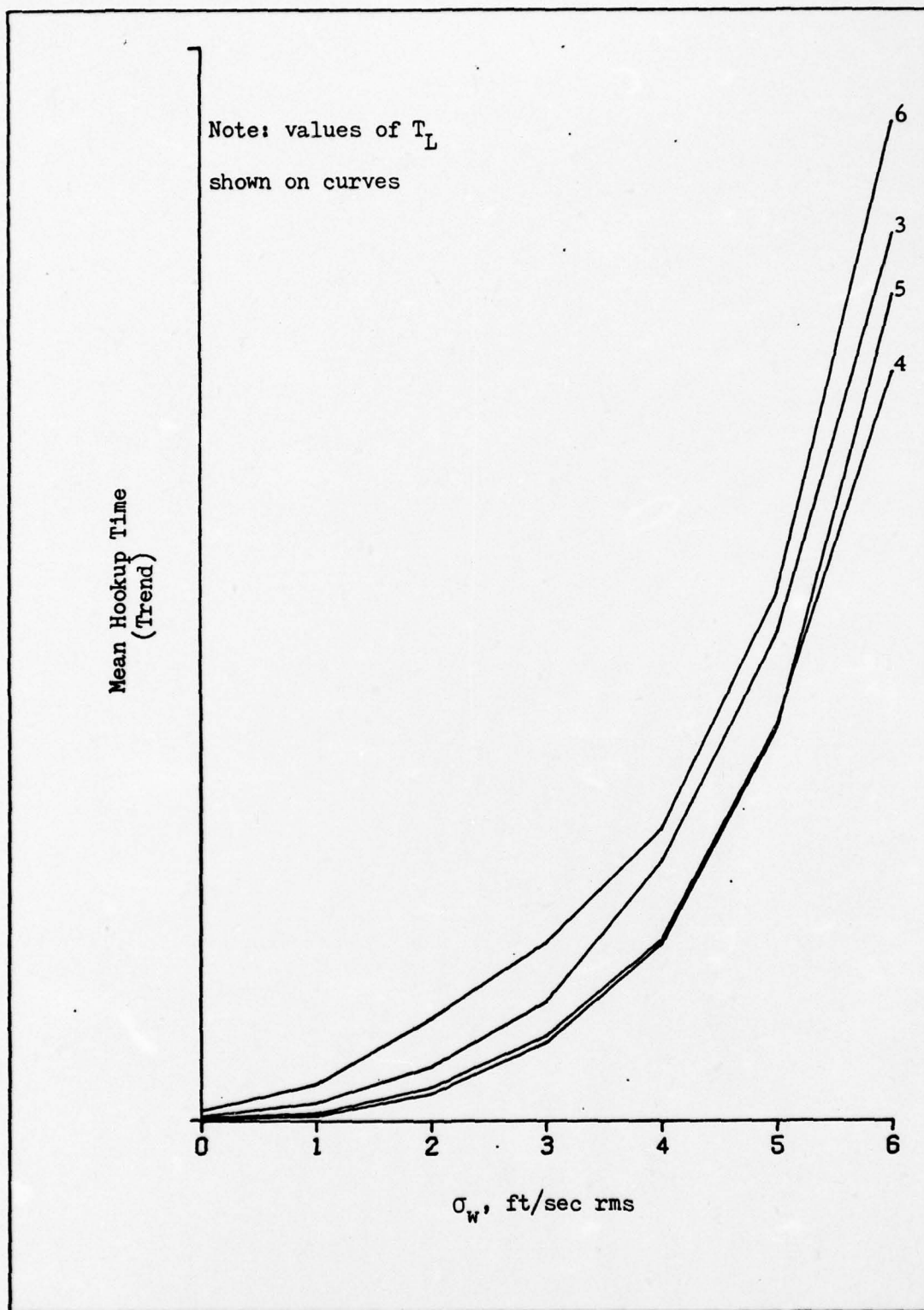


Figure H-5. Mean Hookup Time vs. Gust Intensity for 500 Rads, Thrust Authority A.

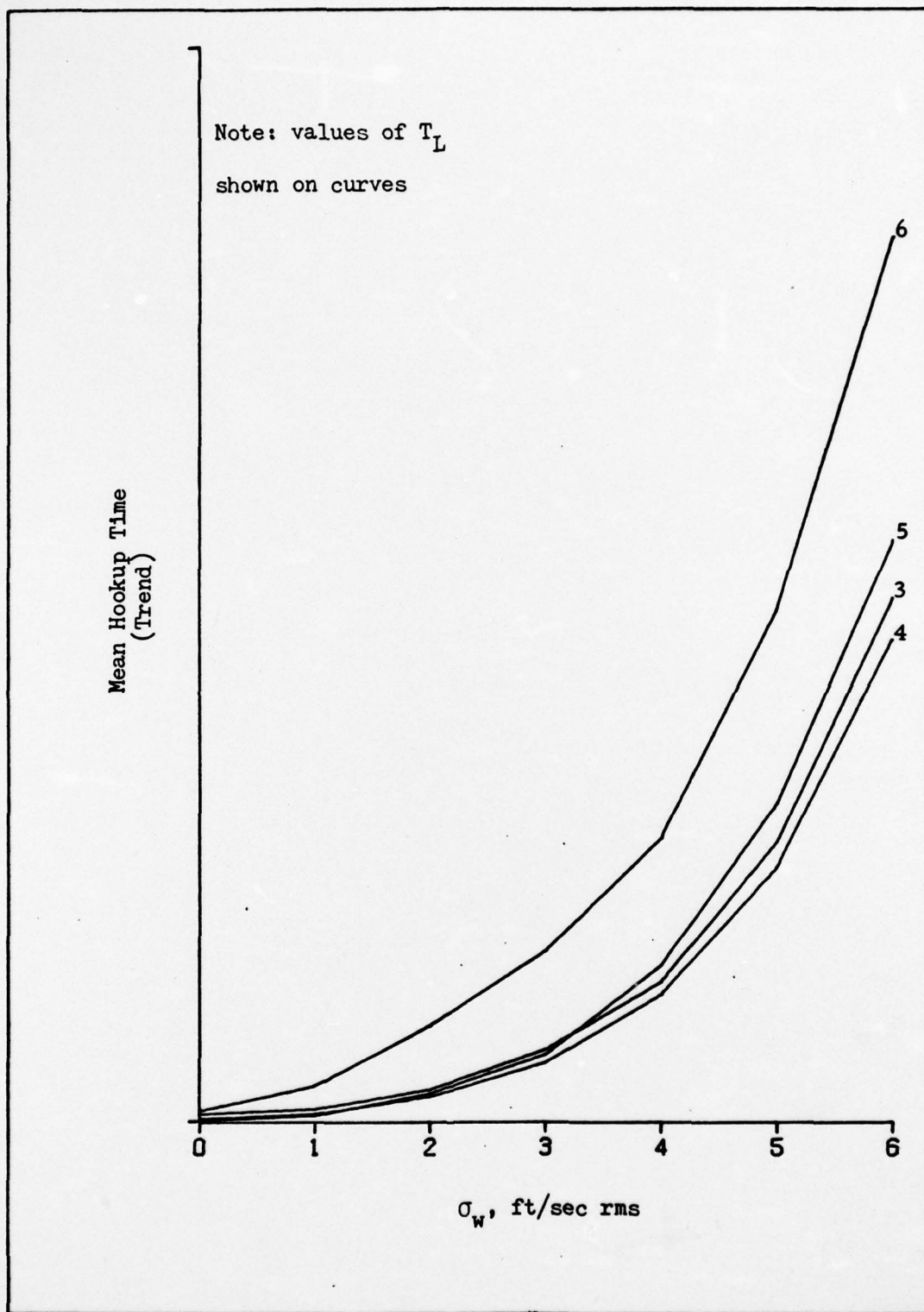


Figure H-6. Mean Hookup Time vs. Gust Intensity for 500 Rads, Thrust Authority B.

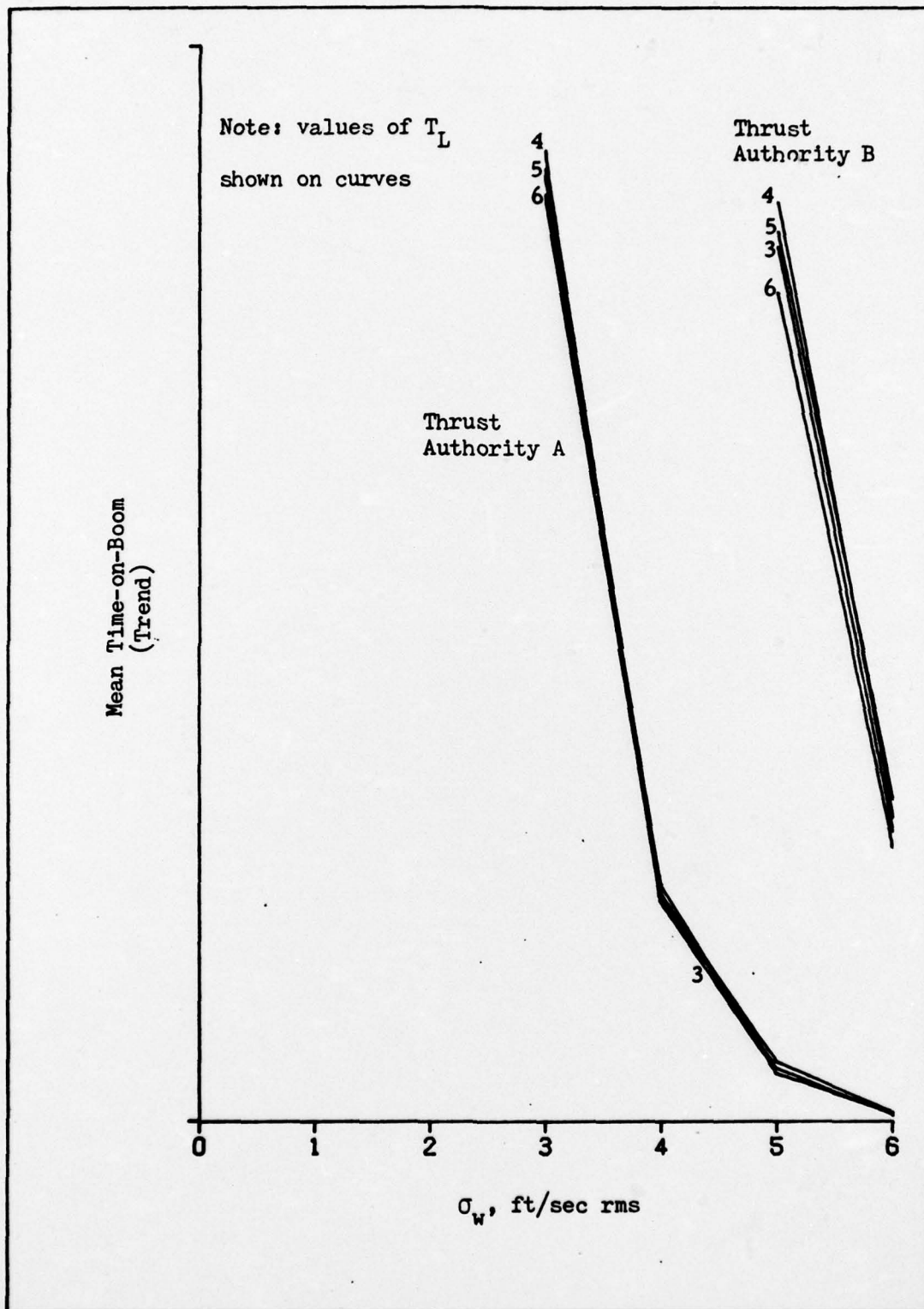


Figure H-7. Mean Time-on-Boom vs. Gust Intensity for 500 Rads.



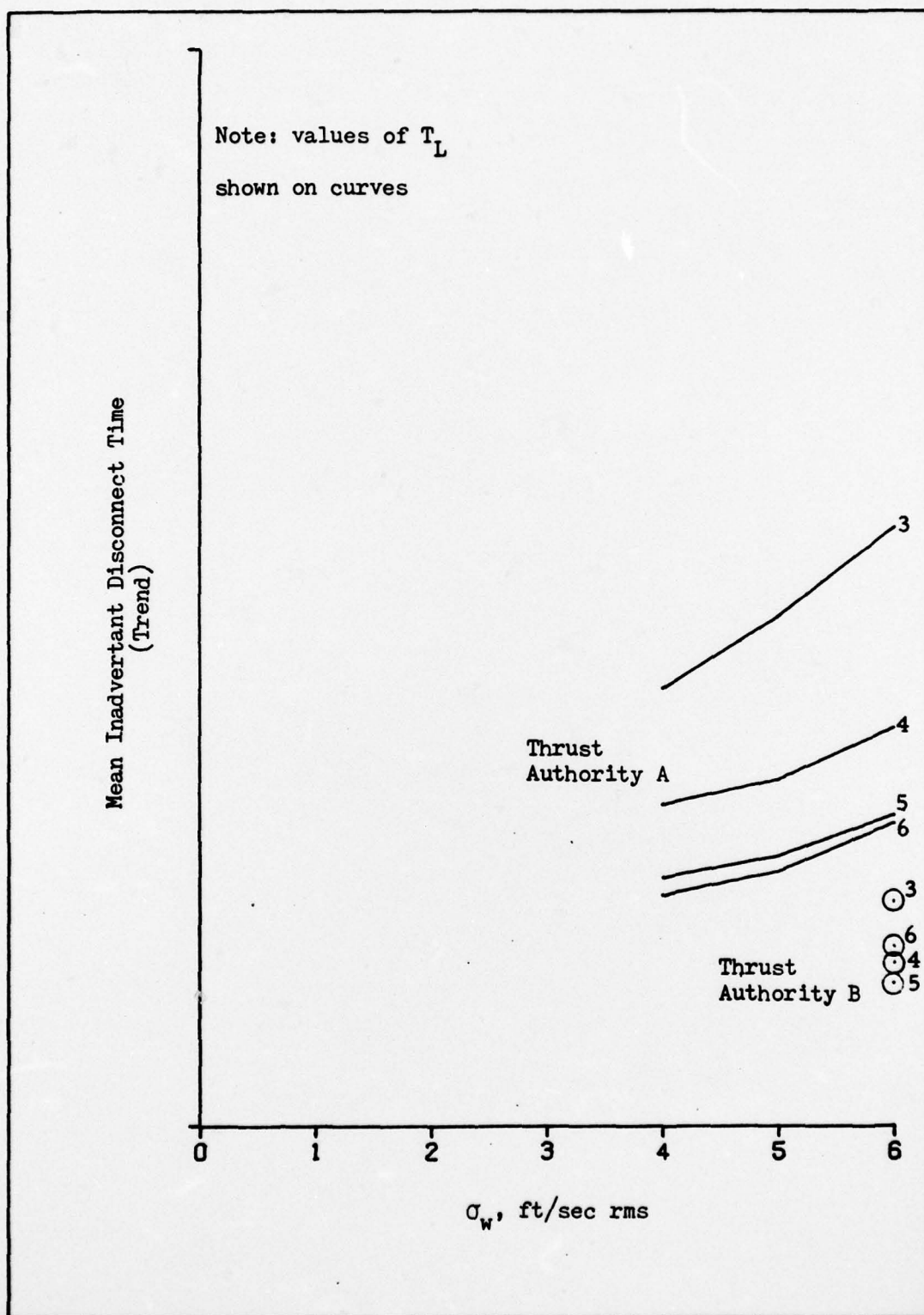


Figure H-8. Mean Inadvertant Disconnect Time vs. Gust Intensity for 500 Rads.

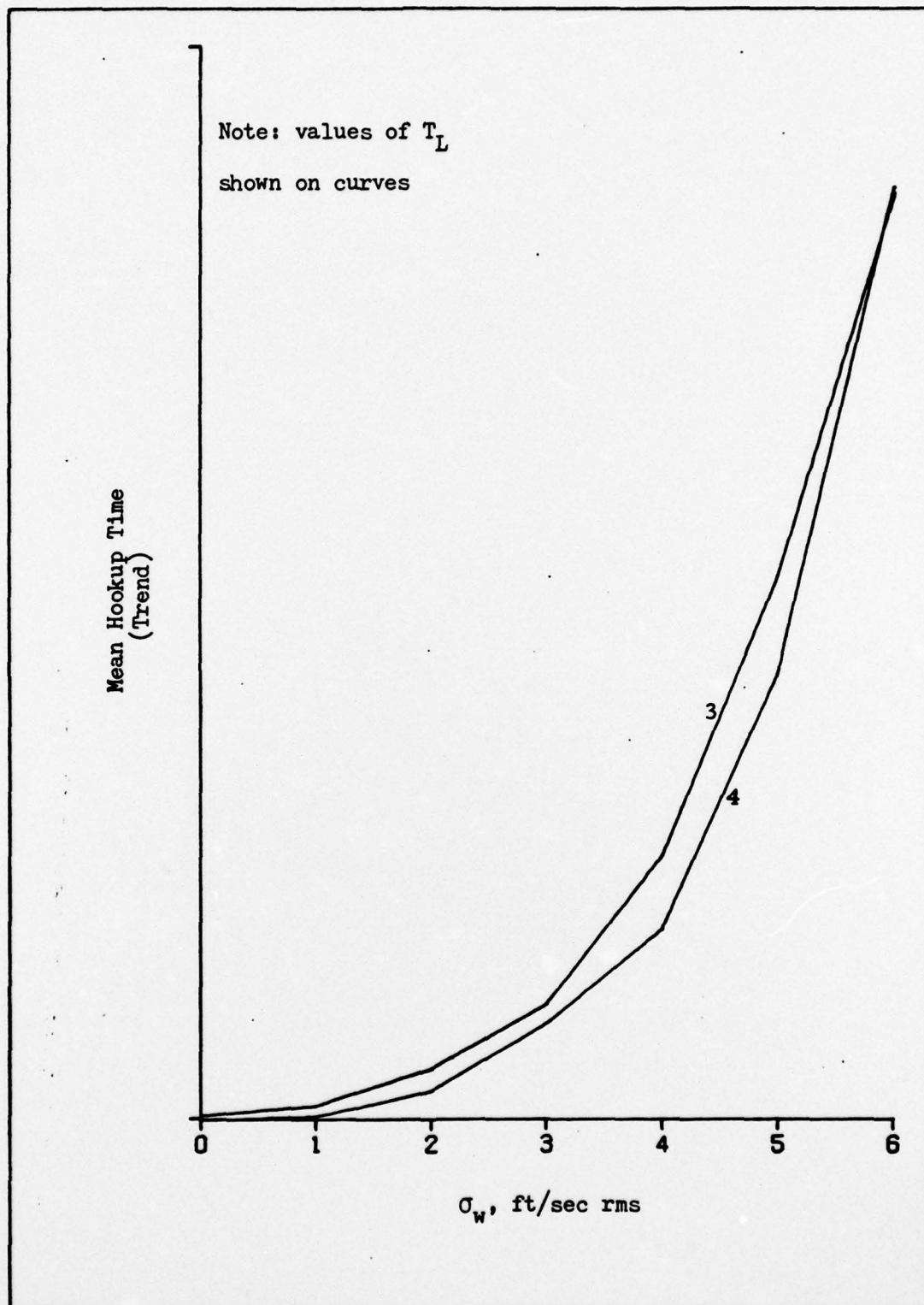


Figure H-9. Mean Hookup Time vs. Gust Intensity for 1000 Rads, Thrust Authority A.

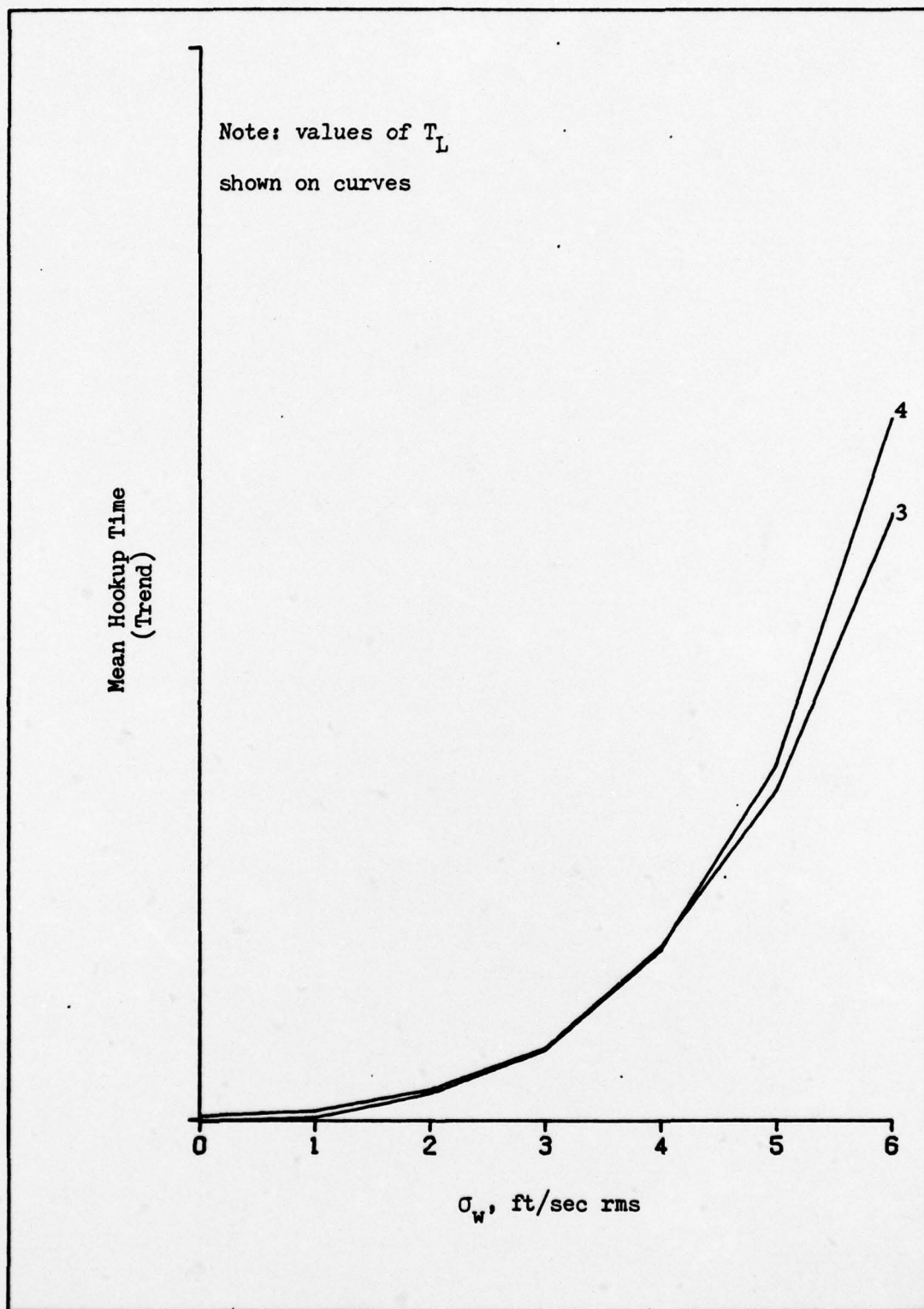


Figure H-10. Mean Hookup Time vs. Gust Intensity for 1000 Rads, Thrust Authority B.

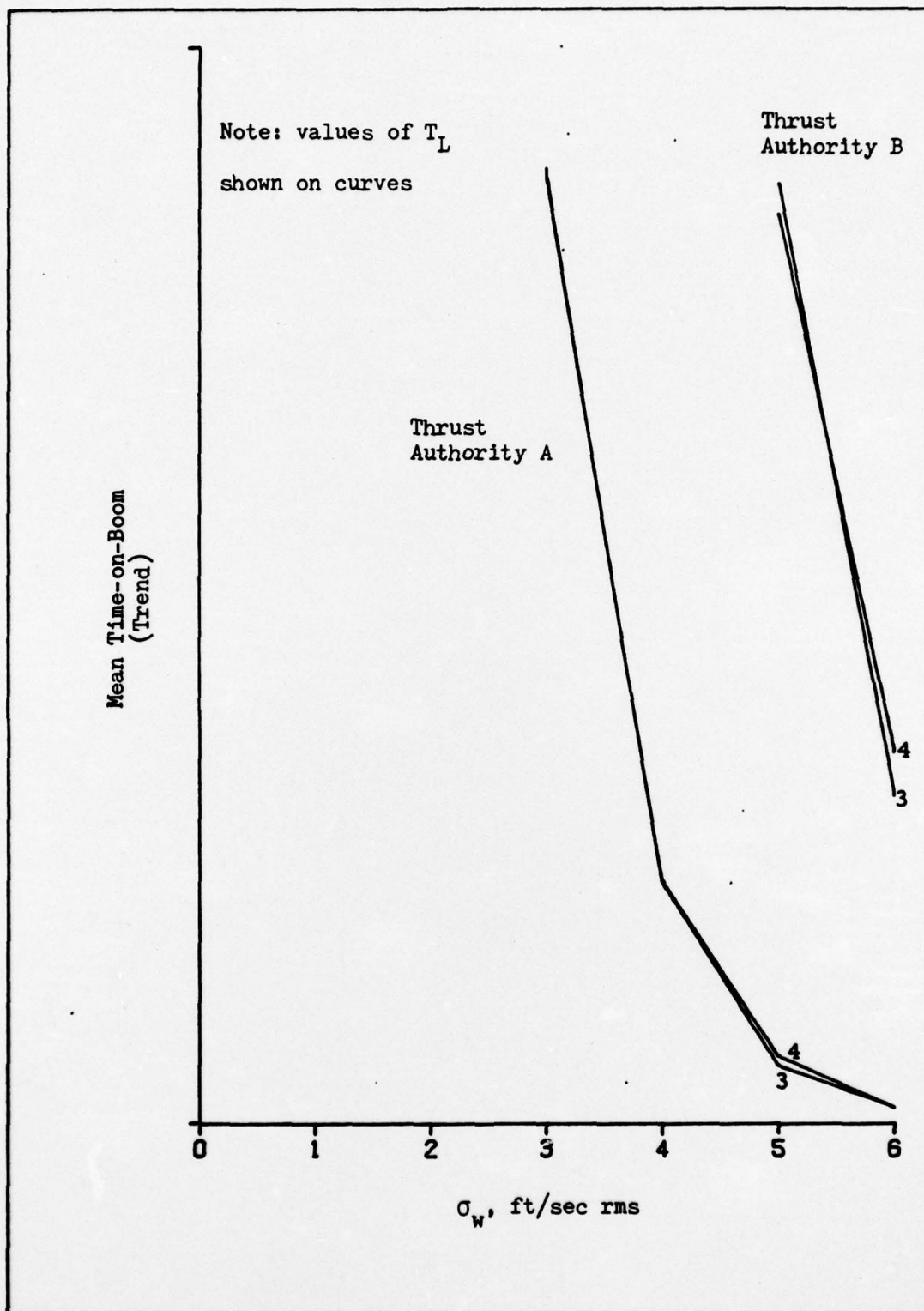


Figure H-11. Mean Time-on-Boom vs. Gust Intensity for 1000 Rads.



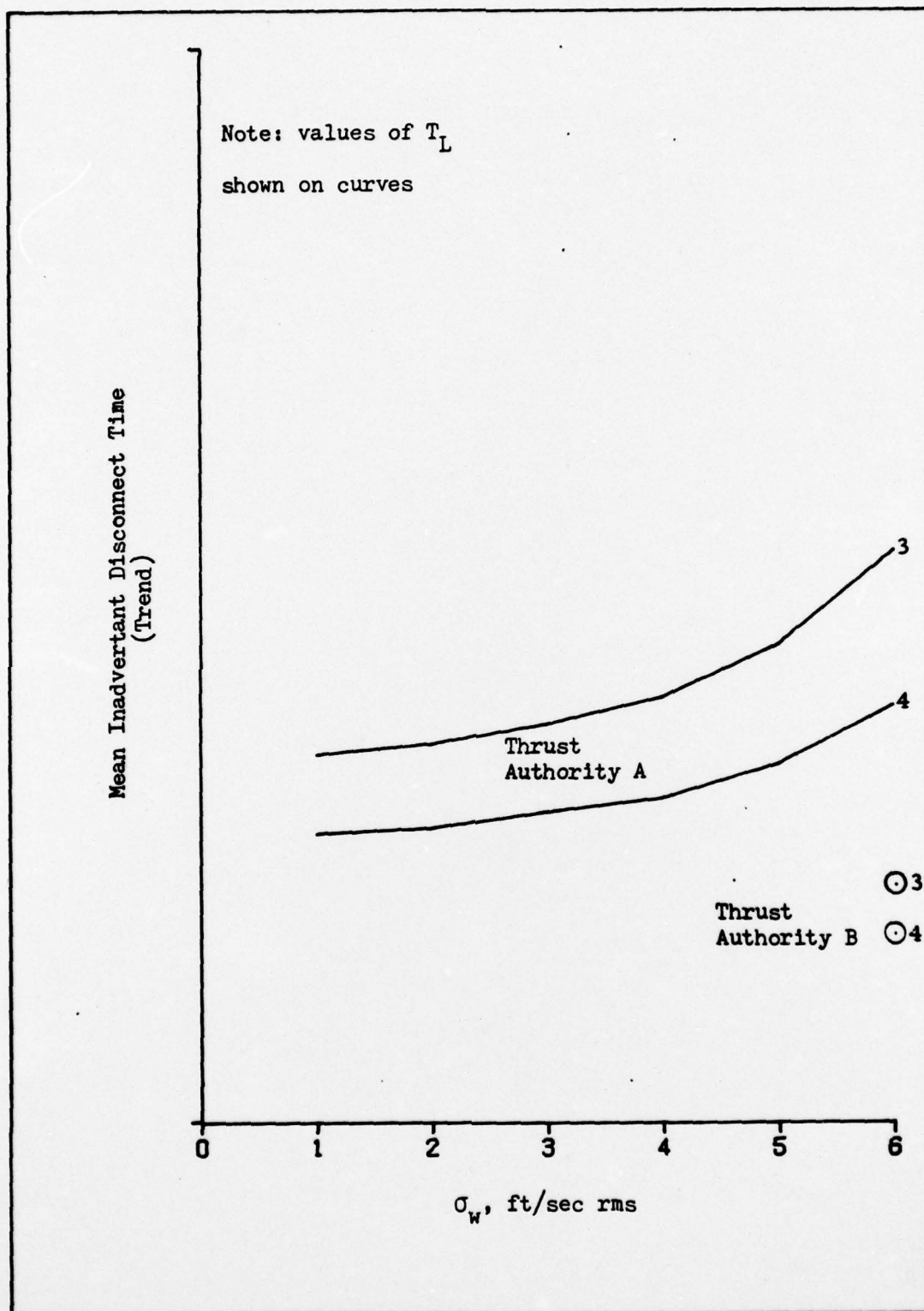


Figure H-12. Mean Inadvertant Disconnect Time vs. Gust Intensity  
for 1000 Rads.

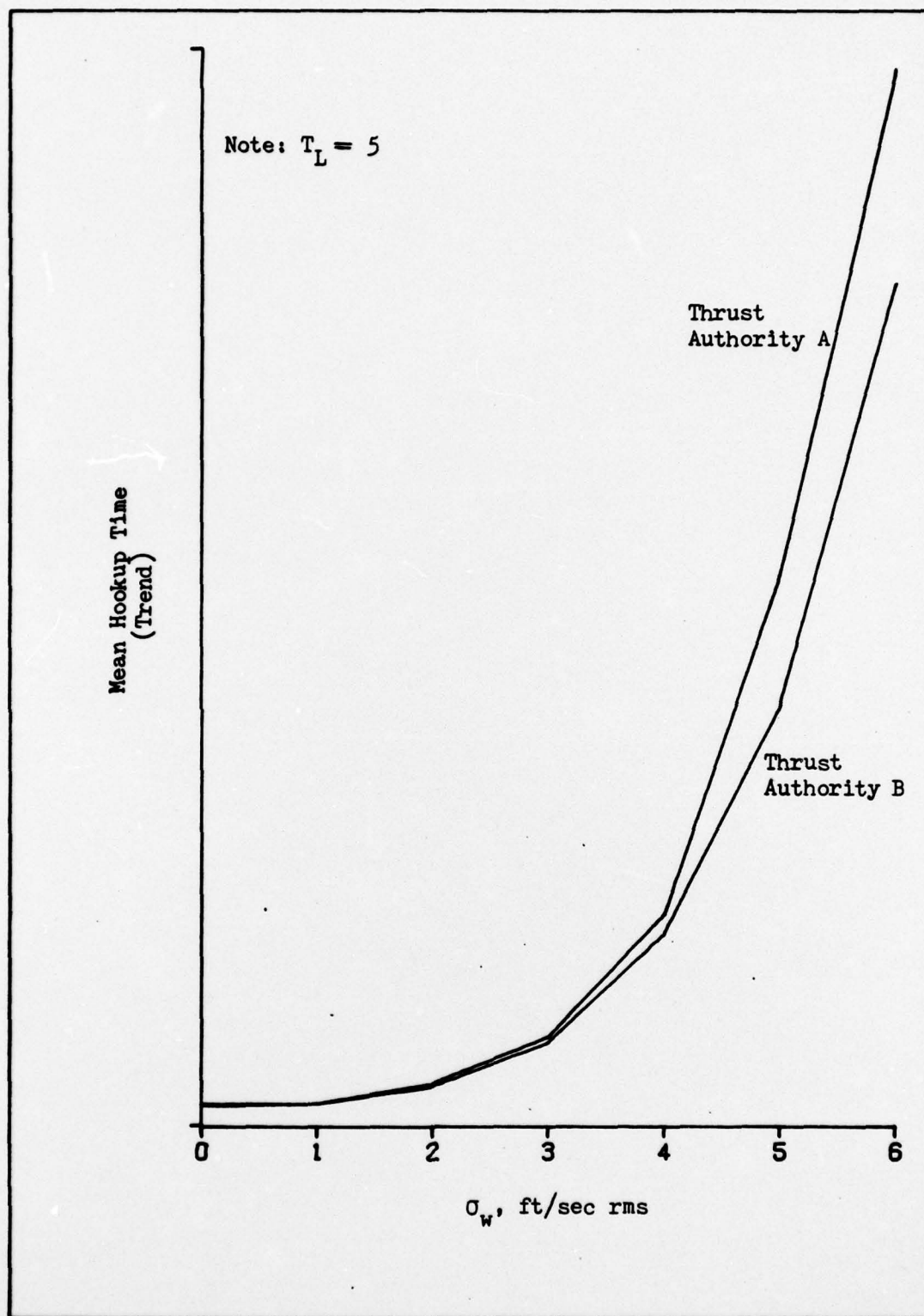


Figure H-13. Mean Hookup Time vs. Gust Intensity for 0 Rads, No Downwash.

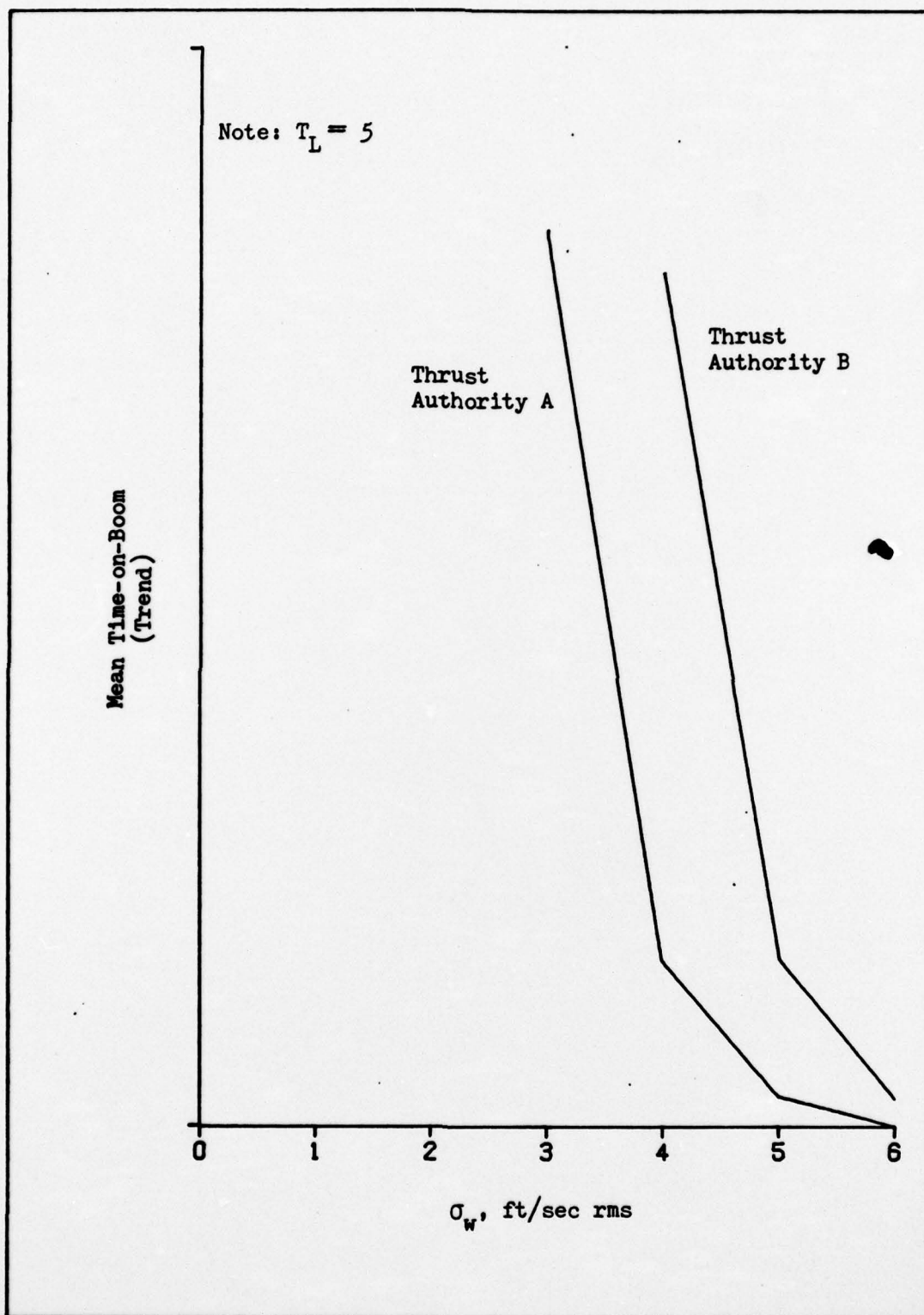


Figure H-14. Mean Time-on-Boom vs. Gust Intensity for 0 Rads, No Downwash.

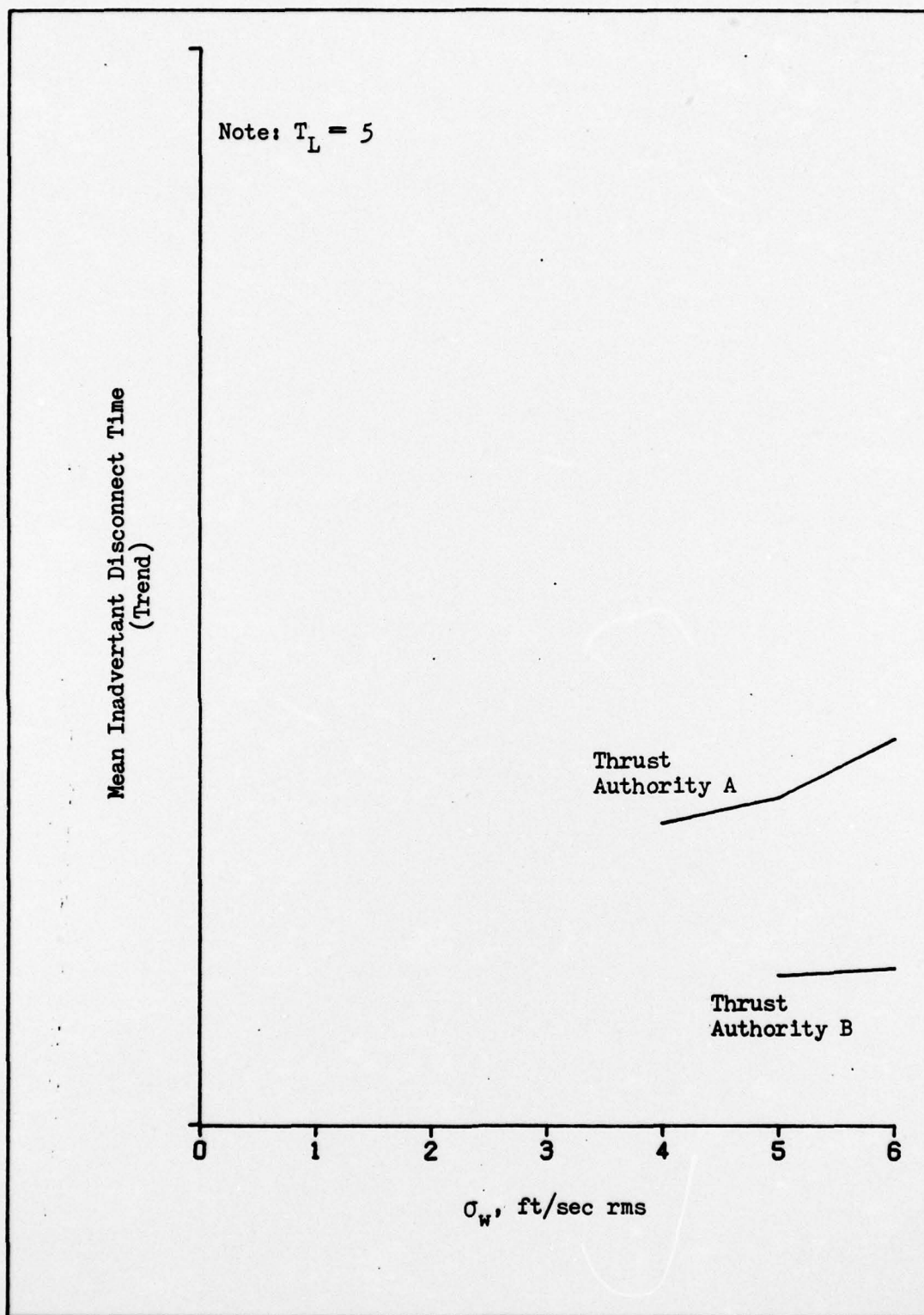


Figure H-15. Mean Inadvertant Disconnect Time vs. Gust Intensity for 0 Rads, No Downwash.



## VITA

John T. Merrifield was born on 14 February 1947 in San Antonio, Texas. He graduated from high school in 1964 and received the degree of Bachelor of Science in Engineering Science from Trinity University in 1968. After an employment as a chemical engineer for the Texaco, Inc. Research Laboratories in Port Arthur, Texas, he entered the United States Air Force in November 1969. He received his pilot rating in February, 1971. He then served as a C-141 aircraft commander, instructor pilot, and operations staff officer with the 437th Military Airlift Wing at Charleston Air Force Base, South Carolina, until entering the Air Force Institute of Technology in June 1975.

Permanent address: 721 Koehler Ct.  
San Antonio, TX 78223

This thesis was typed by Mrs. Anna L. Lloyd

UNCLASSIFIED

SECURITY CLASSIFICATION OF THIS PAGE (When Data Entered)

REPORT DOCUMENTATION PAGE		READ INSTRUCTIONS BEFORE COMPLETING FORM
1. REPORT NUMBER GA/MC/76D-10	2. GOVT ACCESSION NO.	3. RECIPIENT'S CATALOG NUMBER
4. TITLE (and Subtitle) A CONTROL THEORETIC STUDY OF THE NUCLEAR VULNERABILITY OF THE AIR REFUELING TASK		5. TYPE OF REPORT & PERIOD COVERED MS Thesis
		6. PERFORMING ORG. REPORT NUMBER
7. AUTHOR(s) John T. Merrifield Capt		8. CONTRACT OR GRANT NUMBER(s)
9. PERFORMING ORGANIZATION NAME AND ADDRESS Air Force Institute of Technology (AFIT-ENA) Wright-Patterson AFB, Ohio 45433		10. PROGRAM ELEMENT, PROJECT, TASK AREA & WORK UNIT NUMBERS Project 7930-09-12
11. CONTROLLING OFFICE NAME AND ADDRESS Environmental Sciences Division (VNE) USAF School of Aerospace Medicine (AFSC) Brooks AFB, TX 78235		12. REPORT DATE December 1976
		13. NUMBER OF PAGES 146
14. MONITORING AGENCY NAME & ADDRESS (if different from Controlling Office)		15. SECURITY CLASS. (of this report) UNCLASSIFIED
		15a. DECLASSIFICATION/DOWNGRADING SCHEDULE
16. DISTRIBUTION STATEMENT (of this Report)  Approved for public release; distribution unlimited.		
17. DISTRIBUTION STATEMENT (of the abstract entered in Block 20, if different from Report)		
18. SUPPLEMENTARY NOTES  Approved for public release; IAW AFR 190-17 Jerral F. Guess, Captain, USAF Director of Information		
19. KEY WORDS (Continue on reverse side if necessary and identify by block number) Nuclear Vulnerability Survivability/vulnerability Air refueling (B-52) Tanker downwash Analog simulation of air refueling Pilot modeling Pilot irradiation Pilot control of unstable system		
20. ABSTRACT (Continue on reverse side if necessary and identify by block number) A hypothetical air refueling operation involving a B-52H bomber and a KC-135 tanker is modeled on an analog computer for the purpose of determining its vulnerability to air turbulence and pilot gain decrement due to irradiation. The model includes the following elements: (1) the longitudinal small perturbation equations of motion for the B-52H in the downwash flow field of the KC-135; (2) pilot models to operate the elevator and throttle of the B-52H; and (3) a stochastic gust model which provides vertical gust disturbances to the equations of motion. (cont on p 130)		

DD FORM 1 JAN 73 1473 EDITION OF 1 NOV 65 IS OBSOLETE

UNCLASSIFIED

SECURITY CLASSIFICATION OF THIS PAGE (When Data Entered)

UNCLASSIFIED

SECURITY CLASSIFICATION OF THIS PAGE(When Data Entered)

(cont to p 129)  
The controlled elements with and without downwash are derived for the refueling task. Comparison of these transfer functions shows that the downwash causes instability. Stability analyses are conducted on the pilot-aircraft open-loop transfer functions over a range of pilot rate to displacement weighting,  $T_L$ , and pilot gains are found which will stabilize the system for each value of  $T_L$ . (T sub L)

Monte Carlo simulations of the refueling task are run at varying combinations of  $T_L$ , rms gust intensity, pilot thrust authority, and pilot gain decrement due to irradiation. Trends of mean refueling time are predicted. Using mean refueling time as a basis for comparison, optimum values of  $T_L$  are found for the irradiated and the non-irradiated pilot.

130

UNCLASSIFIED

SECURITY CLASSIFICATION OF THIS PAGE(When Data Entered)